Load Testing and Analysis of a 48-year old Out-of-Service Double Tee Girder Bridge

FINAL REPORT
December 2015

Submitted by:

Victor J. Torres, M.S.
Utah State University
4110 Old Main Hill
Logan, UT 84322

Marc Maguire
Assistant Professor
Utah State University
4110 Old Main Hill
Logan, UT 84322

External Project Manager
Joshua Sletton
Utah Department of Transportation

In cooperation with

Rutgers, The State University of New Jersey
And
Utah Department of Transportation
And
U.S. Department of Transportation
Federal Highway Administration

Disclaimer Statement

The contents of this report reflect the views of the authors, who are responsible for the facts and the accuracy of the information presented herein. This document is disseminated under the sponsorship of the Department of Transportation, University Transportation Centers Program, in the interest of information exchange. The U.S. Government assumes no liability for the contents or use thereof.

The Center for Advanced Infrastructure and Transportation (CAIT) is a National UTC Consortium led by Rutgers, The State University. Members of the consortium are the University of Delaware, Utah State University, Columbia University, New Jersey Institute of Technology, Princeton University, University of Texas at El Paso, University of South Florida and Virginia Polytechnic Institute. The Center is funded by the U.S. Department of Transportation.

TECHNICAL REPORT STANDARD

1. Report No.	2. Government Accession No.	3. Recipient's Catalog No.
CAIT-UTC-NC1		

4. Title and Subtitle	5. Report Date
Load Testing and Analysis of a 48-year old Out-of-Service Double Tee Girder Bridge	December 2015
	6. Performing Organization Code CAIT/Utah State University

7. Author(s)	8. Performing Organization Report No.
Victor J. Torres, Marc Maguire	CAIT-UTC-NC1

9. Performing Organization Name and Address	10. Work Unit No.
Utah State University 4110 Old Main Hill	11. Contract or Grant No. DTRT13-G-UTC28

12. Sponsoring Agency Name and Address	13. Type of Report and Period Covered
Center for Advanced Infrastructure and Transportation Rutgers, The State University of New Jersey 100 Brett Road Piscataway, NJ 08854	14. Sponsoring Agency Code

15. Supplementary Notes
U.S. Department of Transportation/Research and Innovative Technology Administration
1200 New Jersey Avenue, SE
Washington, DC 20590-0001

16. Abstract

A 48 year old prestressed double tee girder bridge located on Icy Springs road in Coalville, Utah, was tested for live load. The test measured strains, deflections and rotations. The instruments used for measuring the respective measurements were strain gages, deflectometers ("twangers") and tiltmeters.

From the recorded measurements a finite element model (FEM) was calibrated to validate the modeling techniques based on the test data. The FEM implemented two joint link elements to connect the flanges of the FEM deck to model the transverse load distribution of the bridge deteriorated shear connectors. The abutment restraints were modeled by one joint link elements. The deck and the stems were modeled using shell element.

After validating the modeling techniques, a parametric study was developed to study the prediction of FEM girder distribution factors (GDF). The FEM GDF predictions were compared to the prediction proposed by the American Association of State Highway and Transportation Officials (AASHTO) in the provision AASHTO LRFD 2010. The parametric study considered the variable parameters of span length, slab thickness, number of double tees, angle of skew, and stem spacing.

The AASHTO specification provides an inaccurate prediction, therefore a new statistical model was proposed to better predict GDF. Furthermore, rating factors based on different girder distribution factors were studied for the Icy Springs bridge. The bridge has a passing rate for operating level.

17. Key Words	18. Distribution Statement
Presetressed double tee girder, FEM, GDF, AASHTO LRFD 2010	No restrictions

19. Security Classification (of this report)	20. Security Classification (of this page)	21. No. of Pages	22. Price
Unclassified	Unclassified	166	

Form DOT F 1700.7 (8-69)

ACKNOWLEDGMENTS

First and foremost, I acknowledge my gratitude to my God, Whom I give all the praise and honor of all the fruit of my labor on this earth and the life to come, thank you, Christ Jesus. To my father, Victor, my mother, Luz, and my sister, Ana Torres, for their support and encouragement.

To my major professor, Dr. Marc Maguire, working with you has been a valuable experience. I appreciate all the effort, encouragement and help you had provided along the way. Thank you for entrusting this project to me and giving me the opportunity to work with such a talented person.

Thanks Dr. Gilberto Urroz and Dr. Marvin Halling, for being part of my committee and your input to my thesis. Thanks Dr. Paul J. Barr, for your help regarding research obstacles and questions. To Navid Zolghadri, for all your help and advice during the research process. To Chris Pettigrew, for your help on the initial phase of the project. To Edyson Rojas for the pictures of the live load test.

To everyone that help on the live load test: Dr. Marc Maguire, Dr. Paul J. Barr, Dr. Marvin Halling, Ken Jewkes, Brandon Assay, Edyson Rojas, McKell Bowen, Navid Zolghadri, Nickolas Foust and Wyatt Ellertson.

To the Dominican Republic (MESCyT) for providing the funds for my education at Utah State University. To the Utah Transportation Center (UTC) for the funds dedicated to my research project. Last but not least, to friends and family that provided support and encouragement.

Victor Torres

Table of Contents

LIST OF FIGURES

LIST OF TABLES

INTRODUCTION

The American Society of Civil Engineers published in 2013 the "report card for America's Infrastructure." This publication constitutes an evaluation that the society has performed through research and inspections to rate the infrastructure of the country for further improvement, decision making and planning. According to the report card, bridges in the United States are qualified C+ with C as mediocre and B as good. According to the ASCE report card, an average of 11.7% of the bridge infrastructure of the US is becoming deficient every year. This is 70,200 out of the 600,000 bridges that constitute the bridge infrastructure of the country (ASCE 2013). The United States is home to nearly 600,000 highway bridges (Vaghefi, et al. 2012).

This research consists of the live load testing and analysis of the Icy Springs Bridge. The Icy Springs Bridge, was a prestressed double tee girder bridge in deficient conditions. This bridge is representative of the deficient bridges that constitute the U.S. bridge infrastructure. The bridge had been in service for 48 years prior to removal and replacement by the new Icy Springs Bridge in 2013. The bridge was visibly deteriorated on the deck surface and was load posted. Even though research has been published on testing of old bridge structures, there is no existing research published on a bridge with the deteriorated structural features (double tee girders) like the ones on the Icy Springs Bridge.

Chapter 1 contains the published literature concerning structural identification, AASHTO distribution factors, finite element modeling, live load testing, bridge load rating and live load testing. The purpose of this review of literature is to present the current practice and research that supports the methods used for the project. Furthermore,

to find the needs that the project needs to address regarding the current specifications from testing and analysis results.

Chapter 2 corresponds to the bridge test for live load. The bridge was instrumented for live load testing to record strains, deflections and rotation measurements from four live load cases. The live load was a truck with 61.7 Kips (273.98 KN). During testing the truck was driven at low speed along the path that described each of the load cases. The types of instruments and data processing used for this live load test are explained in detail. Furthermore, interesting observations from test data are commented.

On Chapter 3, a finite element model (FEM) was calibrated from live load testing data to validate the modeling techniques. Shell elements were used for the deck and stems. Link elements were used to model the restraint at the abutments. In addition, due to the deterioration on the deck surface of the tested structure, an innovative modeling technique was used to model the transverse load distribution of live load in the FEM, longitudinal two joint links on the FEM deck. Furthermore, an open application programming interface (OAPI) was used to calibrate the model on SAP2000. Influence lines were obtained from influence surfaces, after the model was calibrated, and compared to the measured influence lines from testing.

In Chapter 4 a parametric study was developed. The parametric study describes the current specifications used in design and rating inspection of bridges. The parameters of span length, slab thickness, number of double tees and skew were varied to compute girder distribution factors (GDF) from FEM. The FEM predictions were compared to the current AASHTO predictions. A new statistical model was proposed to better predict

girder GDF. This new statistical model was developed from the accurate response of parametric FEM models used in the comparison with the AASHTO prediction.

Chapter 5 discusses the rating for the Icy Springs Bridge. Different ratings were calculated for the Icy Springs Bridge to evaluate the conditions of the bridge before removal and the potential that the bridge had to remain operating in service.

Finally, the summary of the project is presented and the final conclusions are reported.

CHAPTER 1. LITERATURE REVIEW

1.1 Structural Identification

The observation of the physical systems by means of experimental testing to validate mathematical models is the basis for structural identification (St-Id) (Moon and Catbas, 2013). System identification originated in electrical engineering as the fashion in which systems can be described by the correlation of inputs and outputs (Aktan and Brownjohn, 2013).

Chiefly, structural identification encompasses testing a constructed system for the validation of a mathematical model based on experimental data. The model represents a structural system validated by the optimization of the measured parameters and the mathematical predictions.

Current design practice of structural systems despite the technological advantages and the implementation of finite element modeling is simplified by the approaches of structural codes resulting in conservative design. Furthermore, current bridge inspection is mostly based on visual inspection and analysis is based on simplified approximated equations that are not able to take into account the physical state and behavior of the system. A constructed system has difficulty being evaluated through the use of a design model, as it will result in an unrealistic approach. Design models are conservative and use a simplified approach to design structural members to resist ultimate loads. Catbas and Moon (2013) stated the importance of St-Id as the bridge that closes the gap between constructed systems and models used in design and assessment.

Aktan and Brownjohn (2013) clarified the importance of using St-It for analytical models by revealing that the use of design models can exceed the prediction of global responses by 500% and the local responses by 1000%. Furthermore, the researchers emphasized that the prevalent shortcomings of predicting structural performance is because engineers cannot model the structural foundation system so that kinetic and kinematic mechanisms are considered for linear and nonlinear behavior. Consequently, St-Id provides the mechanism to improve the reliability of computer models by correlating experimental and analytical data.

Chajes, et al. (2000) stated that the best model to predict bridge behavior is the bridge itself. However, Collins (2010) made the observation that even though this is an impossible task in the design phase, once the system is constructed, testing for load rating or proof testing can provide an accurate model by implementing structural identification.

According to Moon and Catbas (2013) structural identification can be implemented for:

- Determining the load capacity of the system (Load rating)
- Design verification and quality control, especially for “groundbreaking” design
- Delivering a design-build contract in a measurement based fashion
- Evaluation of deterioration and damage mitigation such as: cracking, settlement, vibrations, etc.
- Design for structural modification and retrofit

Numerous research has been published on St-Id application of constructed systems. For instance, the Svinesund arch bridge at the border of Sweden and Norway was tested prior to opening in 2005 for identification of static and dynamic parameters.

The project monitored the bridge during construction, testing period (prior to opening) and the first four years of service. Among the observations from the experimental data the arch was found to be stiffer than it was assumed during the design phase. The calibrated base model represents a mathematical model of the physical undamaged structure that can be used for future condition assessment (Karaoumi, et al., 2006).

Another case of implementation of St-Id among many others is the Qinzhou cable-stayed bridge in China. The bridge is among the longest cable-stayed bridges in the world and prior to opening was tested to confirm that the performance of the bridge satisfies the limits assumed during the design of the structure. It was tested to prove that the design service limits of the bridge deck deflection and displacement of the towers are satisfied by the constructed structure. Furthermore, testing was used to prove adequate load-carrying capacity of the structure. (Ren, et al., 2007).

St-Id can be implemented for all structure sizes. For instance, Sanayei, et al. (2012) tested the Vernon Avenue Bridge in Massachusetts. The bridge is a small structure with three spans; the first and third span are 11.75m (38.55 ft) and the middle span is 23.5m (38.55 ft). The bridge was tested by using static load testing prior to service. The test data was used to calibrate an FE-based model and bridge load rating was studied. Performing a load test and creating a baseline model can reduce the bias or predisposition of future load rating and can be used as a starting point for structural health monitoring (SHM).

1.2 AASHTO Girder Distribution Factors

The current girder distribution factors used by AASHTO LRFD (Load and Resistance Factor Design) were developed as part of the National Cooperative Highway

Research Program (NCHRP) project: "Distribution of Live Loads on Highway Bridges." (Zokaie 2000). This project improved the previous AASHTO method ("S/D method") by including different uncoupled parameters to the calculation of girder distribution factor. Furthermore, the new set of formulas encompassed a broader assortment of bridge types. The new formulas for girder distribution factors developed by Zokaie were adopted by AASHTO in 1994.

Zokaie's live load distribution formulas were developed based on many finite element models loaded to produce the maximum moment. For cases where the simplified formulas do not apply, designers are told girder distribution factors may be obtained by using a "grillage approach" (finite element). Furthermore, Zokaie emphasized that when using the distribution factor formulas, the engineer must understand the limitations, restrictions and when accurate results can be obtained by the use of the formulas. In addition, if finite element modeling is used, the model should be prepared such that it represents the true bridge deck behavior.

Live load girder distribution factors are sensitive to the position of the live load. Edge girders were found to be the most sensitive to live load position; therefore, it is important to determine how close the live load can be placed near the edge for analysis. The closer to the edge the live load is placed, the higher the distribution factor. Therefore, it is important to know how close to the edge the truck can be placed. This distance will be limited by the minimum edge distance, d_e, and any objects on the deck surface, such as parapets and sidewalks. Girder distribution factors are calculated transversely at any position 2 ft (0.61 m) away from the edge of the driving surface (i.e. 2 ft (0.61 m) from curb or parapet). If these restrictions are not considered, then over-conservative values

will be obtained. In addition to the location of the live load in the transverse direction of the bridge, another important parameter is the gauge (axle width). HS20 trucks were used in the study; the HS20 has a gage distance of 6 ft (1.828 m). Another parameter found to be significant on the distribution of loads was the skew of the bridge. The skew modifies the load path of the bridge by causing more load on the girders with the shortest path to the load. (Zokaie 2000)

Two important assumptions were made in the development of the currently specified equations. The study assumes that the parameters can be expressed in the exponential for ax^b where x is the parameter and a and b are the constants that are used to exponentially estimate the parameter x for the calculation of the girder distribution factor. Moreover, the study assumed that the different parameters that affect the distribution of live load are independent of each other, therefore the analysis and development of the equations considered models that changed uncoupled between the parameters chosen. The author of the NCHRP report (Zokaie, 2000) supports the assumption by experimenting with parameters that were thought to be uncoupled by using a scattergram. Zokaie found all investigated parameters to be uncoupled. For example, a plot of girder thickness vs girder spacing is provided by Zokaie in his paper, "AASHTO-LRFD Live Load Distribution Specification," showing significantly scattered data with no clear trend to be fitted to an equation. (See Figure 1.1.) However, one may argue that a line could be fitted and represent a generally coupled relationship between both parameters. If this is the case, a coupled analysis of girder distribution factors based on models of all the possible combinations of parameters should be performed. This would be computationally expensive and perhaps prohibitive.

The use of the girder distribution factors is an approximation of the distribution of live load among the girders of a bridge. When designing a bridge, calculating GDF is an iterative process due to unknown parameters. The AASHTO LRFD equations do not account for the variable cross section, therefore using the moment of inertia that causes the worst case GDF is a conservative approach. Moreover, variable girder spacing is not accounted for. To compensate, the average spacing on both sides of a girder can be used.

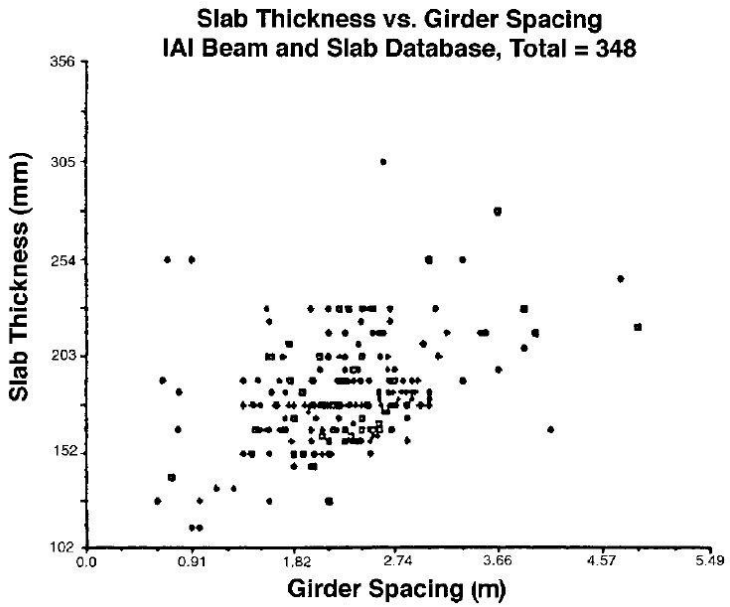

Figure 1.1 Slab thickness and girder spacing, Zokaie 2000

Girder distribution factors are used extensively to perform design and analysis of bridges in current practice. In design, as previously mentioned, GDFs are over-conservative. In analysis, GDF are used to evaluate an existing structure constrained by damage and boundary conditions that can only be observed by live load testing. The use of a theoretical formula to predict the behavior of an existing structure under special boundary restraints and after the damage has occurred will also prove over-conservative. Nevertheless, live load rating as an analysis task is usually performed by theoretical

equations for GDF rather than experimental load rating, due to expense and time even though it can provide more accurate analysis.

Measured girder distribution factors from testing when compared to the AASHTO theoretical prediction, are consistently lower (Kim and Nowak, 1997).

1.3 Finite Element Modeling and Calibration

Bridge behavior such as flexural bending, shear deformation, torsion, deflection, rotation, girder load distribution, natural frequencies and mode shapes, can be modeled with a finite element model (FEM). FEM considers the effects of the parameters that influence the response of the model and the advantages and shortcomings of the elements being used.

Bapat (2009) studied the influence of different parameters on modeling slab on girder bridges. An appropriate modeling technique is considered to be the first step in the development of a finite element model. Shell elements are considered adequate to model bridge deck behavior which is predominantly governed by flexure. Additionally, shell elements can also be used to model bridge girders (Bapat, 2009). Another feasible combination is the "beam offset model," which uses shell elements to model the deck surface and frame elements to model the girder (Bapat 2009). Both elements are connected by "link" elements, which can have partial fixity or full fixity to model partial- or full-composite behavior respectively. Moreover, Bapat pointed out that the change of material properties can be used to model the presence of slab reinforcement. Therefore, the use of shell elements is appropriate for structures that have different types of layers.

Furthermore, Bapat (2009) studied the effects of including the bridge parapets on the model and the effects due to boundary conditions. It was found that the flexural modes of vibration were sensitive to the boundary conditions and the guardrails. Guardrails provide stiffening effects to the bridge either by having a connection that is partially or fully composite. The study investigated no composite action and full composite action. The support conditions provided higher values of natural frequencies when fixed restraint was used. In addition, it was noted that the higher frequencies were the frequencies less susceptible to boundary conditions.

Finite Element Calibration is the procedure by which an engineer modifies a finite element model based on an objective way to quantify the difference in the experimental response and the analytical finite element response (Wang, et al., 2007). Using an objective function to optimize the difference in the experimental response and the analytical response of the FEM model calibration is a task appropriate for computer programming. Wang specified the awareness of the civil engineering community to the limitations of visual inspection for condition assessment of bridges and how model calibration can simulate the response of a bridge to improve condition assessment. The purpose of the FEM calibrated is to predict the global behavior of the bridge. The maximum response of a unit influence line (UIL) is one of the most important properties of the influence line used in the calibration of the FEM.

Goble, et al. (1992) studied 34 bridges across the United States to demonstrate the use of FEM calibration based on live load experimental data. The bridges were tested and the experimental data was used by a computer program to optimize the FEM based on an iterative algorithm that used an objective function to calibrate the FEM response to the

measured data. The algorithm used to optimize the model's basically estimated properties initially was set to upper and lower limits of $\pm$ 50% or more. The program optimizes based on the number of load cases (n). If the lateral distribution of loads was not correct, the truck position was adjusted $\pm 12ft$ ($\pm$ 3.66 m) in any direction. If the error was acceptable, new properties were reassigned based on average and standard deviation of the parameters changed for calibration. New upper and lower limits were set. Furthermore, the program determines which parameters will continue to be optimized.

Goble pointed out the importance of parameters that needed to be included when modeling beam-slab types of bridges, such as:

- Longitudinal Stiffness
- Lateral load distribution ability
- Geometry of the structure being modeled
- Load geometry
- Rotational Stiffness of support and connections.
- Torsional Stiffness of beams and girders.

When calibrating an FEM, the major changes in the diaphragm properties change the overall strains slightly. Because of this, diaphragm properties were estimated and assumed to be a fixed parameter for the calibration of the model. However, lateral load distribution is influenced by the deck elements and the relative stiffness of the exterior and interior beams.

In order to have enough data for calibration, Goble recommends that more than one lateral truck position must be considered. When calibrating, the engineer will use the experimental influence lines to find the location of maximum deformation, using proper

load geometry, the truck will be positioned at the same location in the model. After the static analysis is performed, the FEM response is compared to the experimental measurement by an objective error function. Based on an optimization algorithm or manual iteration decisions are made to optimize the model based on the discovered sensitive parameters.

Sanayei, et al. (2012), made the distinction between a design model and a calibrated model. Design models are not intended to represent the actual structural response but they are intended to provide design values for the ultimate conceivable demand. This is a valid conservative approach because the probability that all structural members will experience their respective ultimate capacity at the same time is low. On the other hand, a calibrated model represents the actual response of the structure under a defined load condition. The defined load conditions used for model calibration come from the different load cases that constitute the load test.

1.4 Live Load Testing

Live load testing of bridges consists of loading the bridge with a known load along a predetermined path to record measurements that indicate the deformation of the structure as the load is applied throughout the test. The bridge is instrumented to record measurements at points of interest for different purposes such as load rating and FEM calibration.

Ren, et al. (2007), describes live load field testing as the most vital way to understand the behavior and fundamental characteristics of bridges. In addition, the reasons behind live load testing include uncertainties in materials, numerical prototypes (FEM) and concerns for the serviceability of the constructed system. Ren, et al. (2007),

explains that through field testing, it is often observed that bridges have a greater load carrying capacity that the one predicted from analytical methods. The reasoning for this is that during design, conservative assumptions are made to account for the things that are uncertain in the analysis. Therefore, live load testing provides a more accurate estimation of a bridge load carrying capacity.

Collins (2010) comments how instruments such as displacement transducers had been used successfully to measure the absolute movement of girders, and the relative movement between deck and girder. Likewise, rotation measurements have been recorded from bridge testing by using inclinometers and tiltmeters. Collins also pointed out that one major application of live load testing is the computation of an experimental girder distribution factor, as a way to quantify from experiment the ability of a bridge to share load transversely. Barr, et al. (2006) observed through the use of live load testing that the AASHTO equations used to calculate girder distribution factors are excessively conservative. Moreover, the use of live load testing has been commonly used to determine load ratings of bridges with more accuracy (Hodson, et al., 2012). Experimental GDF are typically calculated using strains or deflections on each girder at midspan and are different for different truck positions.

1.5 Bridge Load Rating

Due to the complexity of the load distribution on bridges, engineers often times rely on code provisions to determine distribution factors used for inventory and operating ratings (Barr, et al., 2006).

AASHTO has developed bridge load rating provisions that are consistent with the load and resistance factor design (LRFD) philosophy. The provisions contained in the

AASHTO load and resistance factor rating (LRFR) determine load posting, bridge strengthening or renovation and assist in the decision making of overweight vehicle permitting (AASHTO LRFR, 2013).

Figure 1.2 from the AASHTO provisions is the flowchart recommended for the assessment of highway girder bridges regarding based on load rating. The process suggests rating a bridge for the LRFD design loads in what is called the inventory level. If this level is exceeded by the bridge, no further action is required. If the inventory level is not met, then the bridge can be rated to what are considered the AASHTO and state legal loads. These loads are considered the operating level, i.e. a bridge passing this stage can operate if the rating factor is greater than one. The rating factor is the ratio of the capacity of the bridge and the live load effects on the bridge. Otherwise, the bridge can be posted or strengthened. When overweight loads are considered, a pass or fail can be determined for the bridge and the corresponding load.

Bridge rating was developed using structural reliability for the strength limit state. Furthermore, guidance for service limit state is available as well. The rating only considers permanent loads and vehicle loads. Other loads such as earthquake, vessel collision, wind, flood, ice or fire are not considered for load rating. The AASHTO LRFR specification is for highway bridges that are not long-span bridges and movable bridges (AASHTO LRFR, 2010).

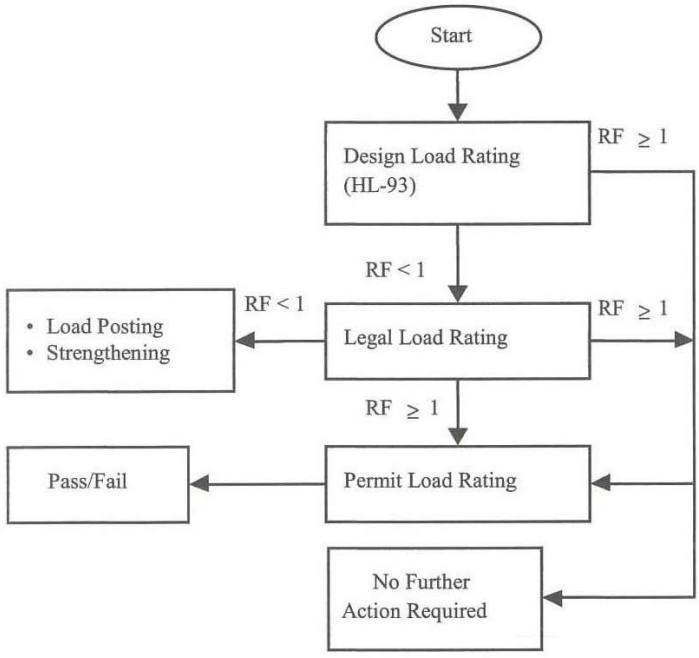

Figure 1.2 AASHTO LRFR rating flowchart (AASHTO LRFR, 2010)

Bridge rating is similar to the approach used for bridge design. However, when rating bridges, a conservative evaluation can require rehabilitation or replacement to become necessary (AASHTO LRFR, 2010).

CHAPTER 2. BRIDGE TESTING

2.1 Bridge Description

The Icy Springs Bridge was a bridge that had been in service in Coalville, Utah, for 48 years until it was replaced in the fall of 2013 by a new bridge. The bridge was located on the global coordinates: 40.912037 latitude and -111.406173 longitude (Figure 2.1). The bridge was located on Icy Springs road, which is road 280 that overpasses the interstate I-80 (Lincoln Hwy).

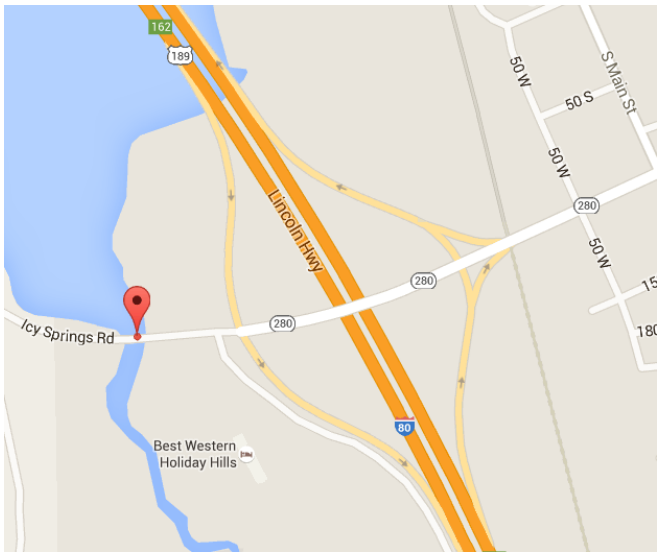

Figure 2.1 Bridge location (red tag) in Coalville Utah

The superstructure consisted of three double tee girders spanning over 51 ft (15.54 m). The bridge was a single span bridge with semi-integral abutments. The abutments were cast into the wing walls which had an angle of about 45°. For the bridge plan see Figure 2.3. The stems of a single double tee girder were separated at a distance of 4 ft (1.219 m). Moreover, the spacing of the stems in between adjacent double tees was 2 ft (0.61 m). See **Error! Not a valid bookmark self-reference.** for the bridge cross section dimensions. Every stem had 16 strands of 0.438 in (11.11mm) diameter each. The

stems had a variable cross section that tapered from the bottom of the stem to the deck. From 0.43 ft (13cm) to 0.62 ft (19cm) in a trapezoidal cross-section shape. The strands were harped in a two-point harped pattern ("two-point depressed") that varied linearly from the abutments to 0.38L with different slopes per strand (i.e. fanned). The pattern

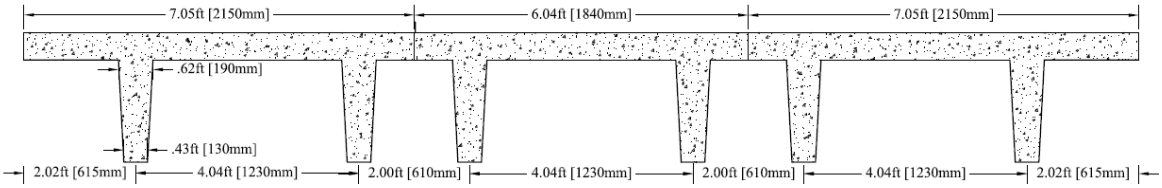

Figure 2.2 Bridge Cross Section Dimensions

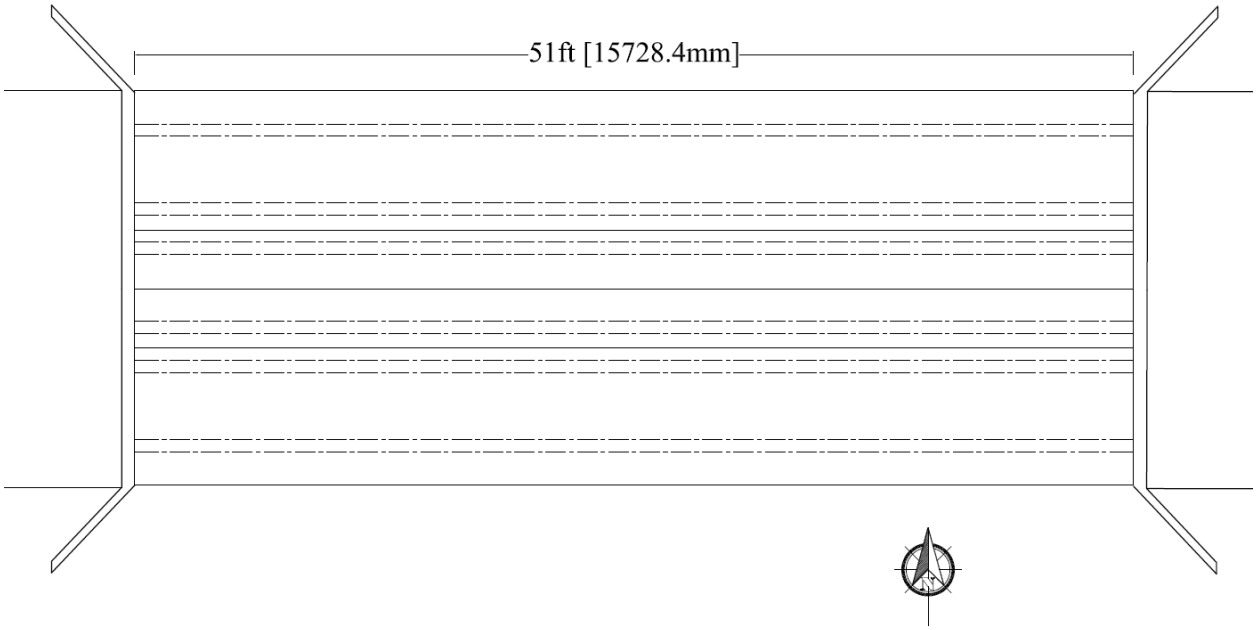

was symmetrical about mid span.

The bridge deck was considerably deteriorated. The asphalt driving surface was worn and had little protection for the deck surface against water deterioration and the wearing of the surface. In addition, there were spalls and cracking on the deck and deteriorated shear connectors between the stems. It is important to emphasize that since

Figure 2.3 Bridge Plan View

the asphalt wearing surface was absent in many sections of the deck, many spalls were located on the concrete deck itself. Shear connections between girders were deteriorated to an extent that in some cases no connection existed. Rebar was exposed by the damaged surface, both from spalling and near shear connections of the bridge.

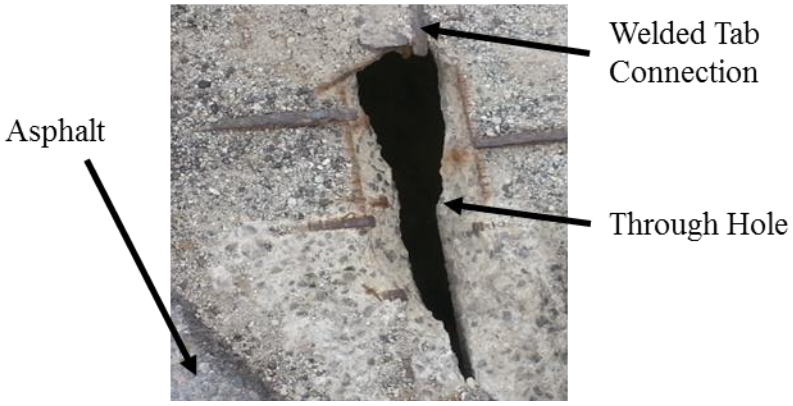

Figure 2.4 Deteriorated deck surface at girder connection

shows the concrete exposed at deck surface with no wearing pavement to protect the top flange. Furthermore, rebar was exposed in many places and a hole through the deck was found in between two girders. Girder connections are significantly important for the distribution of live load, and many were potentially compromised. Connections of girders are important when evaluation an existing structure, especially with respect to transverse load distribut

Figure 2.5 Pothole on the bridge superstructure structural deck component

Figure 2.6 Damaged superstructure deck surface

, 2.5 and 2.6 show the damaged deck surface, where the majority of the structural deck concrete was exposed, without protection against water, snow and wearing from the vehicles crossing the bridge. In many locations the gaps between girders were visible. In addition, potholes were present in many locations on the structural deck and rebar was exposed with no concrete cover.

The stems of the double tee girders were in good structural conditions, there was no cracking present, which indicated that the bridge had not yet been loaded significantly. Figure 2.7 demonstrates the good structural condition of the double tee girders with no visible cracking or spalling. Moreover, the bridge included steel pipe hand rails on the sides that were measured to use the dimensions and weight for further analysis. The rails

were attached to the edge of the exterior girder flanges through welds to an embedded angle on the exterior flanges.

Figure 2.7 Girders showing no cracking

Figure 2.8 shows a load post sign for 8000 lbs. The allowable load to cross the bridge was significantly low and should had been determined by the process of load rating according to the bridge load carrying capacity. Using conservative assumptions deck punching shear capacity was the controlling limit state, according to the rating engineer.

Figure 2.8 Bridge load post sign

2.2 Desired Data

The desired data for the bridge determines the type of instrumentation to place on the bridge for testing. For live load testing, the desired data to be acquired was: displacement, rotation and strain

This data was intended to be used to study the load carrying capacity of the structure based on experimental data, and to demonstrate the use of finite element modeling (FEM) for further experiments and comparisons with the current bridge specifications. A finite element model could be validated based on experimental data for: further study of the bridge, decision making and to demonstrate the adequacy of finite element techniques to model bridge behavior. The calibrated bridge model could also be used to compute live load shear distribution factors, which were not experimentally collected. Furthermore, the bridge can be load rated based on the factors for flexural distribution of live load from load testing.

2.3 Instrumentation Layout

The instrumentation for the strain transducers layout consisted of three sections: at midspan (0.5 L), quarter span (0.25 L) and twice the girder height from the abutment (2H). The instrumented side of the bridge was the west side of the span. Only one side of the bridge was instrumented due to access and water depth issues.

Figure 2.9 is the plan view of the instrumentation sections located on the west side of the bridge (instrumented side). Figure 2.10 shows the sections and instruments located at the respective section. The bridge was instrumented for deflectometers along the midspan (0.5L) transverse direction. Tiltmeters were located on the interior stem at the abutments. T1002 was located at stem S5 and T1001 at the south double tee. The purpose of these instruments was to obtain the response of the bridge for strain,

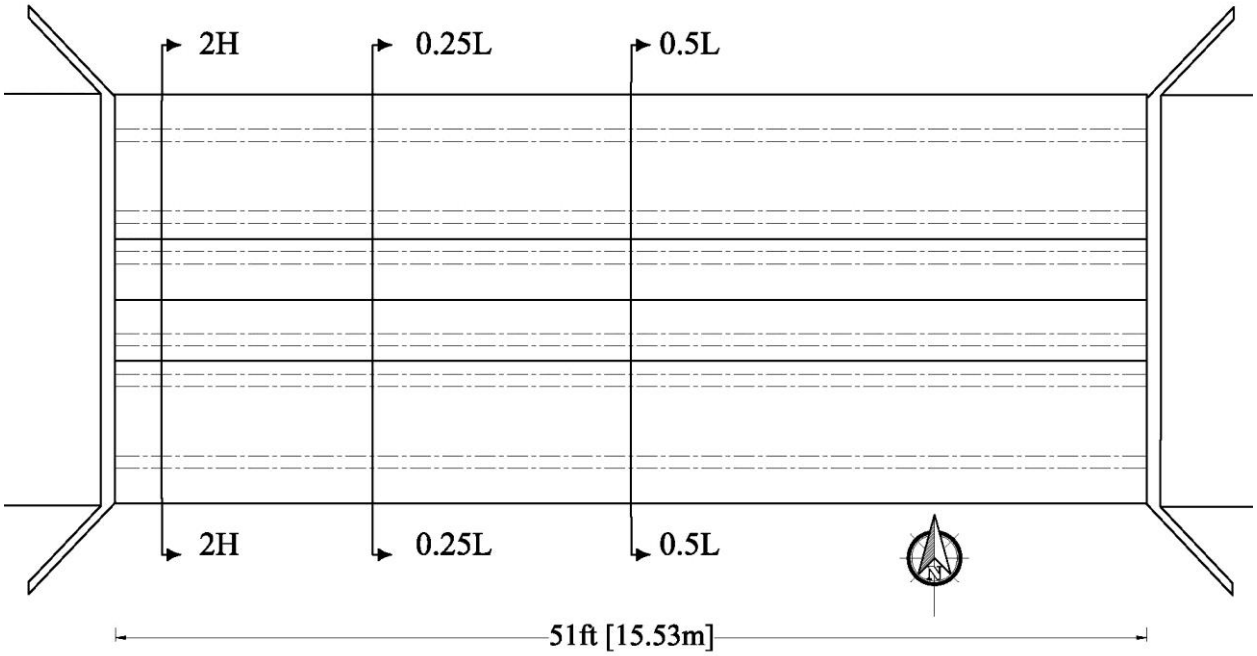

deflection and rotations in order to calibrate a finite element model to validate the modeling techniques. The 2H section was intended to provide information about the fixity of the bridge at the supports. The deflectometers and strain transducers were to ensure that the calibrated model represented the global behavior of the bridge corresponding to strength and service.

Figure 2.9 Instrumentation sections bridge plan view

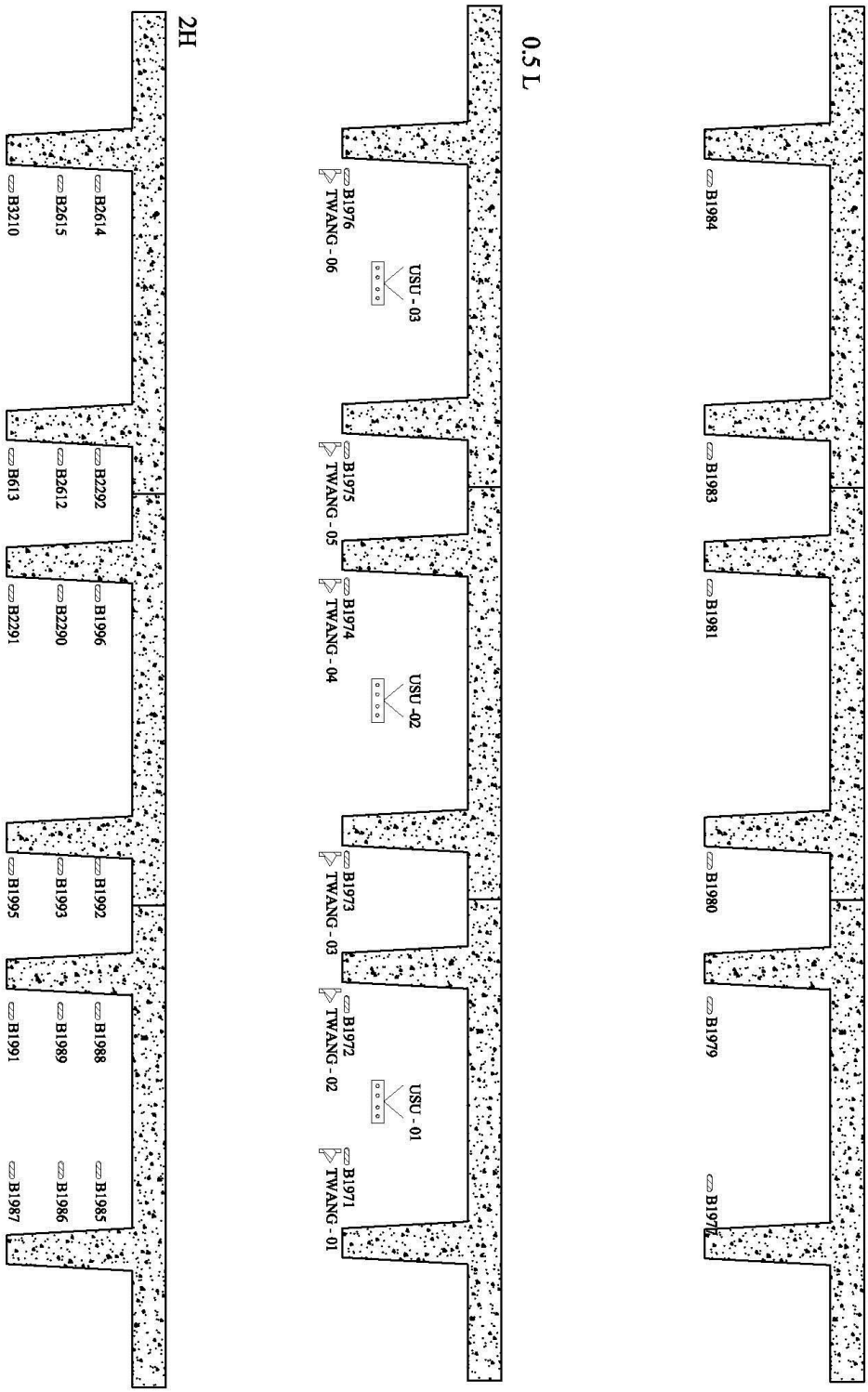

Figure 2.10 Instrumentation sections at 0.25H, 0.5L & 2H

2.4 Live Load Test Instrumentation

2.4.1 Strain Transducers

Strain Transducers are instruments that are designed for measuring strains under live load testing conditions. The duration of live load tests is usually short; therefore a negligible change of temperature for the test can be assumed (Bridge Diagnostics Inc. 2012a). The instrumentation used to measure strain on the test was ST350 BDI strain transducers. These instruments were able to measure strain accurately to less than plus or minus 1 % of the measured value. The ST350 strain transducers are designed for dynamic, pseudo static or static tests. The instrument consists of a typical "Wheatstone Bridge" electrical circuit with four 350Ω foil gages (resistance). Flexural bending can be determined from axial strain measurements as long as the small angle theory applies. The installation of the gages was according to the "tab and glue system" on concrete according to the installation manual.

Figure 2.11 Instant adhesive Loctite 410

Figure 2.12 Accelerometer Loctite 7452

Figure 2.11 is the glue used to attach the instrument to the location of measurement. To accelerate the time in which the glue reacted to connect the instrument tab to the structure an accelerator was used, this accelerator is shown in **Error!**

Figure 2.13 Strain gages installed on double tee girder stem

eference source not found..

Strain gages were tested and calibrated by the manufacturer within one year of the test. The manufacturer certifies the instruments were calibrated according to NIST (National Institute of Standards and Technology) standards. Figure 2.13 shows three ST350 strain transducers installed on the bottom, middle and top of the stem at 2H.

2.4.2 Tiltmeter

A Tiltmeter is an instrument used to measure the rotation of structural elements from their initial position due to loading of the member being tested. This type of instrumentation uses a liquid bubble correlated to its electrical excitation to measure rotation. The liquid bubble device is similar to the principle of equilibrium and leveling used in a carpenter's level.

Due to the small settling time of the liquid bubble system, the response of the instrumentation is considered to be inadequate for dynamic testing. However, the instrumentation is considered suited for live load testing (pseudo static). This is due to the slow loading that live load test undergoes. When testing bridges the live load from truck loads is applied to the structures by driving at constant crawl velocity (1-3 mph). The tiltmeter is recommended for bridge girder rotation and it is one of the usual applications for this type of sensor (Bridge Diagnostics Inc. 2012b). Figure 2.14 shows a tiltmeter installed one foot from the bridge abutment using glue and tabs. The rotation measurement at the abutment is important to determine the level of restraint that the abutment has to rotation.

Figure 2.14 Tiltmeter installed at the bridge abutment.

2.4.3 Deflectometer

Deflectometers were the instruments used to measure deflections; this type of instrumentation is colloquially called “Twanger.” The sensor consists of an aluminum plate attached to the bottom of the girder and a cantilever aluminum plate that extends to the side of the girder. The cantilever plate has an initial weight hanging from the farthest outer distance. Four strain gages in a Wheatstone bridge configuration are placed between the cantilever plate and the plate that attaches to the girder, the transducer measures strains as the beam deflects and through calibration can correlate the change in strain and the change of the cantilever deflection to the actual girder deflection.

Figure 2.15 shows how the twanger is attached to the stem on the girder. The cantilever end is pre-deflected by hanging a weight from the tip of the plate to the ground. When the girder is loaded, the deflection in the cantilever plate will change. A gage can correlate the difference in deflection to the change in resistance to compute a deflection measurement.

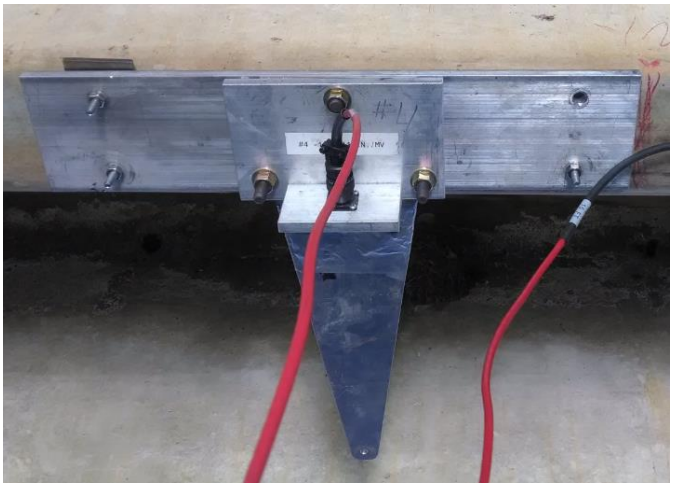

Figure 2.15 Deflectometer installed on girder

2.4.4 STS Wi-Fi System

The STS Wi-Fi System is a wireless system that uses a Wi-Fi router to communicate to the nodes. The nodes are data acquisition (DAQ) hardware instruments that are connected to the different types of instruments used for testing (deflectometers, tiltmeters, twangers, lvtds, etc.) via short cables. During testing the nodes will collect the data from the instruments via cable and send it wirelessly to the base station. The base station can be connected to a computer wirelessly or by cable. The computer has software to record test data in which the test data can be seen during and after testing. All the instruments with their respective labels are displayed in the computer software. Labels are assigned automatically by the STS system based on pre-installed calibration files and the BDI intelliduceder plugs to avoid errors, the labels correspond exactly to the instrumentation label unless manually changed.

Figure 2.16 shows the STS Wi-Fi base station and Figure 2.17 shows a node connected to the strain transducers. During testing, the node sends the data wirelessly to the STS base station which can be seen in the display of a computer and stored for further use.

Figure 2.16 STS Wi-Fi Base Station

Figure 2.17 STS node connected to strain transducers ST530

2.5 Test Load

The load used for the static live load test was a dump truck with two axles. The front axle was 7.08 ft (2.16m) apart and back axle was 6.53 ft (1.99 m) apart. The front wheels were 16.50 ft (5.03m) to the first set of back wheels. The back wheels were 4.58 ft (1.40m) spaced out. Figure 2.18 shows the plan view dimensions of the test truck. The front axle weight was 18.2 kips (80.95 KN) and the back axle weight was 43.46 kips (193.3 KN). The truck had a total load of 61.7 Kips (274.25 KN). Figure 2.19 illustrates the test truck axle weight distribution. Note that the bridge was posted for 8,000 lbs. (35.58 KN) which is 13% of the test load. Usually over conservative load posting are not based on load testing, and motivated by engineering judgment from visual inspections.

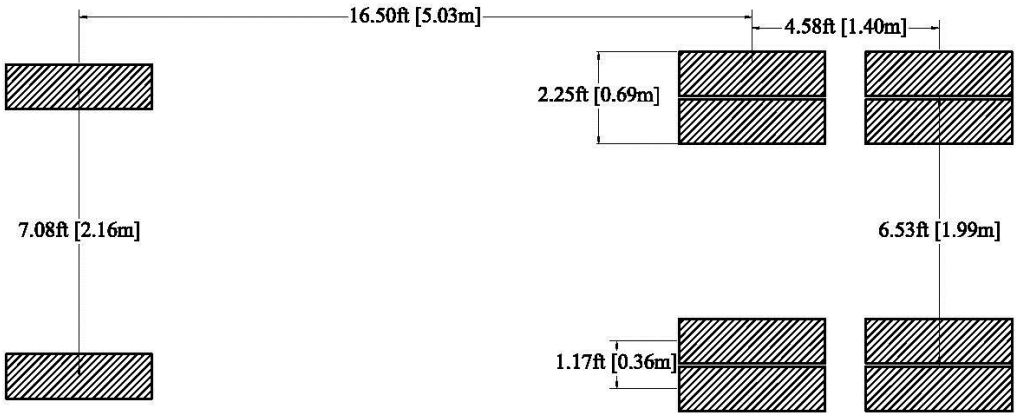

Figure 2.18 Test truck dimensions

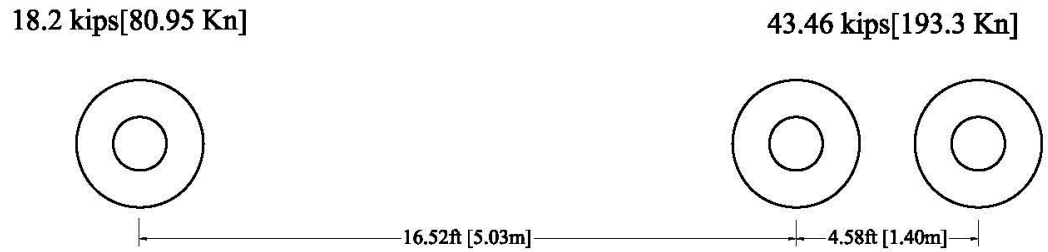

Figure 2.19 Test truck axle weight distribution

2.6 Load Cases

For the static live load test, different load cases were considered to gather the desired data: strain, deflection and rotation for each load case. The load cases were selected so that the acquired data provides important information that can be used to analyze the live load carrying capacity and the bridge behavior under different loading scenarios. For this purposes, it was necessary to drive the test truck at different positions transversely along the bridge.

In **Error! Reference source not found.** are the different load cases used for esting. Four different load cases were considered for static testing. Load Case A (LC-A) starts 2 ft (0.61 m) from the outer edge of the south girder (Girder 2). This position is 2 ft (0.61 m) from the outer edge of the girder according to the AASHTO specification for calculating exterior live load distribution factors

LC-A represents the most vulnerable case for load distribution. On this case the truck is positioned as closest to the edge as possible and the load can only be distributed in one direction. Furthermore, LC-A provides special insightful information about the load transfer between S1-S2 and S3-S4 when the load is close to the exterior girder S1. Besides, LC-B is located in between the stems S2 and S3 and also provides information to analyze the load transfer particularly between S1-S2 and S3-S4. LC-C is important in the sense that is driven just over the connections between all girders. LC-D is the load case that provides more information about load distribution from S6 and S5 to the others girders.

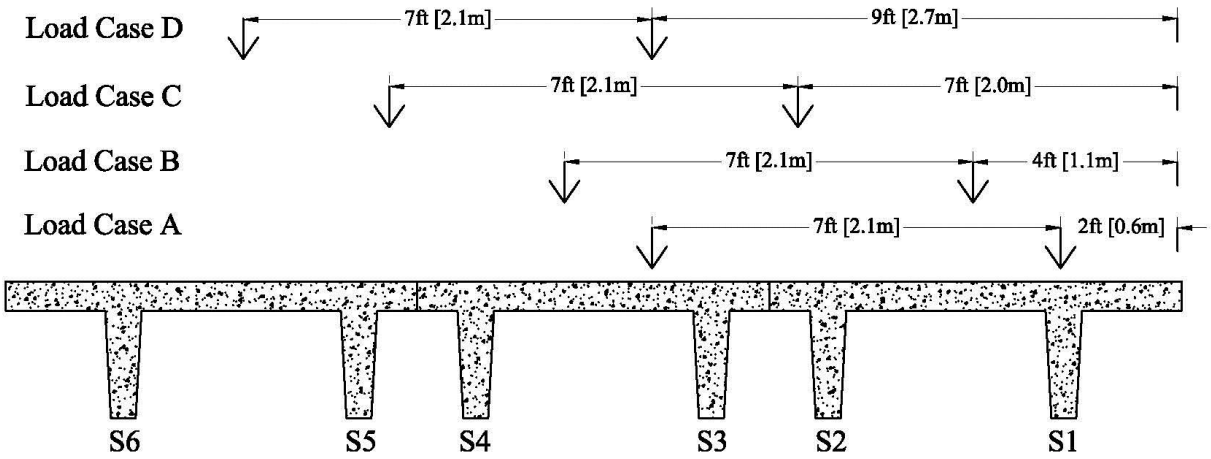

Figure 2.20 Static live load cases

2.7 Test Results

2.7.1 Data Processing

The test results were recorded by the data acquisition software into text files corresponding to the live load tests. The test file contains all the instruments used during the static test and their respective measurements, as a function of time. The data was recorded in the time domain. In order to analyze the data it is necessary to convert the

data from the time domain to the position domain. While testing, “clicks” where taken to specify the time where a particular front tire position had been approached. Click indications were performed on the data at the starting time of the test (i.e. when the first tire stood on the bridge), 0.25L, 0.5L, 0.75L, L and when the last wheel excited the bridge. The purpose of using the clicks is to create intervals of time with known positions, so that the data can be converted to the position domain. This is done by assuming a constant velocity and therefore a linear relationship between time and distance. Even though the truck is driven at a significantly low speed (i.e. crawl speed), it does not mean that the truck is driven perfectly at a constant speed at all times throughout the test duration, which introduces error in the time domain. However, if the total length is divided into stations where indications (“clicks”) are made in the data; then a linear relationship between these intermediate locations is a more accurate assumption for converting the data to the position domain. The position domain will contain all the data from when the first wheel stood on the bridge until the last wheel got off the bridge. Therefore, the influence lines will have a total distance of the bridge span plus the truck length. The position refers to the front truck tire.

Once the data was converted from the time domain to the position domain, further data processing was necessary before using the data. The instruments will typically have an initial measurement before the bridge was loaded and this should be subtracted out of the data this process is referred as “zeroing”. The first data point in the data will be subtracted from each measurement, making the first point zero and the last one zero, assuming there was no thermal drift. Thermal drift is a phenomenon that happens when using electrical resistance transducers due to the thermal expansion of the resistor,

thermal effects of the surroundings and the thermal expansion of the system (in this case the bridge)are being measured as well. This often shows up as drifting, up or down of various sensors. The data that starts at zero will finish above or below the x axis. To correct for the thermal drift, the last data point of each sensor will be corrected linearly among all the data points of each sensor. Before correcting for thermal drift, the data were also plotted to see if mayor drifts occurred to the data. In such case, the drift could not be attributed only to thermal drift but to nonlinear effects due to overloading with the test truck or any previous nonlinear deformation from previous loading. The data did not exhibit any mayor drifts, but only minor drifts so thermal drift was a safe assumption according to standard bridge testing practice. The procedures described above, after the data were converted to the position domain, were executed by programmed routines. The codes automated the process to ensure proficiency, ease and uniformity when processing the data. The codes were tested several times and were proofed to work as expected by plotting all the test results and observing the expected data. Figure 2.21 depicts the process of using the raw recorded data, which have an initial reading, zeroing the initial reading and linearizing the thermal drift.

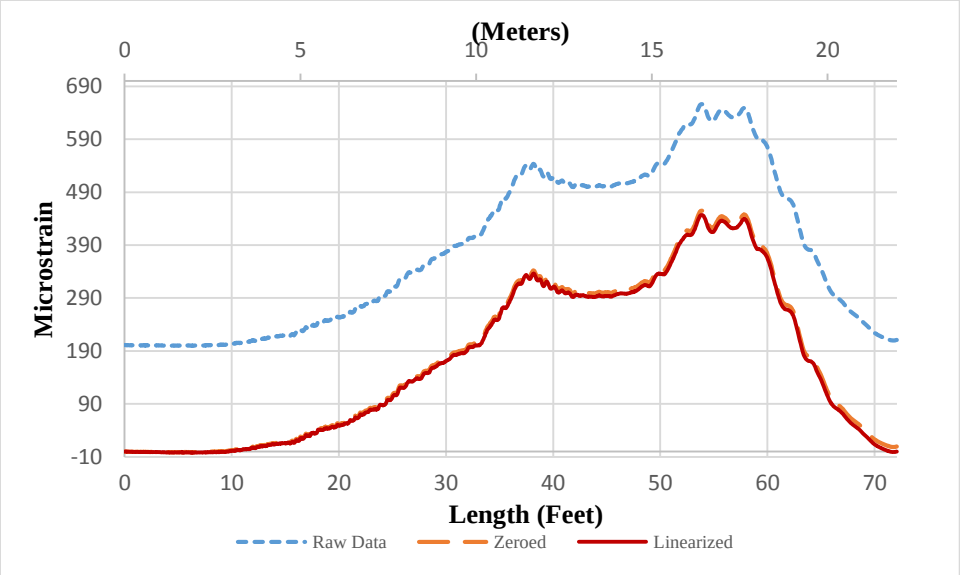

Figure 2.21 Plot of initial reading, zeroed and linearized data

2.7.2 Strain Results

The strain results indicated what is expected from a linear elastic system under static live load conditions at mid span and quarter span. Figure 2.22 shows the data corresponding to LC-A for the gages at midspan. On the x axis is the truck front tire position and on the y axis is the strain recorded in microstrains ($\mu\epsilon$). The x axis is the sum of the bridge span plus the truck length 72.08 ft. (21.97 m). Figure 2.22 has the maximum value of strain at S1 which was the closest stem to LC-A and besides is an exterior stem. Exterior girders are forced to carry more load when the load is closer to the edge of the corresponding girder due to the nature of the load path. S3 is the second largest value being a gage close to the load and interior stem, the result is as anticipated.

Another important observation is how different in magnitude are the different sensors across the bridge. S1 and S3 carry 29.4% and 20.8% of the total load respectively, whereas S6 is carrying 2.5% of the total load. This is significant because the bridge is only 20.14 ft. (6.14 m.) wide and the truck is 7 ft. (2.18 m.) wide. This shows

that the bridge has relatively low live load transfer in the transverse direction. Hence, the double tees are working more as an individual girder system than as a bridge; this is a consequence of deteriorated girder connections and deck wearing surface deterioration.

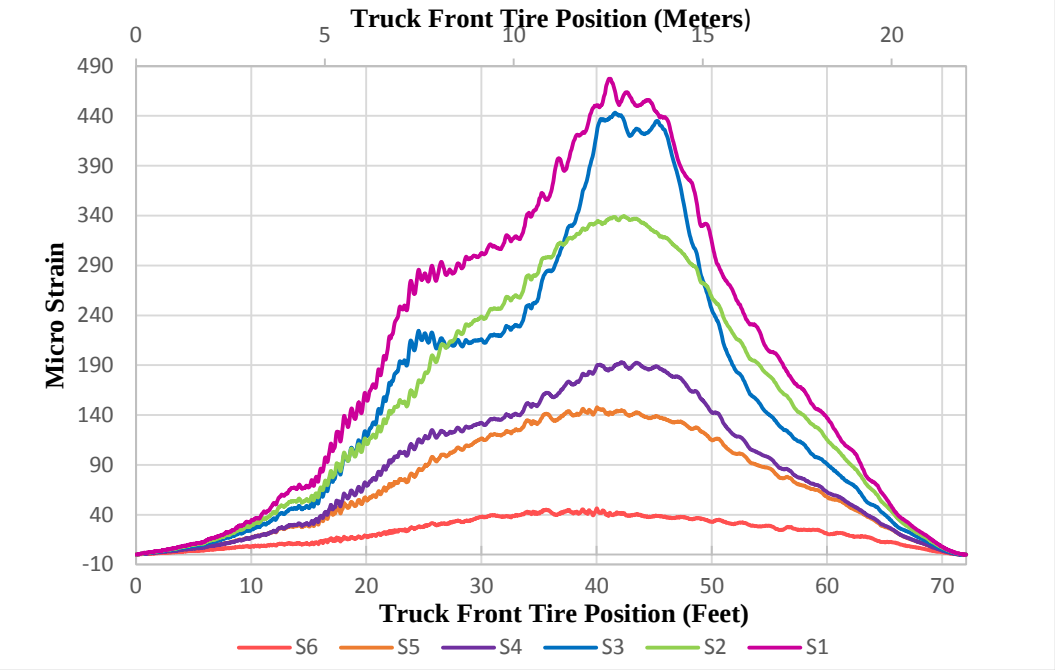

Figure 2.22 LC-A strain transducers results from midspan

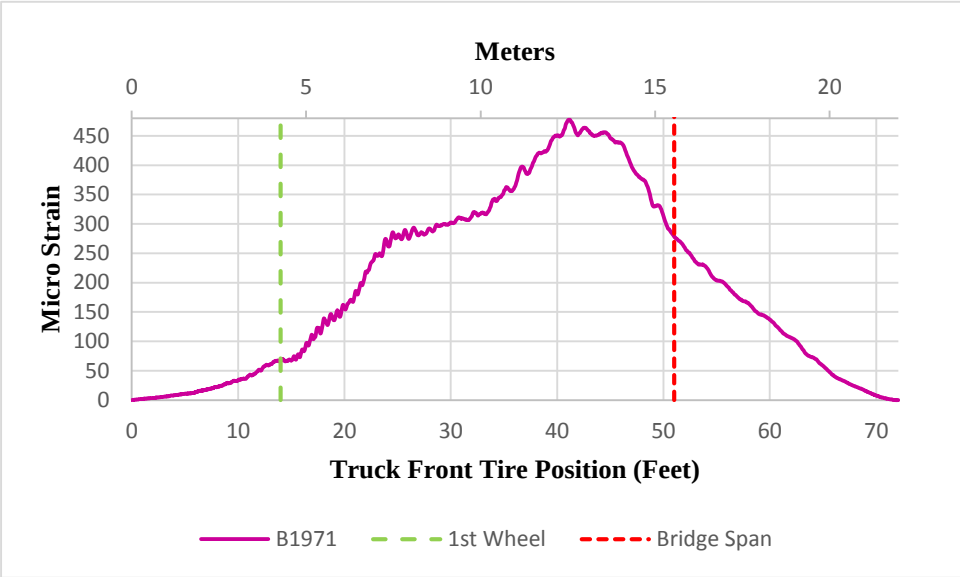

Figure 2.23 Strain from gage B1971 (S1) with 1st wheel at first peak

Error! Reference source not found. indicates the position of the first axle were he first peak was reached.

At that location the only load on the bridge was the first axle. The strain starts from zero and increases to a peak where it slightly levels out. When the second wheel from the back axle starts to load the bridge, the strain increases to a new peak. This new peak represents the location were the first and second wheel achieve their maximum value before the third axle starts loading the bridge. This is shown in Figure 2.24.The figure also shows the distance from the first wheel to the second. At this point the truck load has reached the maximum deformation before the third wheel of the back axle starts adding to the flexural deformation of the structure. When the third wheel gets on the surface, the load starts to increase until all the load is applied to the bridge and the truck moves to the point that causes the maximum deformation.

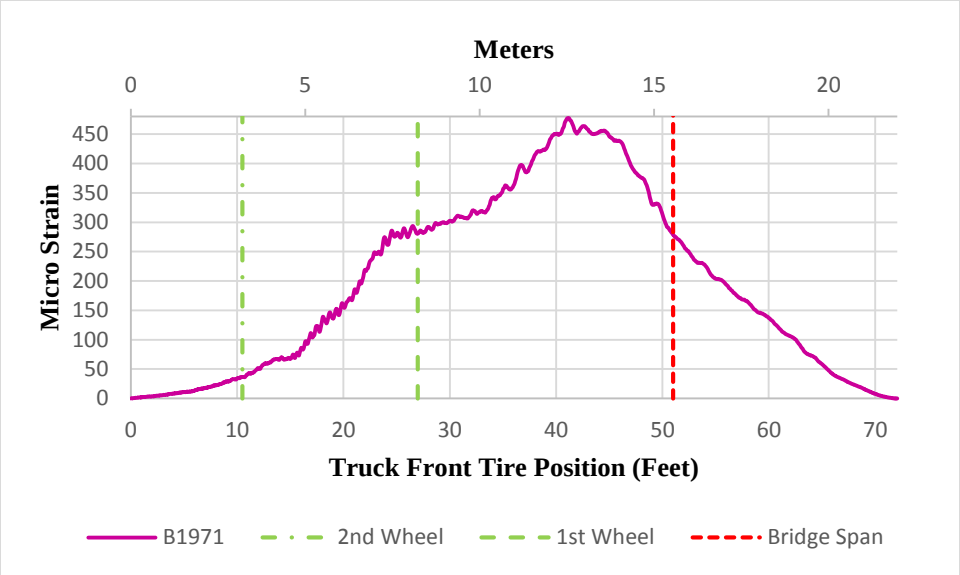

Figure 2.24 Strain from gage B1971 (S1) with 1st wheel at first peak.

Figure 2.25 shows the test truck first wheel positioned at the maximum strain for the test.

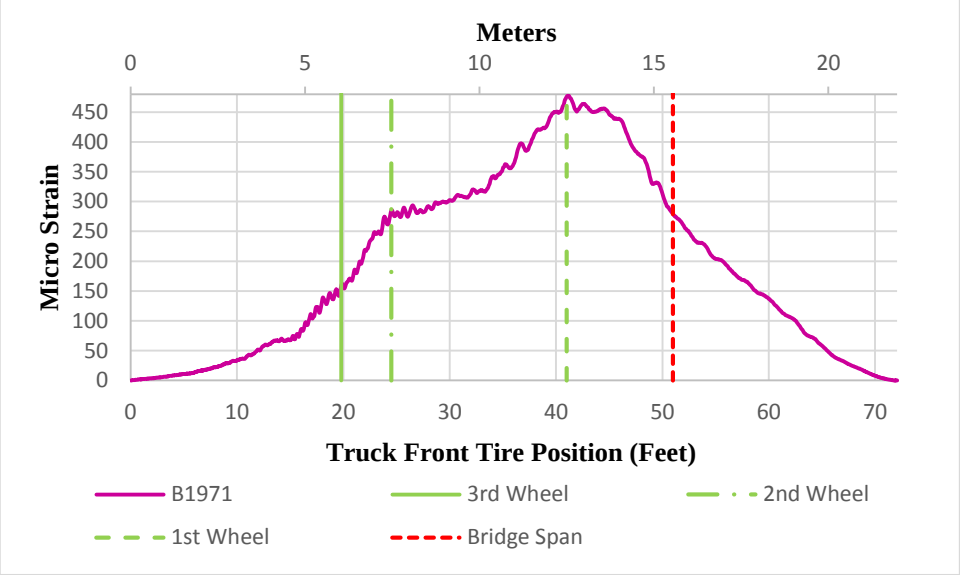

Figure 2.25 Strain from gage B1971 (S1) with 1st wheel at third peak.

Table 2.1 contains the measured strains at mid span and Table 2.2 contains the measured strains at quarter span. At midspan, LC-A yields the maximum response in comparison to the others tests. This result was anticipated due to the nature of the load location. When girder bridges are loaded on the exterior girder the exterior girder is forced to carry more load because is only able to distribute load to one side. Even though LC-D is not all the way at an exterior girder, the loading should be superior to the one on LC-C. Strains at quarter span are less than at midspan. However, an important observation can be made about the quarter span strains maximums compared to the mid span strains maximums. The order of maximum stem strains is not the same for quarter span maximum than for midspan. And the maximum strain occurs at different stems at quarter span than at midspan. The maximum value at quarter span occurs at LC-D, which was the smallest value at midspan. The second largest value is LC-A, which was the maximum value of midspan. The descending order at midspan for the respective LC-A, B, C and D was: 1,3,2,4. Whereas for quarter span was: 2,4,3,1. This information is relevant because it provides measured data of how the bridge lateral distribution of live load changed as the truck was driving over the same load path along the bridge. This is something that can only be shown by testing since a theoretical approach only considers a uniform transverse load distribution. Transverse load distribution of girders is an important property of a bridge for condition assessment that can only be quantify and taken into account by load testing.

Figure 2.26 results from a simply supported beam with the same longitude and load used on the test. The unit influence is used to obtain the axle influence line by timing

the influence by the weight of the axle. The individual influences are offset according to the distance in which they start acting on the bridge (i.e. truck configuration). The total influence line is obtained by superimposing the individual influence lines corresponding to the axles and spacing them according to the truck configuration. Note that the figure y axis is moment; this figure is meant to only exemplify the use of superposition to obtain a total influence line.

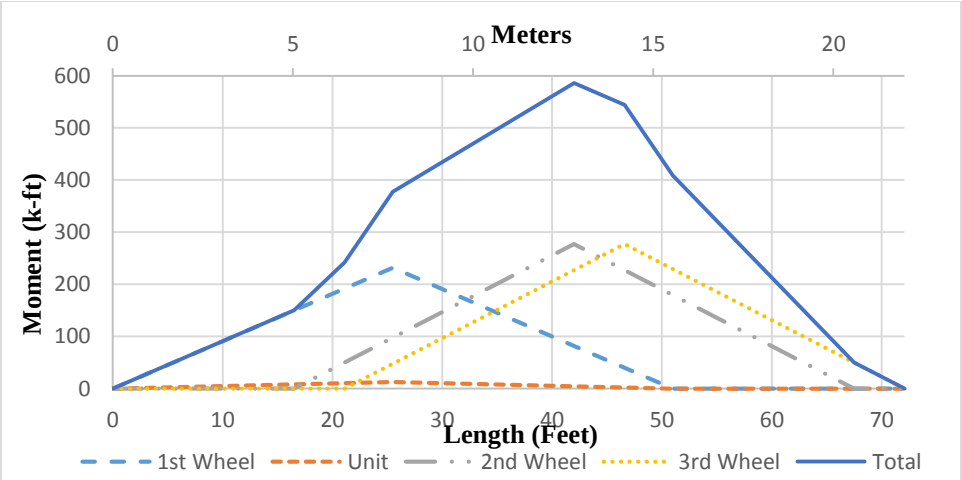

Figure 2.26 Superposition of influence lines for a simple supported beam

LC	Mid-Span Max ($\mu\varepsilon$)	L/2 Order	Max Strain Stem
A	479.37	1	S1
B	406.39	3	S3
C	417.83	2	S3
D	364.86	4	S5

Table 2.1 Midspan maximum strains

LC	Quarter-Span Max ($\mu\varepsilon$)	L/4 Order	Max Strain Stem
A	301.196	2	S1
B	228.50	4	S1
C	297.27	3	S2
D	354.43	1	S3

Table 2.2 Quarter span maximum strains

The cross-section at 2H was selected to be twice the distance away from a discontinuity region. According to St. Venant's principle, members behave linearly elastic throughout the member a distance H (greater cross-sectional dimension) away from discontinuities. These discontinuities induce strains from load and cross section changes at a distance H from the discontinuity. The regions in a beam are B regions, were beam theory applies, and D-regions, were discontinuities induce nonlinear behavior (Nilson).

Discontinuities are changes in geometry of cross-sections that produce high stresses. Stress concentrations appear at the point of loading, when a load acts over a small area it produces high stresses in the area near the point of application. St. Venant's principle is an observation from theoretical and practical experience. Near the source (loading or change on geometry) the stresses will depend on the load and the cross-section shape of the member (Gere).

Figure 2.27 shows the beam line strains at 2H for top, middle and bottom gages for LC-A. As it can be seen, the gages do not manifest a linear behavior since the gages do no plot in a linear order. This linear order will always plot the middle gage in between top and bottom, for either compression (top straining positive) or tension (top straining negative). Due to stress concentrations at a discontinuity region (the abutments) and the high load from the reactions, nonlinear stresses are measured according to St. Venant's principle. H should have been considered to be the width of the double tees instead of the depth, which is the longest dimension in the cross section. This way the 2H rule of thumb for St. Venant's principle would have positioned the sensors in a B region. Due to this inconvenient the 2H strains from test were not used for further analysis.

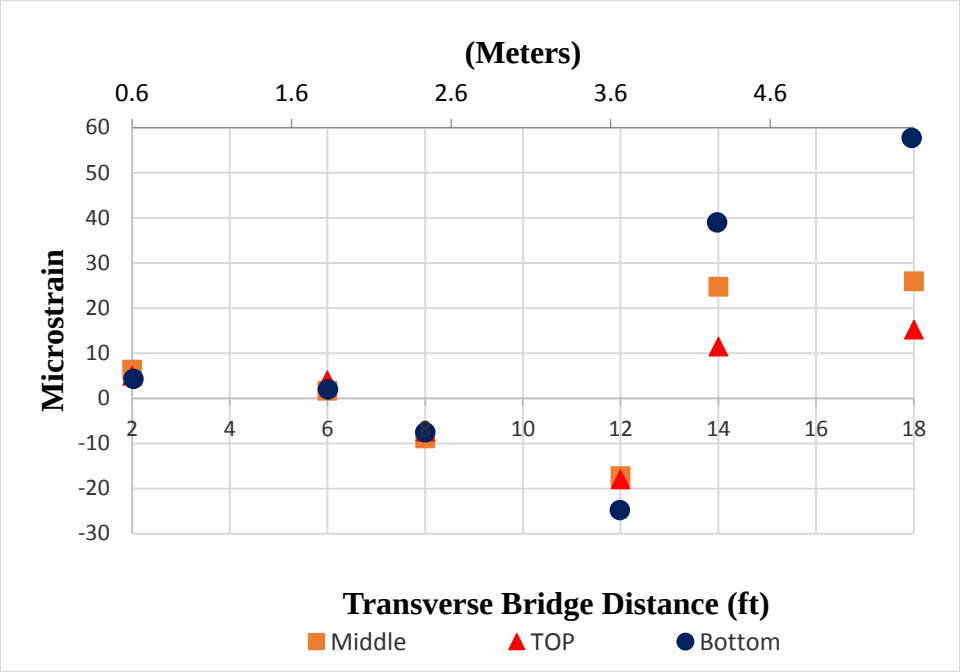

Figure 2.27 Section 2H for LC-A beam line strains top, middle and bottom

2.7.3 Deflection Results

The deflection results were measured at midspan; initially six twangers were used for the test. However, after testing and plotting all the data, it was realized that three twangers were measuring a constant value. After the test the twangers were functioning, therefore it was determined that not all the twangers were installed properly. Table 2.3 shows the deflection values that correspond to the position of maximum strain at midspan. The maximum deflection was recorded from Twang-01 which was the closest to the load path in LC-A.

Table 2.3 Deflection (In) at midspan at the position of maximum strain

Deflectometer	LC-A	LC-B	LC-C	LC-D
TWANG-04	0.265	0.341	0.418	0.415
TWANG-03	0.545	0.585	0.594	0.443
TWANG-01	0.789	0.661	0.437	0.214

By observing the others load paths and the corresponding results, one can comment that the deflections increase as the load path is close to the instrument. This is constant for most of the test measurements. However, on LC-C the load from LC-D should have caused a bigger deflection than the load from LC-C for twanger at S3. This is important because it shows the effect of the damaged girder connections, end conditions at the abutments, and possibly the changes in cross section (potholes) on the service of the bridge.

From mechanics of materials, deflection is related to curvature by the basic differential equation of an elastic beam (Equation 1), also known as the moment curvature equation. The equation is derived from the constitutive relationships between strain (ϵ) and rotation (θ) of an infinitesimal stress block from a simply supported beam with radius of curvature ρ and curvature κ. Moment is one the variables contained in this equation. Recall that moment is a function of loading and length (Equation 2). Since the loading and span length is the same for all tests, deflections should be proportional to the closeness of the load according if assuming constant flexural rigidity (EI) across the entire bridge.

$$\kappa = \frac{\varepsilon}{c} = \frac{d^2y}{dx^2} = \frac{M}{EI} \quad (1)$$

$$w(x) = \frac{dV}{dx} = \frac{d^2M}{dx^2} \quad (2)$$

However, this is not true in reality, but if the bridge is in good conditions one can assume that a constant flexural rigidity is a reasonable assumption. This is not the case for Icy Springs Bridge. The connections are damaged to an extent that the transverse load distribution is not constant along the bridge and the cross section changes due to the damaged structural deck (potholes on the structural deck with no pavement). Hence, the flexure rigidity changes along the bridge when truck travels on the same path corresponding to a test. Even though the bridge behaves in the linear region which is displayed by the test data showing no permanent deformation, the bridge may have minor nonlinear behavior induced from local effects. These nonlinear effects are caused by the change of flexural rigidity at a local level in the structure. Since in theory the moment curvature equation is derived from Hooke's law (as shown below), it is important to know that when measuring a damaged structure local effects can influence the linear behavior of the structure by induced nonlinear change of flexural rigidity. This applies to all measurements since they are related by differentiation.

$$\sigma = E \cdot \varepsilon; \quad \frac{\varepsilon}{c} = \frac{\sigma}{E \cdot c} = \frac{M \cdot y}{E \cdot I \cdot c} \quad for \ y = c \quad \frac{\varepsilon}{c} = \frac{M}{E \cdot I} \quad (3)$$

Figure 2.28 shows a plot corresponding to LC-C for deflectometers. The plot shows the measurement of deflection as the truck moved along the bridge. On the y axis deflection is plotted and on the x axis distance corresponding to the first wheel of the truck is plotted.

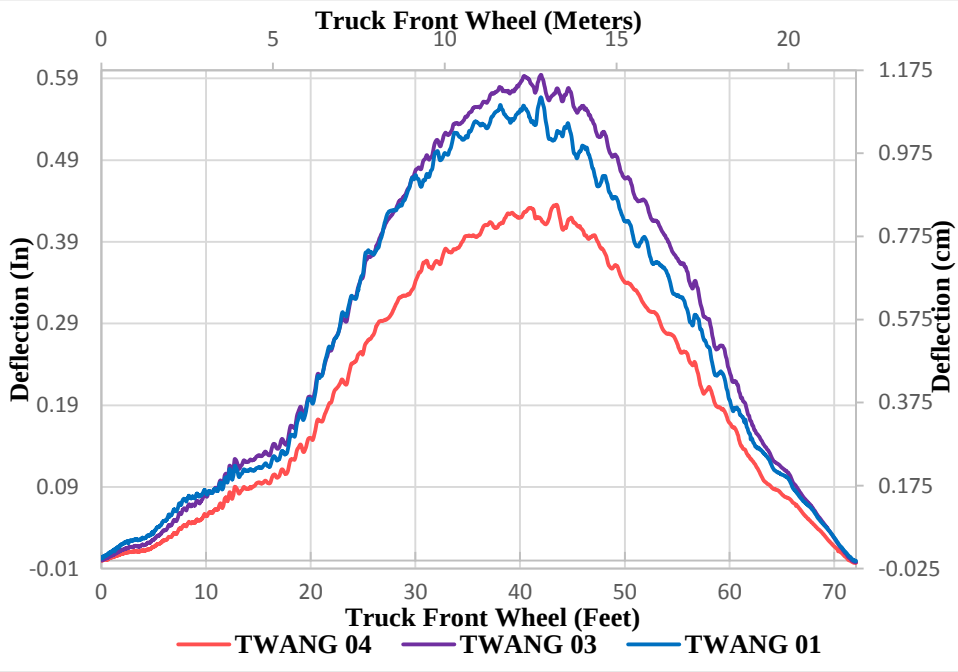

Figure 2.28 Deflectometers (Twangers) influence lines corresponding to LC-C

2.7.4 Rotation Results

Two tiltmeters were installed 1ft (30.48 cm) from the abutments to measure the rotation of the stems at the abutments. These types of abutments were cast in place of a semi integral abutment, in which the ends of the girders were cast into the abutment. The abutment behaves between the ideal end conditions of a pinned-pinned and fixed-fixed

simple span beam. The pinned-pinned will produce the maximum value of rotation and the ideal fixed-fixed will have zero rotation.

For further analysis this rotations will help to calibrate a finite element model and validate that the ends conditions or boundaries conditions to represent restraint of the actual structure. Figure 2.29 plots the influence lines from rotations measurements collected from LC-C. Recalling that the bridge was loaded from the instrumented side to the instrumented side, it can be observed that the rate of change of rotation increases as the load approaches the instrumented side of the abutment. The rate of rotation decreases as the load is moving from the point of maximum deflection to the abutment, of the instrumented side, as the bridge is getting unloaded.

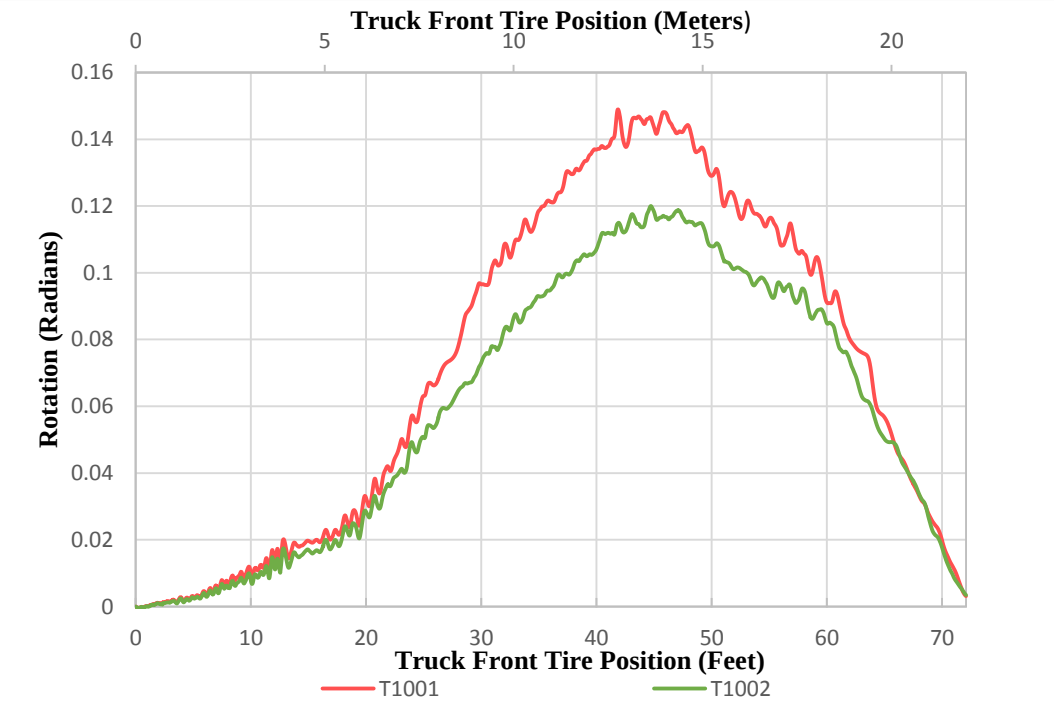

Figure 2.29 Rotation influence lines from LC-C.

Table 2.4 is a summary of the rotations recorded in radians for the different static load cases. The table contains the rotation measurements at the same position where the

maximum strain for the load cases was recorded. The tiltmeters shows agreement with the load cases. T1001 was installed on the stem S5 and T1002 was installed on the stem S2. The rotation increases as the load is close to the girder. For LC-A and B the greater value is at T1001 which is closer to the load and for LC-D the same happens with T1002. LC-C is special since the load case is symmetrical about the centerline of the bridge and so are the location of the tiltmeters. Accordingly to this remark in a perfect bridge the rotations should be about the same. However, the measurements for this test show that they are different. This is due to the different boundaries conditions at the abutments and along the connections of the girders.

Table 2.4 Rotation measurements in radians at the position for maximum strain

Tiltmeter	LC-A	LC-B	LC-C	LC-D
T1001	0.154	0.152	0.147	0.082
T1002	0.068	0.085	0.115	0.118

2.7.5 Live Load Transverse Distribution

For girder bridges one of the most important factors for design, analysis and decision making is the girder distribution factor (GDF). In a two-dimensional beam, a single beam will take all the deformation for any given load. For a three-dimensional structure, the load is distributed transversely. In order to easily describe the ability of a bridge to distribute load transversely a girder distribution factor is used. The experimental GDF represents the true ability of the bridge to distribute load transversely, this is an important measurement that can only be obtained from testing. Experimental GDF may be used in design if enough load cases are considered or a FEM can be calibrated to produce worst case scenarios.

Kim and Nowak (1997) commented on how girder distributions factors are calculated from maximum strain at each test from the same section on the bridge. Equation 4 presents the definition of an experimental GDF: the maximum strain at a section is divided by the sum of all the strains at the section.

$$GDF_i = \frac{M_i}{\sum_{j=1}^{k} M_j} = \frac{ES_i\varepsilon_i}{\sum_{j=1}^{k} ES_j\varepsilon_j} \quad (4)$$

$$GDF_i = \frac{\varepsilon_i}{\sum_{j=1}^{k} \varepsilon_j} \quad (5)$$

Where

- M= Moment
- E= Modulus of Elasticity
- S= Section Modulus
- $\varepsilon =$ Strain
- $i =$ Stem at which maximum response occurs
- $j =$ Particular stem
- $k =$Total number of stem

Equation 5 assumes a constant section modulus for each girder to not account for a weighted section modulus. This is the way girder distribution was calculated for the project, which is standard practice.

Table 2.5 contains all the strains used to calculate the experimental girder distribution factors for the static live load cases. Bolded values indicate the maximum strain observed in a stem for that LC. This strain corresponds to the location at which the load caused the most strain for a given load case. At the same position, the other gages will report their results and a GDF can be computed from the experiment. LC-A has the

larger distribution factor from the test. Since LC-A is the extreme load on an exterior girder, the exterior girder will deform more since it is only able to distribute load to one side of the bridge. In theory this is an external girder distribution factor and as explained previously it controls when compared to the internal distributions factors. LC-C is the second test of largest magnitude. Even though this test is standing at the center of the bridge, very close to the connections to the center girder, the maximum strains for this load case are recorded at S2 and S3. This is evidence that the north girder (girder 3) is the most rigid of the three girders. Observe that for LC-A, B and C the sum of the strains averages 1645 microstrain and for LC-D the summation is 1465 microstrain. This also validates that the northern girder (Girder 3) is stiffer that the other girders. In a perfect bridge the strains at the cross section will add to be the same for any load path. However, this data shows that in the real structure, girders may have different stiffness due to girder material properties, damage, connections and boundaries condition.

Table 2.5 Experimental GDF and strains used for calculation

Strain Gage	**Micro Strains at midspan max effect**			
	LC-A	**LC-B**	**LC-C**	**LC-D**
B1976 (S6)	41.15	76.30	137.67	293.78
B1975 (S5)	142.73	198.66	276.33	**364.86**
B1974 (S4)	186.75	285.07	302.62	280.24
B1973 (S3)	439.76	**406.39**	**417.83**	302.32
B1972 (S2)	339.12	353.96	320.88	143.14
B1971(S1)	**479.37**	349.55	181.61	80.32
Σ	1628.87	1669.94	1636.95	1464.66
Experimental GDF	**0.294**	**0.243**	**0.255**	**0.249**

Figure 2.30 plots the data from Table 2.5. The plot illustrates the previously discussion regarding load transfer in the transverse direction of the bridge. On the y axis are the microstrain used to compute girder distribution factors and on the x axis is the transverse distance of the bridge, starting from the south to the north (i.e. from S1 to S6).

Note that on a bridge with good structural conditions pertaining to transverse load transfer, the plot should look symmetrically about the centroid as the truck load case is moved transversely. Even though the load cases are not symmetrically it can be said that in the case of symmetrical load cases that the Icy Springs Bridge is far from showing acceptable transverse load transfer. Figure 2.31 shows the same plot but for quarter span. When compared to *Figure 2.30* the shapes are different showing evidence of the change of transverse load transfer longitudinally. Even though the magnitude has to be smaller as it is, the shapes from midspan and quarter span will have more similar shapes if the bridge will show a more constant transverse load distribution longitudinally.

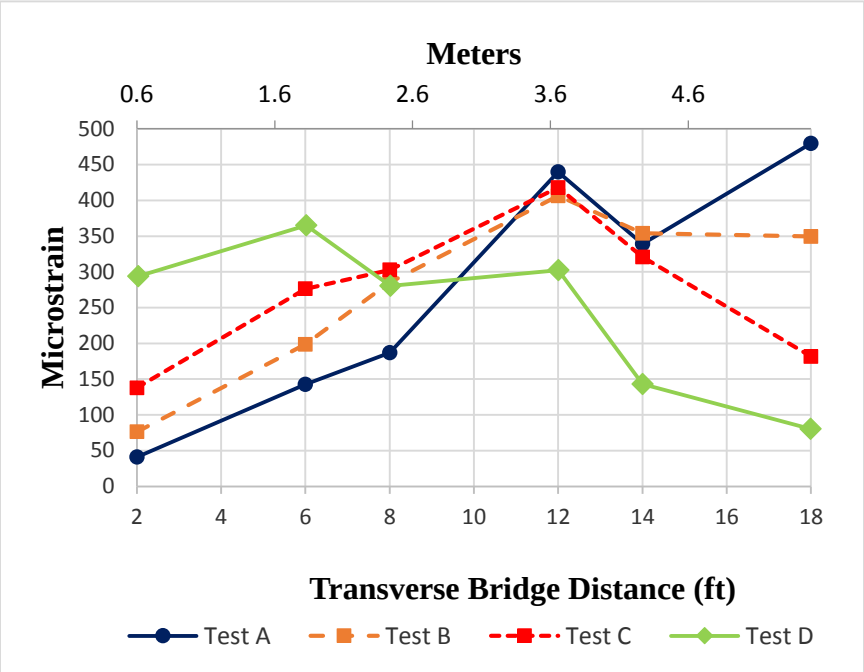

Figure 2.30 Midspan transverse load distribution

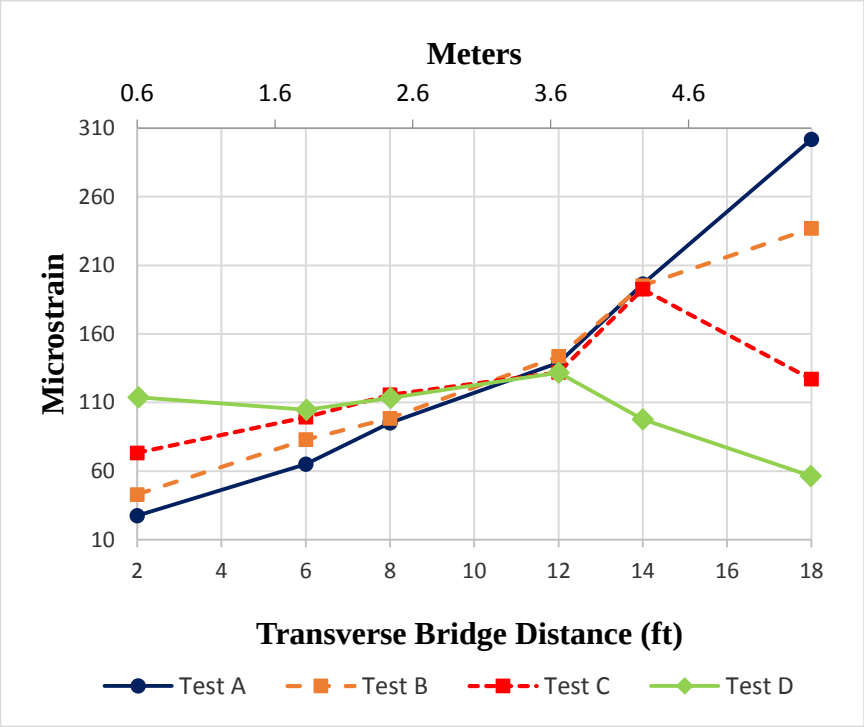

Figure 2.31 Quarter span transverse load distribution

CHAPTER 3. FINITE ELEMENT MODELING

3.1 FE Model Description

The finite element model (FEM) was developed using the finite element structural analysis software SAP 2000. The FEM had 7456 shells, 96 tendon objects (discretized by SAP into more objects), and 6646 joints. The model was created using shell elements for the stems and the deck. The shell elements used by SAP2000 are a six degrees of freedom per node triangular and quadrilateral flat shell described by Ibrahimbegovic and Wilson (1991). Shell elements are suitable for modeling deck and girder behavior of bridges (Bapat, 2009). The shells on the stems had variable thickness shells that varied with the cross section according to the measurements of the variable cross section of the stem. The shell elements were three or four nodes elements. Shell elements combine membrane and plate behavior (Computers and Structures Inc., 2013).

The flanges were separated at a distance of 0.5in (1.27cm), and connected with "link" elements at each node that have stiffness in the vertical translational direction only (i.e. shear stiffness). This type of link element is considered to be "two joint links" in SAP2000. The reason behind the link elements, longitudinally along the deck, is to model the degraded shear transfer from girder to girder. It was observed during the collection of the experimental data that the deck had deteriorated transverse load transfer connections, and in some cases no connection existed at all. This spring stiffness reflects an average of shear stiffness along the joint. In the real structure there were potential locations were significant shear was transferred, and were little or none was transferred.

After analyzing the collected data, it was observed that the bridge had significant local problems corresponding to the girders transverse load transfer (see results section 2.7.5). In addition, the pavement surface which would provide significant load transfer was worn or missing and therefore provided highly variable transfer between girders.

The support conditions were modeled with one joint links. The links had stiffness in the longitudinal and transverse direction. In the vertical direction the springs were fixed. The model was not sensitive to fixity in the transverse direction. The longitudinal degrees of freedom were the ones uses for calibrating the model; rotational degrees of freedom were free to rotate without restraints.

Figure 3.1 displays the finite element 3D view of the Icy Springs Bridge FEM model. Note the trapezoidal pattern at the stems (see Figure 3.2).

Figure 3.2 shows the cross section of the FEM. In this figure the longitudinal link connections can be seen in-between the girders. The FEM was also divided into different section properties for calibration purposes. The model was divided into three deck properties (one per double tee) and six stem properties. Each stem had two springs at each end to model the boundary conditions. The two link couple at a single stem end shared the same properties, to model the end restraint conditions for calibration. Therefore, 24 links were used to model 12 stem end support conditions.

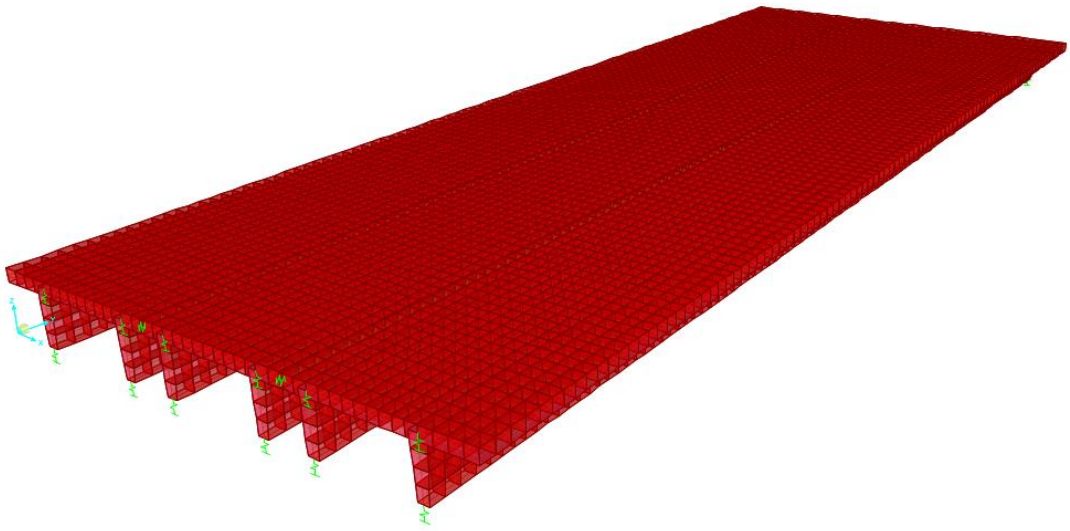

Figure 3.1 Finite element model extruded view

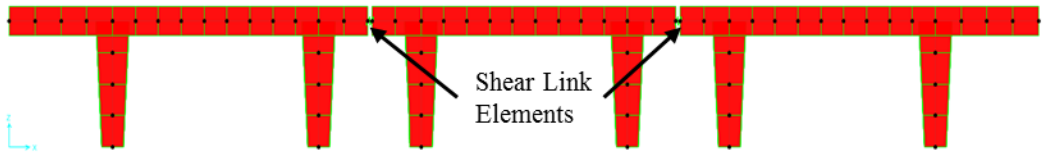

Figure 3.2 Finite Element Cross-Section, shell joint pattern at stems

Figure 3.3 demonstrates the use of springs at the abutments. The springs were fixed in the vertical translational direction and had stiffness along the longitudinal translation degree of freedom. The springs also had stiffness in the transverse direction; however, the model was insensitive to this during calibration.

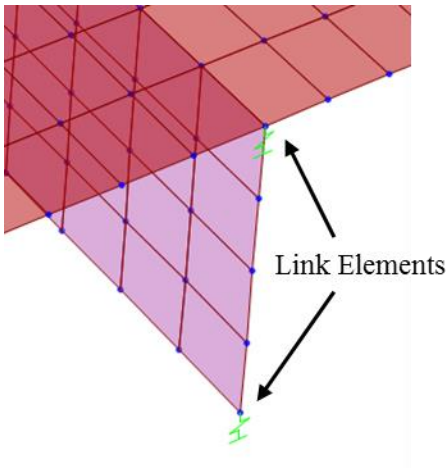

Figure 3.3 Abutment with springs for end restraint modeling.

Figure 3.4 represents the configuration of link elements used for calibration. The link couples used for the modeling the end restraint were the ones labeled S1 through S12. Note that the link configuration of Figure 3.3 is the one corresponding to S1; therefore each S property uses two link elements, one at the bottom and one at the top of the girder. In addition, the longitudinal link elements were the ones used to model the transverse load transfer, these are the ones label DS1 through DS4. Effectively there were four zones trying to capture the variable load transfer. Significant difference was noticed on the bridge deck wearing surface from the east to west end, thus the four different sets of limits. Note that DS4 and DS3 go from the instrumented abutments to one third of the span. As this is where a significant change in asphalt quality was visible (see Figure 2.6). And DS1 and DS2 occupy the rest of the length of the model.

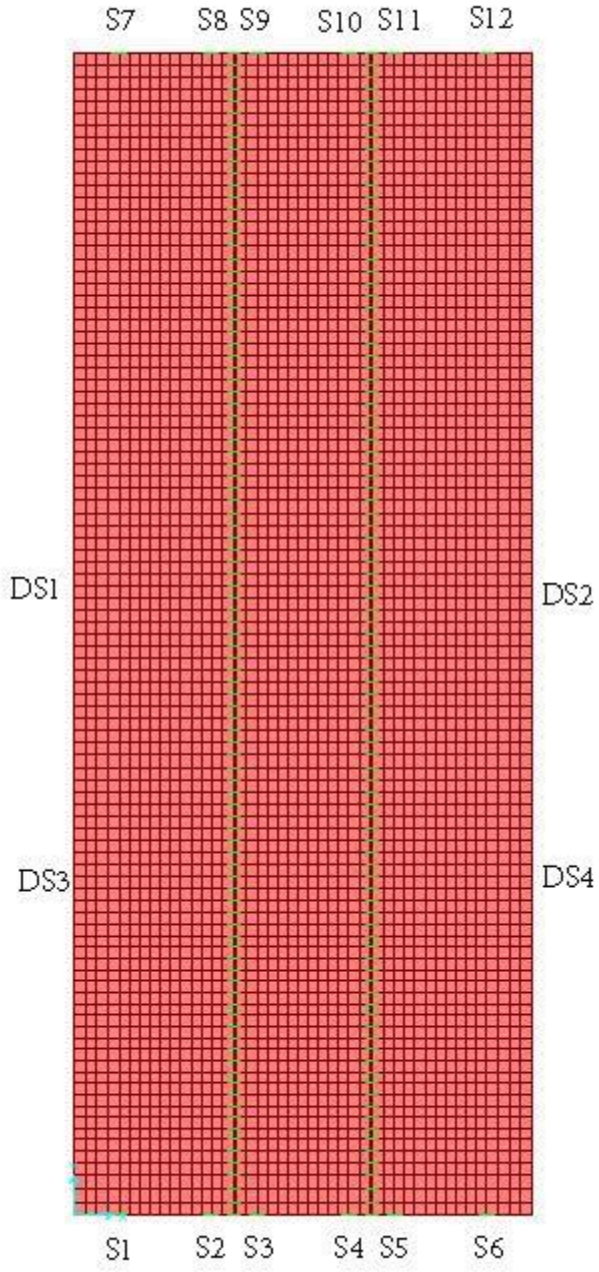

Figure 3.4 Link elements configuration for calibration.

The sensitivity of the shell meshing was studied to compare the accuracy of the model when meshed in different dimensions. The model used approximately 6 in (15.24 cm) shell elements. The geometry of the shells used angles of 90 degrees. The aspect ratio of the shells is approximately one in all instances, when comparing width and length. The aspect ratio is significantly less than four, the maximum aspect ratio recommended by the developers of SAP2000 (Computers and Structures Inc., 2013). Furthermore non-rigid connections are modeled by releasing and restraining the adequate translational and rotational degrees of freedom and incorporating respective stiffness.

3.2 FEM Calibration

In order to use the FEM to predict the measured behavior of the bridge, the FEM had to be calibrated to test Data. Once the FEM was calibrated, the model would constitute a calibrated version of the bridge that could be used for further rating, study and also as a validation for the modeling techniques used to describe bridge behavior. This calibrated model represents the approximate global behavior of the experimental structural response. The calibration of the model included the change in stiffness of the longitudinal springs along the deck and the springs at the support conditions. In addition, the modulus of elasticity of the deck and stems was changed. This is a valid approach since the end conditions showed on the experimental data to have different end conditions at the abutments and shear girder connections. This is common practice for calibration models (Goble, et al., 1992). There was extensive structural deck damage to account for deteriorated deck by changing the modulus of elasticity of each girder.

The process of model calibration is summarized as follows. From the

experimental data, the location where the maximum position occurred was obtained. At this very position, all the instrument responses were gathered. This was the static position and response to which the bridge was to be calibrated. On the finite element model a static load case was created for every single test load case. The respective load case will load the bridge at the maximum response position with the same load and geometry of the truck for a given test. Note that only live load is applied in the model. Other loads such as dead load and pre-stressing are not measured by the test and therefore are not included in the analysis for calibration. The responses of the FEM (at the location of the experimental instrument) was obtained from the model and compared with the experimental measurements. The comparison was made by using objective error functions, discussed in detail in a later section. These functions will account for the error and how optimal was the analyzed model. From this point, calibration is an iterative process that consists of changing the boundary conditions and material properties to optimize the model as quantified by the objective functions. Table 3.1 contains the final calibrated values for the FEM and the experimental values used for static calibration on each test.

Table 3.1 Experimental values and final calibrated FEM values for each test

	LC-A		LC-B		LC-C		LC-D	
Instrument	**EXP**	**FEM**	**EXP**	**FEM**	**EXP**	**FEM**	**EXP**	**FEM**
B1984	27.50	31.09	42.95	42.33	73.29	62.75	113.69	194.52
B1983	65.03	63.78	82.93	86.76	99.32	96.58	104.72	174.78
B1981	95.15	87.80	98.42	102.68	115.57	123.81	113.22	118.78
B1980	138.94	160.38	143.63	148.92	131.89	130.32	131.73	160.94
B1979	196.41	210.61	195.23	197.72	192.53	186.97	97.59	89.29
B1977	301.70	301.20	236.89	228.50	127.06	137.44	56.34	62.97
B1976	41.15	48.15	76.30	65.77	137.67	113.21	293.78	311.74
B1975	142.73	129.43	198.66	176.49	276.33	297.27	364.86	354.43
B1974	186.75	205.31	285.07	274.34	302.62	320.24	280.24	307.87
B1973	439.76	413.78	406.39	382.89	417.83	420.47	302.32	322.65
B1972	339.12	359.09	353.96	361.66	320.88	297.59	143.14	162.73
B1971	479.37	478.81	349.55	347.19	181.61	178.67	80.32	92.91
TWANG-04	0.27	0.31	0.34	0.38	0.42	0.45	0.41	0.45
TWANG-03	0.55	0.52	0.59	0.49	0.59	0.50	0.44	0.39
TWANG-01	0.79	0.69	0.66	0.50	0.44	0.26	0.21	0.13
T1001	0.15	0.17	0.15	0.16	0.15	0.14	0.08	0.07
T1002	0.07	0.05	0.08	0.07	0.11	0.09	0.12	0.12

3.3 Objective Error Functions

The objective error functions used to assess the calibration were the mean absolute error (MAE, see equation 6) and the mean absolute percent error (MAPE, see equation 7). These two objectives function were used to quantify the optimization of the model due to the different magnitudes in types of measurements being optimized. Rotations, deflections and strain measurements were of very distinct magnitudes and units. When using data in a wide range of magnitudes and units, it can be difficult to quantify the error in a meaningful way. If large magnitudes are considered, for example strain transducers in this test, the difference in the measured and the predicted value can be significantly large compared to the same difference of a sensor with smaller

$$MAE = \frac{1}{n}\sum_{i=1}^{n}|M_i - P_i| \tag{6}$$

magnitude, in our case the rotation measurements. In the first case, the difference may be larger, but the percent difference magnitude was small. In the case of MAE, if the data will contains large differences (i.e. strains) and very small differences (i.e. rotations), the average can exhibit relatively low error. This is the case of MAE.

$$MAPE = \frac{1}{n}\sum_{i=1}^{n}\frac{|M_i - P_i|}{|M_i|} \tag{7}$$

Where

- MAE = Mean absolute error
- MAPE= Mean absolute percent error
- M= Measured value from testing
- P= Predicted value from FEM
- n = number of instruments

When using MAPE with small values the difference can be a small number, but because it is divided by a small number it will be a greater error than if just taking the error to be the difference that MAE does. MAPE provides a straightforward error measurement, but provides poor information when using small values (Maguire, et al., 2015).

Another approach to quantify the optimization of the FEM was to use a comparison between the FEM and experimental values using linear regression with the sum of the least square residuals. Equation 8 show the linear regression fit where a_1 and a_0 are the slope and intercept of the line and ε is the error associated with the experimental values and the FEM prediction. Solving for ε and squaring gives the square of the residual, and for a number of values n gives the sum of the squares of the residuals, (see equation 9).

$$M = a_1 \cdot P + a_0 + \varepsilon \tag{8}$$

$$\sum_{i=1}^{n} \varepsilon^2 = \sum_{i=1}^{n} (M_i - a_1 \cdot P_i - a_0) \tag{9}$$

$$R^2 = \frac{\sum_{i=1}^{n}(M_i - \bar{M})^2 - \sum_{i=1}^{n} \varepsilon^2}{\sum_{i=1}^{n}(M_i - \bar{M})^2} \tag{10}$$

Where

- R^2 = Coefficient of determination
- a_1 = Slope of the prediction
- a_0 =Intercep of the prediction
- $\bar{M}$ = Average measured value.
- M= Measured value from testing
- P= Predicted value from FEM
- n = number of instruments

Note that $\sum_{i=1}^{n}(M_i - \bar{M})^2$ is the sum of the spread of the data around the mean value which is the numerator of the standard deviation. When the residual ε is zero, then $R^2 = R = 1$. Hence, the formula is normalized to$\sum_{i=1}^{n}(M_i - \bar{M})^2$. Moreover, on this case $a_1 = 1$ and a_0=0. R^2 is the coefficient of determination and R is the coefficient of correlation (Chapra and Canale, 2010).

The shortcomings or drawbacks of using the coefficient of determination are present when dealing with data with significant spread. On this case the residual is a smaller number than the term that corresponds to the spread around the mean, resulting in higher coefficient of determination. Moreover, the significance of coefficients of the fitted equation is not very reliable when including instruments in different units with very

different magnitudes, similar with the drawbacks with MAE. Nevertheless, the coefficient of determination is evidence of the correlation between the measured and predicted value. It is commonly used to show the correlation, but it is usually in company of other objectives functions. MAE and MAPE are good measures of accuracy and R^2 is a good measure of precision. There is no statistical model that can resolve the difference in types of measurements (units and differences in magnitudes) perfectly. The objective functions are to facilitate the calibration of the model and to elaborate optimization algorithms. The best way to observe the prediction of the global behavior of the bridge is by plotting influence line of the FEM and the experimental data.

Table 3.2 contains the coefficient of determination, MAPE and MAE for the final FEM model on each test. The table shows that the bridge globally predicts the experimental data to acceptable accuracy. This means that the boundary conditions simulate the conditions of the bridge and that the finite element modeling techniques used are appropriate to model the bridge behavior. Especially the incorporated longitudinal springs (link elements) to model the transverse shear transfer of live load. Note that LC-D presents a slightly higher error. LC-D only had three clicks during the experiment, due to human error. Therefore, the assumption of uniform velocity between clicks location may not have been very consistent. Nonetheless, the error at mid-span sensors was MAPE 9.15% average and since the test was the only load case that provided load transfer from stem S6 and S5 to the rest of the bridge, the model is considered relevant.

Table 3.2 Statistical values of the FEM final calibration.

Test	R^2	MAPE	MAE
A	0.994	9.48%	7.88
B	0.996	7.54%	6.01
C	0.992	7.72%	7.72
D	0.960	18.71%	18.19

Figure 3.5 shows the correlation between the experimental measured value and the FEM predicted value. The model globally behaves as the measured values, this global correlation is demonstrated by closed approximation of a one to one relationship of FEM and measured values.

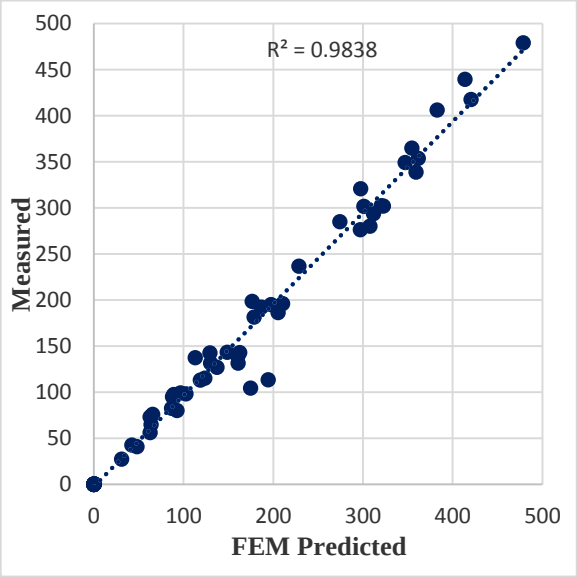

Figure 3.5 Experimental and final FEM correlation

3.4 Transverse Shear Distribution Modeling

From field observation and the experimental data collected, it was noted that the Icy Springs Bridge had fractured girder connections, patchwork ripping surface and

consequently had unreliable transverse shear connections. Although this was an observation of major importance, the calibration of the bridge neglected modeling the longitudinal shear connections at first. When comparing the transverse load distribution of FEM and experimental, it was evident that, to achieve a good calibration, the shear connections had to be modeled to represent transverse load distribution due to the deteriorated structure. Initially, the longitudinal springs had a single property along the length; it is a single value of spring stiffness over the entire bridge. However, when comparing the mid-span and quarter-span transverse load distribution plots as well as photos of the bridge deck, there was still a need for different stiffness along the deck. To accommodate for this, the longitudinal stiffness was divided into two regions: a third of the span from the instrumented abutment (for the quarter-span gages, DS1 and DS2) and the rest of the springs along the bridge for the mid-span gages (DS3 and DS4, see Figure 3.4). Although in reality the bridge was in worse local condition that indicated an inconsistent stiffness along the bridge, this modeling approach was practical and yielded acceptable outcomes for modeling the global behavior of the structure. Figure 3.6 presents the stem strains of test B at mid-span. Both FEM and experimental measurements are plotted. The FEM approximates the shape of the measured values very well, which indicates the modeling techniques were acceptable. Likewise Figure 3.7 shows the transverse load distribution for LC-A at quarter span. The plots for mid-span transverse load distribution for all test (FEM and experimental) are available in Appendix B.

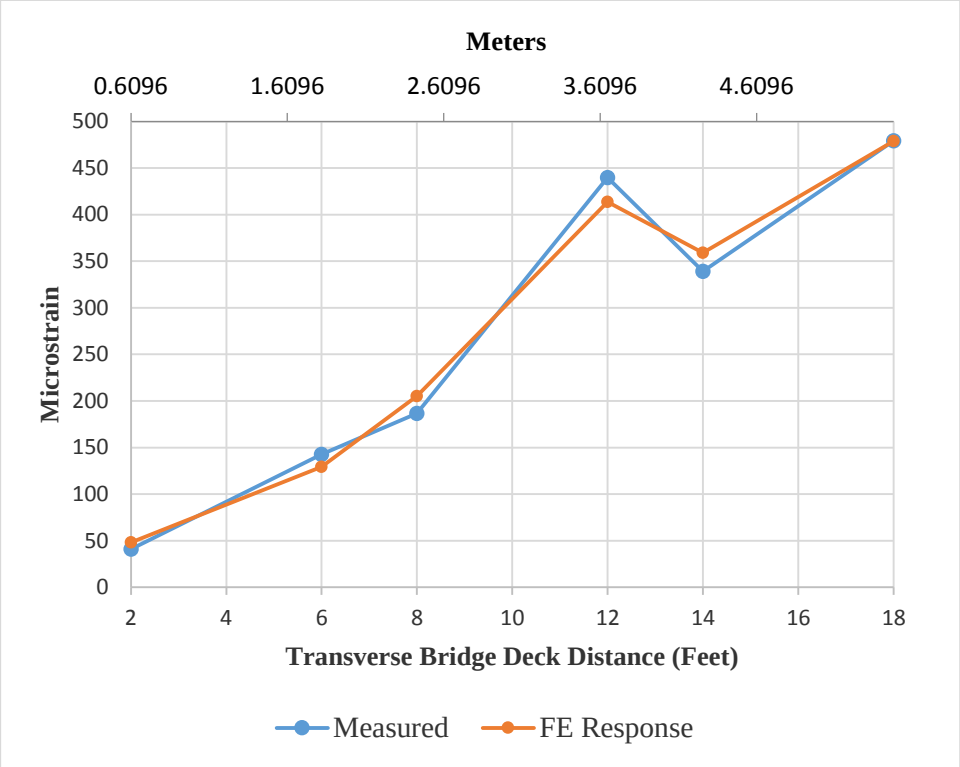

Figure 3.6 Transverse load distribution of LC-B at mid-span

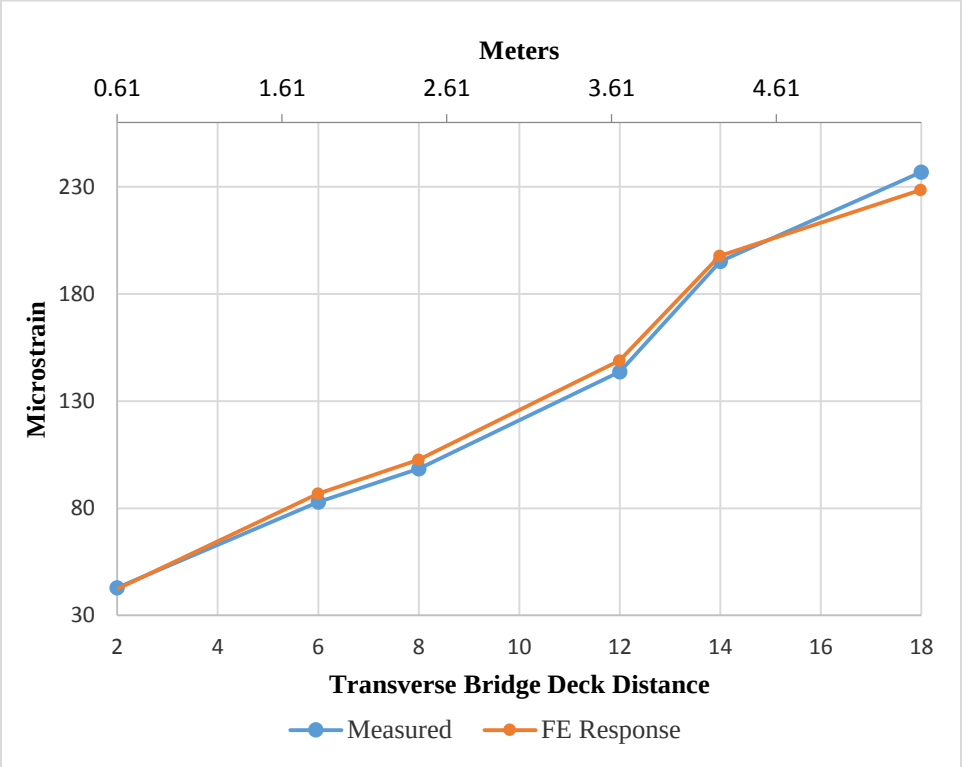

Figure 3.7 Transverse load distribution of LC-A at mid-span

Another way to describe the ability of the model to predict the transverse distribution of load is to calculate the girder distribution factor as experimental and compare it to the actual experimental values from testing. Table 3.3 presents the comparison of FEM experimental girder distribution factor and live load testing experimental values. The values are considerably close, which demonstrates that the model has a very close prediction of the transverse distribution of the load when compared to the tested capacity of the bridge.

Table 3.3 FEM and experimental GDF

Test	FEM GDF	EXP GDF
A	0.293	0.294
B	0.238	0.243
C	0.258	0.255
D	0.228	0.249

3.4.1 SAP 2000 OAPI

SAP2000 includes on its license a programming object based set of functions that can be used to control the software from a third party software. All the functions that are used in the GUI (Graphical User Interface) of SAP2000 are available to use as programming functions. This set of programmable functions that can be used to operate SAP2000 as a programmable object is called the OAPI (Open Application Programming Interface). An OAPI help file can be found in the folder of the installed software of SAP2000. The file contains help on all the functions that SAP2000 uses.

The OAPI was used to facilitate the calibration process by communicating SAP2000 to Microsoft Office Excel using Visual Basic for Applications (VBA). Multiple sets of functions were programmed on an Excel spreadsheet so that the model could be

change for boundaries condition and the material properties. Based on the conditions entered, the spreadsheet will communicate with SAP2000 and perform the analysis. After the analysis was performed the spreadsheet will request the response from SAP2000 and obtain an organized analysis of the FE response and the experimental measurements.

Figure 3.8 is an illustration of how the finite element software SAP 2000 was able to execute the analysis based on the boundary conditions specified on Excel, and how, after the analysis was completed, Excel was able to request from SAP2000 the responses at the specific locations for further analysis and comparison of results. Both Excel and SAP were communicating with each other through VBA by using the programmable functions from SAP2000 OAPI. Note that Excel and SAP2000 cannot communicate without the VBA interface.

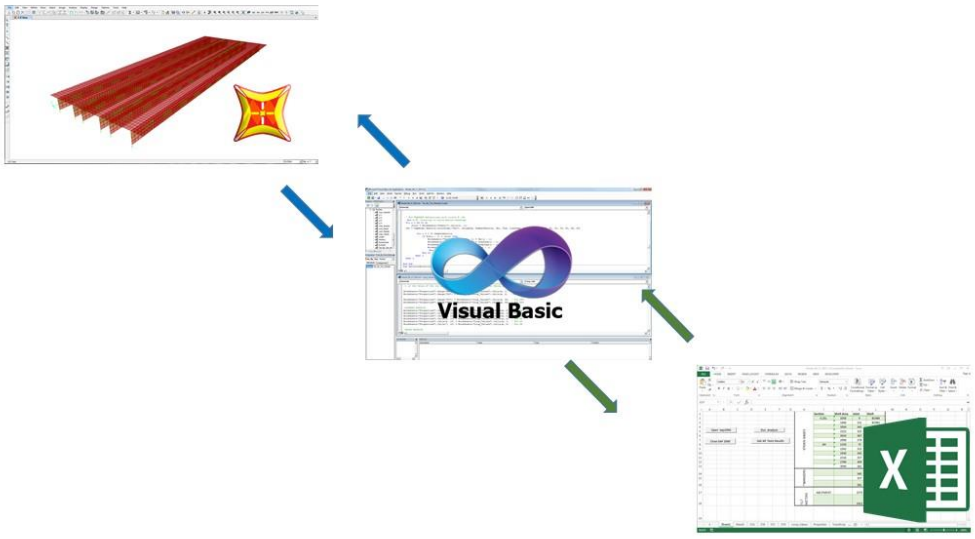

Figure 3.8 Interaction diagram describing the calibration process

FEM calibration is an involved and repetitive task that can incorporate the advantage of computer programming to facilitate the process of calibration. Without the use of a programming interface the process of calibrating an FE model to an experimental data can be more difficult and tedious. Taking into account the different boundary conditions and properties that have to be changed for calibration, requesting the specific response from the nodes and the numerical analysis of the comparison between FEM and experimental data, it is certainly a task that can be programmed to be partially or fully automated.

The OAPI made possible the communication between a programmable spreadsheet in Excel, through VBA programming, and SAP2000. Once the FEM was developed using the SAP interface, the OAPI was used to automate the operations that otherwise would have to be done by a user in a step by step basis. The OAPI was able to open the SAP model in order to create an object that will be associated to the FEM model in VBA. After the model was opened, the stiffness values corresponding to each spring element, and the modulus of elasticity of each stem and deck, will be assigned by the OAPI from values specified by the user in the spreadsheet. Based on the assigned values, SAP2000 can be set to run a static analysis from load cases that correspond to the experimental static load case. Once the analysis was complete, the spreadsheet will tell SAP2000 exactly which type of responses (rotations, deflections or stresses) will be reported and from which elements (shells and joints). These elements correspond to the same location of the experimental instruments. Taking into account the number of elements in the model and the number of responses SAP2000 can provide and time available, this was the best approach to request for the exact information the analysis

needed from a vast set of values available from the entire model. Once the responses were obtained, the spreadsheet organized the FEM prediction in the corresponding Excel tables for each test. Note that SAP 2000 will not give strain as an output, shell stresses corresponding to a node had to be requested and divided by the modulus of elasticity of the stem according to Hooke's Law. Once the data was available, the spreadsheet computed the values for the objective error functions. The spreadsheets also included plots of the measured and predicted values for the mid-span and quarter-span strain measurements. This plots could only be seen at the end of a single analysis. If multiple analyses are to be run, the spreadsheet will report the values of the different objective errors and the predictions per analysis.

After debugging and making sure that the spreadsheet works as intended, it can be a reliable mechanism to change material properties and boundaries conditions for experimental purposes. The programmed approach helped to facilitate a consistent analysis that was reliable run after run, whereas the step-by-step approach will be susceptible to user mistakes. Even though a fully automated model update could have been implemented, it was decided not. This could have helped calibrated the model faster but would have required considerably more time. Even when optimization algorithms are proposed by the user, fine tuning by the user is usually a final step. The user relied on a semi-automated interface to perform the calibration consistently through every analysis in this project.

3.5 CSi Bridge Influence Surface & Surface Post Processing

Once the model was calibrated, the calibration had to be compared to the experimental measurements by creating influence lines and plotting both influence lines

(i.e. experimental and theoretical) to observe if the model could model the global behavior of the bridge.

In order to obtain the influence lines corresponding to the calibrated finite element, the model was exported from SAP 2000 to CSi Bridge. Once the final model was exported to CSi Bridge, a lane was defined with the same width of the bridge. The influence surface is the surface of the superstructure where the load can act upon it (Computers and Structures Inc. 2014). CSi Bridge creates the unit influence surface depending on the load case associated with a lane. Therefore, in order to obtain an influence surface on the entire bridge the lane must be defined with the same dimensions of the bridge deck surface.

The output surface from the CSi moving load analysis will always be a unit influence surface. Nodes will have influence surfaces available for rotation and displacement. Shells will report stresses at nodes by the corresponding influence surface. From here, strains will have to be computed using Hooke's law using the modulus of elasticity of the stem.

Figure 3.9 is the influence surface for the calibrated model corresponding to the gage B1974. The influence is given in units of kip/kip-in^2 for the local stress of the shell that correspond to the bending of the shell in the longitudinal direction, reported at the node of the experimental gage location in the model. In order to get the influence of a point load of a known weight at a known location, multiply the weight of the point load by the influence corresponding to the location of the load, the result will be in kip/in^2. Strain can be computed with Hooke's Law. For a position located between two adjacent points in the surface, linear interpolation can be used to compute the influence from the

available points and then proceed to compute the response from the influence. The influence for deflection is in/kip and for rotation is rad/kip.

Any response corresponding to a given weight can be known at the surface at any position, transverse and longitudinal. Additionally the structural model is behaving linearly elastic (i.e. the FEM response is from a static analysis). Based on this observations, the principle of superposition can be used to obtain the influence line of a load configuration by taking into consideration the magnitude of the load and when the load starts acting on the structure and when the load stops acting on the structure. For the case of a truck load, the aforementioned weight and load distribution will correspond to the weight of the axles and the spacing between the axles.

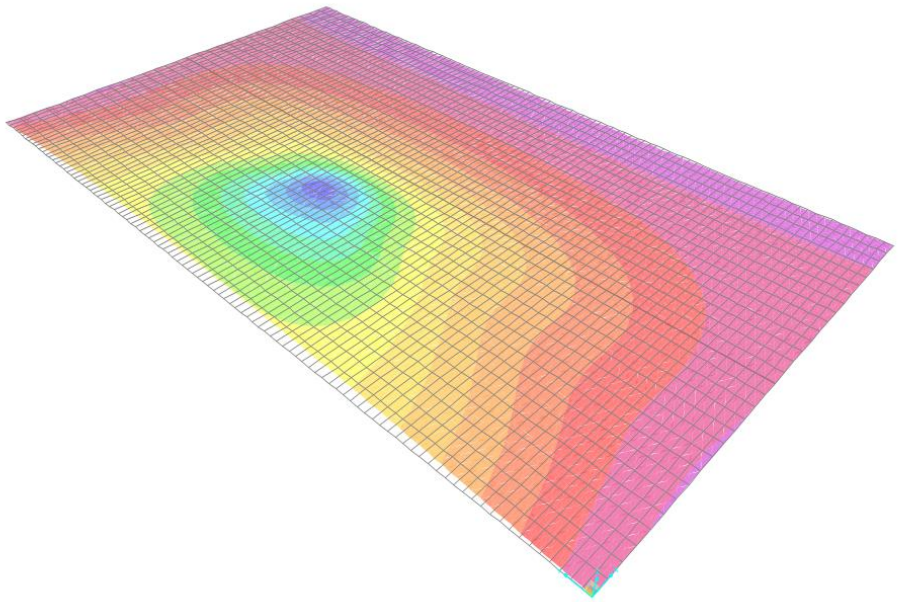

Figure 3.9 Influence surface for the node corresponding to the gage at S4

Using the principle of superposition, truck positions can be defined and respective influence lines are obtained by interpolating for the response of the truck position with the available surface coordinates. Finally, the individual influence lines per truck wheel are superimposed, combining them in a single influence line.

Figure 3.10 displays how the principle of superposition is used from an influence surface to obtain an influence line that describes the load and its distribution (i.e. axle weight and axle distance of the test truck for a lane of wheels) at a given transverse position.

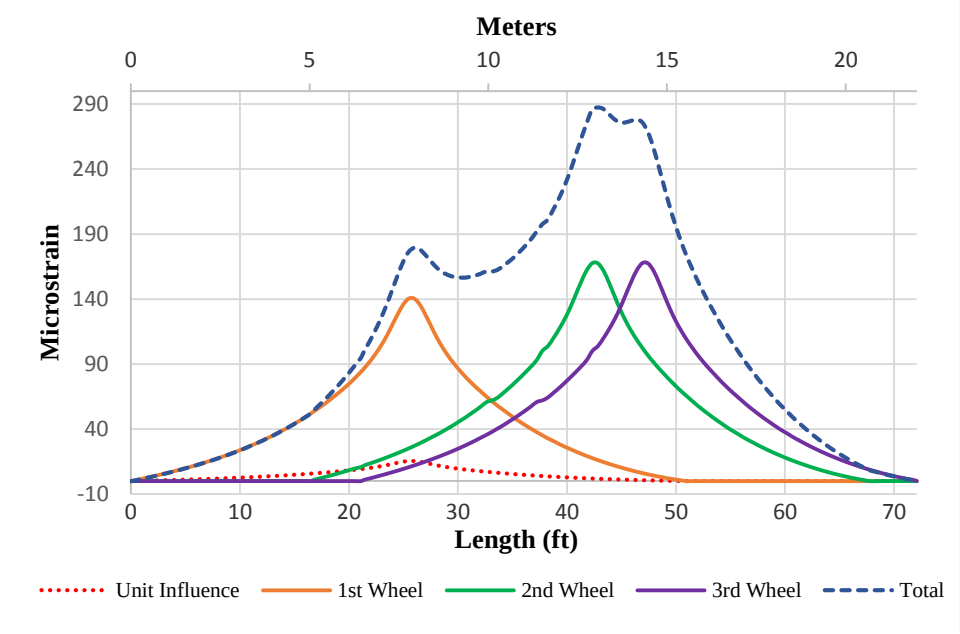

Figure 3.10 Unit, individual axle and total superimposed influence lines

First the influence line that corresponds to a unit load at the transverse position along the bridge is found (the unit influence line). Then this influence line can be used to find the influence when the load corresponds to the weights of the load from each wheel (in other words to multiply the unit influence line by the weight of the load to find the wheel's influence line). In addition, the position of when the loads start acting on the

bridge has to be incorporated by offsetting the wheel influence lines by the wheels distance. By adding all the wheel's influence lines the influence line of the wheels in one side of the axles is obtain (i.e. on side of the truck wheels). Figure 3.10 shows that each peak is one of the axle's loads in the respective side of the truck. To find the truck influence line, the other axle side influence line is computed by the same approach in a transverse position offset by the axle width in the direction of driving. Once both sides of the truck are represented as an influence line, the total truck is the summation of both truck wheel lanes, which essentially is the sum of all the wheel loads together when the influence lines are offset by the corresponding axle's distances.

The use of influence surface to obtain influence lines for a load configuration that corresponds to the test truck was used to compare the FEM influence prediction with the measured influence lines. Since this is a repetitive process that was performed for every single instrument in all tests, it was feasible to program a spreadsheet. A programmed spreadsheet was developed in which the truck axle weights, the distance in between wheels, the modulus of elasticity (in the case of strain gages) and the transverse position of the truck were specified. From this the spreadsheet would interpolate to find the unit influence line, multiply the weights and concatenate the influence lines according to the axle position. The influence lines were added by the spreadsheet taking into account the units and the use of Hook's law to find strain from stress. Note that the tests were defined by the transverse position in which the truck was acting on the surface over the length of the bridge. Every element has its own surface and any position can be specified. The elements correspond to the place of the instrumentation. The predicted influence lines from FEM that correspond to a test are all the influence lines from FEM at all elements

(instrument locations in FEM) for the transverse position of the truck that define the test truck position.

3.6 Experimental and FE Predicted Comparison

After the calibration culminated, the FEM response was compared to the measured influence lines by obtaining the predicted influence lines and plotting both responses. The plot illustrates that the calibration and modeling techniques can model the general behavior of the measured bridge response.

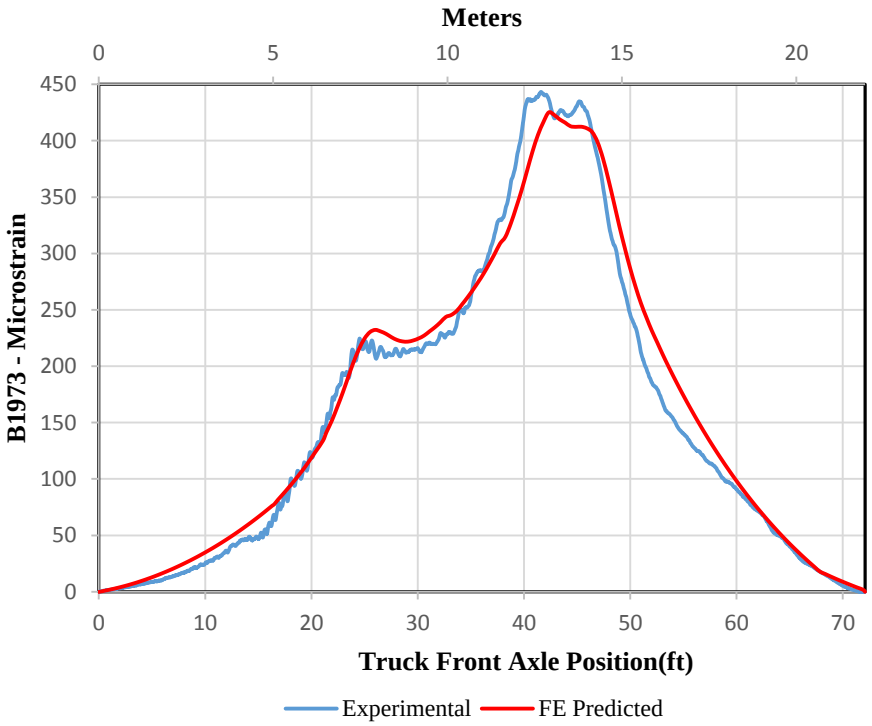

Figure 3.11 Experimental and FE predicted influence line for B1973 LC-A

Considering the structural conditions in which the Icy Springs Bridge was at the time of testing, it can be said that even though there were many local issues that made the calibration difficult, the calibrated model represents the global structural response of the Icy Springs Bridge. Figure 3.11 is the prediction of B1973 by the calibrated FEM plotted with the actual measurement from LC-A. Figure 3.12 shows one of the quarter span gages for B1980 on LC-B. Several plots of experimental and calibrated influence lines are available on Appendix C for the different experimental load cases and instruments.

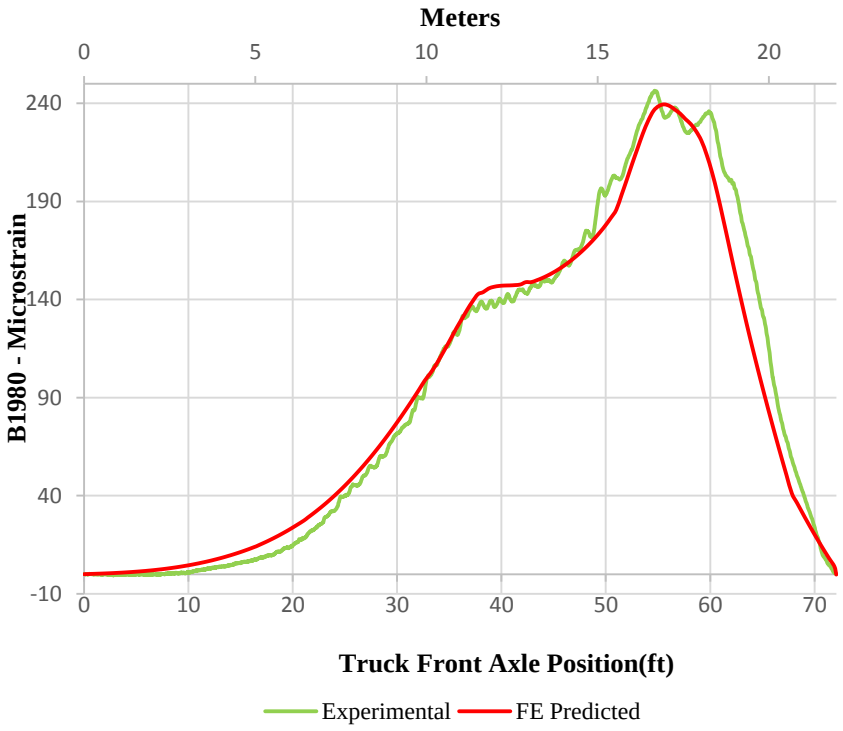

Figure 3.12 Experimental and FE predicted influence line for B1980 LC-B

CHAPTER 4. PARAMETRIC STUDY

In the preceding chapter, a shell element-based modeling technique was demonstrated and validated for a double tee structure. This model can be used to investigate double tee specific phenomena, through parametric study. The purpose of the parametric study outlined below, was to investigate girder moment and shear distribution factors from the parameters affecting transverse load distribution, such as:

- Span Length
- Number of girders
- Slab thickness
- Stems spacing
- Skew

The goal of this study is to develop more accurate distribution factors from finite element models using the validated modeling technique. To evaluate the existing AASHTO LRFD GDF formula, the prediction has to be compared with an accurate result. The distribution factors obtained from a finite element analysis are considered to be an accurate analysis (Zokaie, 2000) and will be used as the "ground truth" in the following study. Once the distribution factors from finite element were calculated, the distribution factors will be compared to the current specifications from the AASHTO code. Based on the observations from finite element and the current specifications, the study will propose an equation to estimate the finite element distribution factor.

The study computed the distribution factors for interior girder and exterior girder. In addition, the loading conditions considered were single lane loading and double lane loading.

4.1 FEM Parametric Model Description

To compute the finite element distribution factors a base model was selected. From that base model the different parameters were varied to produce additional models that represent the variation of different parameters. Table 4.1 contains the parameters considered for the development of finite element models to compute the distribution factors. The base model is a model of 40 feet long (12.19 m), 8 feet (2.44 m) spacing between girders, 6 inches (15.24 cm) slab thickness and zero skew angle. The models used for the parametric study set the longitudinal spring (flange connector) to a near infinite value of stiffness, in order to mimic the AASHTO code assumption of full shear transfer. Variable shear connection was studied as part of the parametric study and discussed at the end of this chapter. All other models are a variation of the base model described above.

Error! Reference source not found. displays one of the skew parametric odels. On this model, the parameter of skew was considered at 30°. The non-skew length and all the cross sectional properties are the same as the base model. Hence the only parameter changed from the base model is the skew angle.

Figure 4.1 30° Skew parametric model

Table 4.1 Parametric models variation

Parameter	**#Double T**	**L (ft)**	**S (ft)**	t_s**(in)**	θ**(°)**
Base Model	3	40	8	6	0
# of Girders	2	40	8	6	0
# of Girders	4	40	8	6	0
# of Girders	5	40	8	6	0
Length	3	20	8	6	0
Length	3	80	8	6	0
Length	3	100	8	6	0
Length	3	140	8	6	0
Skew	3	40	8	6	15
Skew	3	40	8	6	30
Skew	3	40	8	6	45
Slab Thickness	3	40	8	4.5	0
Slab Thickness	3	40	8	8	0
Slab Thickness	3	40	8	10	0
Slab Thickness	3	40	8	12	0
Spacing	3	40	10	6	0
Spacing	3	40	12	6	0

4.2 FEM Distribution Factors

The equations developed for the AASHTO specifications were developed on the basis that the parameters are uncoupled (Zokaie, 2000) (See Figure 1.1 on section 1.2). Investigating the parameters as if they were coupled would be much more computationally expensive and unnecessary based on Zokaie (2000).

Five parameters were varied, the amount of distribution factors calculated were 68. From each model four distribution factors are calculated due to the different loading conditions (single or double lane loaded) and the type of factor (interior or exterior). Since this applies for both moment girder and shear girder distribution factor, the study compared 136 distribution factors from FEM analysis and used in the following statistical analysis.

To calculate a distribution factor in the truck position that causes the maximum response (shear or moment) is needed. To accomplish this, all the influence lines were available for the critical response locations (i.e., reactions for shear and midspan for moments). For any given position a moment girder distribution factor (MGDF) can be computed by using equation 11.

$$MGDF = \frac{M_{max}}{\sum_{i=1}^{n} M_i} \tag{11}$$

Where:

$MGDF$= Moment distribution factor

M_{max}= The maximum moment for a load case at a beam line

M_i= The moment at stem i for a beam line of n stems

Note that when calculating the interior distribution factor only the interior stems are considered to find the maximum strain, likewise when calculating exterior factors. Shear distribution factor is calculated in the same manner as for moment, but using the reactions at an abutment in place of M_{max} and the M_i's.

The AASHTO specifications were developed including multiple presence factors depending on the load conditions in order to account for the worse case condition (AASHTO LRFD 2010). The multiple presence factor has to be included when calculating the FEM distribution factor when comparing to the theoretical AASHTO LRFD provisions, since the provision have already include it. Table 4.2 contains the AASHTO multiple presence factors for the different loaded lanes used in the study.

Table 4.2 AASHTO Multiple presence factor for the type of loaded lane

No. of Loaded Lanes	**Multiple Presence Factor**
1	1.2
2	1

The function of the GDF is to use the load from a single truck beamline analysis to estimate the maximum possible effective load in a single girder, or stem in this case. For this reason, GDFs for a single lane loaded case are calculated assuming that the total load on the bridge is only a single truck. For a two lane load case where the load are two trucks, the experimental analysis only finds the fraction of the load applied, GDF must be multiplied by two so that when multiplied by the forces from the single truck beamline analysis can account for the increase in load (See Figure 4.2).

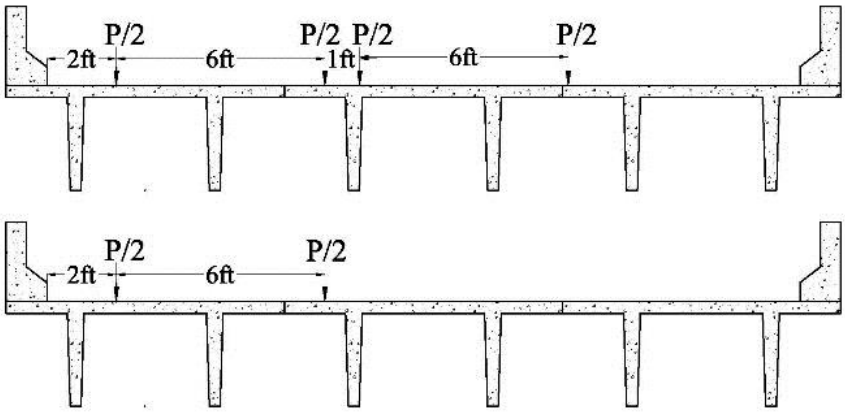

Figure 4.2 Load P considered for GDF for one and two lanes

Figure 4.3 is a plot of the different influence lines at the bottom of the stems on the FEM from each beam at mid-span. The transverse position corresponds to the allowable outermost transverse position. From this data the response in all beams at the position of maximum response can be found and the distribution factor can be calculated. This approach ensures that all the positions longitudinally are considered when calculating the distribution factor for a given transverse load case. Note that each influence line is representing strain on the stem where the factor is being calculated. For convenience, all influence lines are calculated from the corresponding influence surface. When using the double lane loaded case, the influence lines for a single truck was found for multiple positions and then added together. Once the response was represented in a single influence line, the distribution factor was calculated. This was done for all possible combinations of trucks and transverse positions.

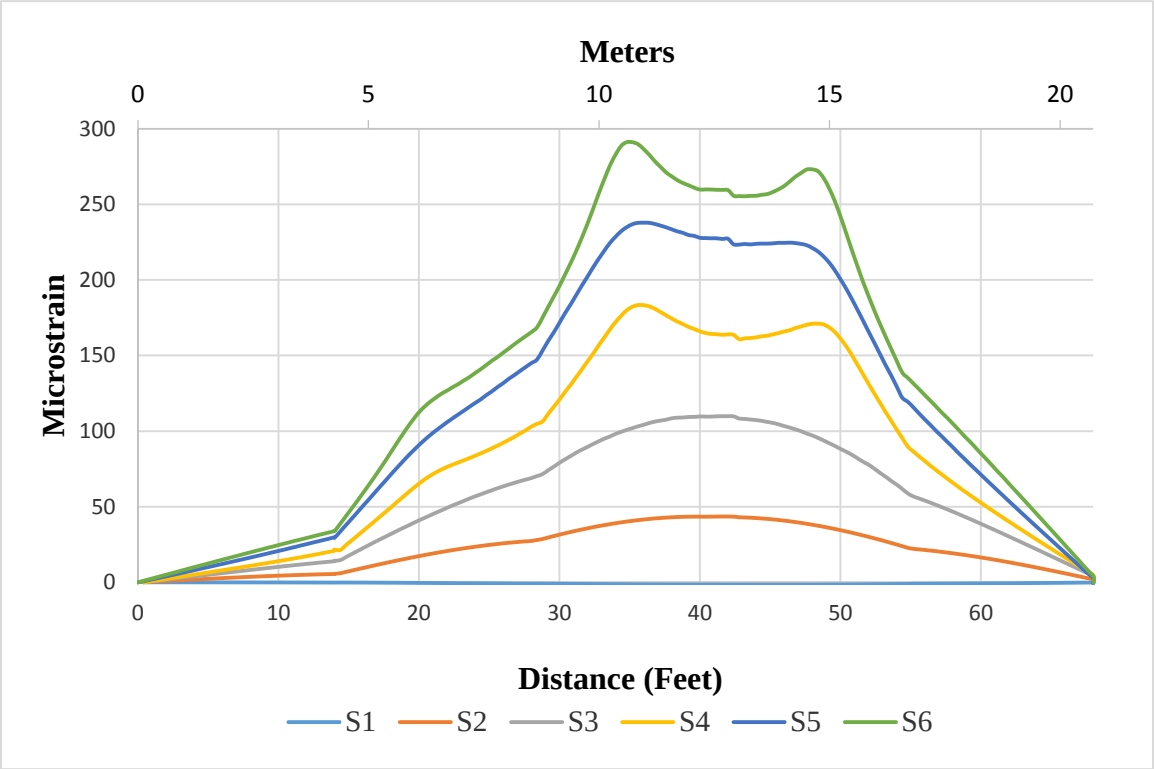

Figure 4.3 Influence line for the beam line at mid-span for the base model.

Figure 4.4 displays six influence surfaces used to compute the influence lines on the beam line to compute the FEM distribution factor at any given transverse position for the base model. Depending on the parametric model the number of girders changed and therefore the number of influence surfaces changed as well.

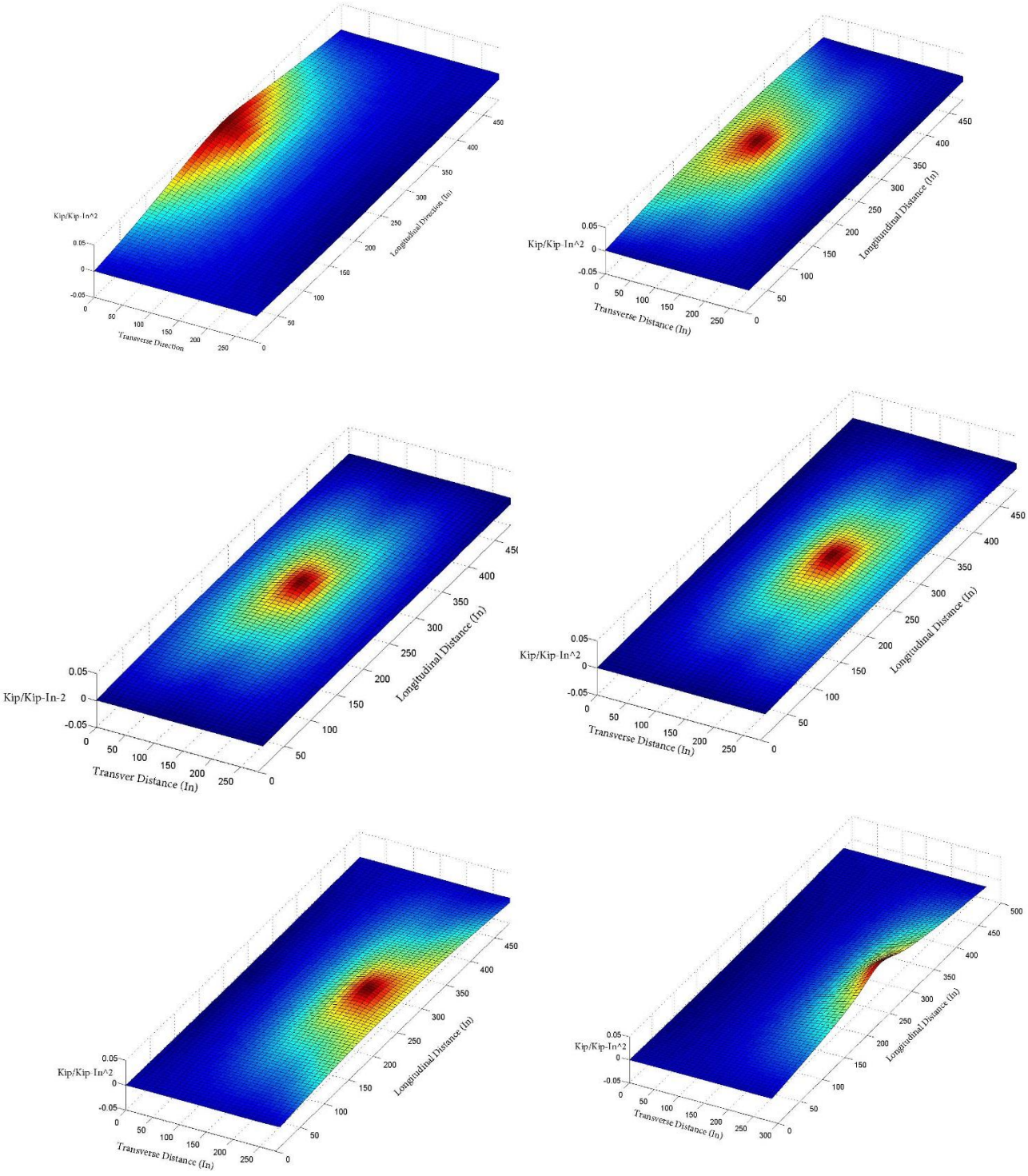

Figure 4.4 Influence surfaces for base model

To calculate the distribution factors for a given parametric model a programmed spreadsheet was developed. The spreadsheet used the influence surfaces to generate the influence lines corresponding to appropriate response and numerically calculate the distribution factors. Once all the distribution factors for every transverse position were calculated, the maximum distribution factor will be reported as the girder distribution factor for the girder type (i.e. exterior or interior). For the case of SGDF, the influence surface corresponded to the reactions at the pinned abutment. For MGDF, the influence surface corresponded to the strains obtained from shells at midspan.

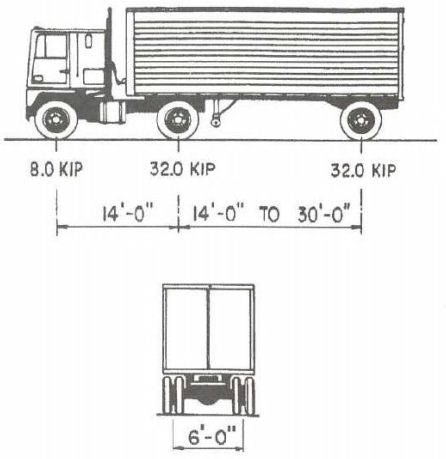

Figure 4.5 AASHTO HS-20 Truck (AASHTO LRFD).

Figure 4.5 illustrates the axle weight and axle distribution of the HS-20 truck, which is used in HL-93 loading. This truck is a permit truck and it is the appropriate loading to use when computing the distribution factors. The distance between the second and third axle was used at 14ft (4.26 m) in all cases. This distance was selected to produce the load that would generate the worst case scenario for the computation of the factors.

When calculating MGDF for interior and exterior, it was observed that the governing GDF for moment is always obtained when the truck is placed as close to the edge of the exterior girder between one or two feet away from the allowable edge distance. When calculating SGDF is necessary to use different transverse positions, the governing factor is usually obtained when the truck is place closer to the interior girders.

4.3 AASHTO Distribution Factors

The theoretical prediction of the AASHTO LRFD specification was calculated to be compared with the actual girder distribution factors from FEM and how the theoretical values changed as the parameters were varied. Equation 12 and 13 are the equations from the AASHTO specification for the calculation of the interior girder distribution factors. Equation 12 corresponds to one design lane loaded and equation 13 to two or more design lane loaded. According to the AASHTO equations there is relevant correlation in between spacing (S), Length (t_s) and the slab thickness (t_s). The longitudinal stiffness parameter is (K_g), is used to incorporate cross sectional and material properties.

$$GDF_{interior} = 0.06 + \left(\frac{S}{14}\right)^{0.4} \cdot \left(\frac{S}{L}\right)^{0.3} \cdot \left(\frac{K_g}{12 \cdot L \cdot {t_s}^3}\right)^{0.1} \tag{12}$$

$$GDF_{interior} = .075 + \left(\frac{S}{9.5}\right)^{0.6} \cdot \left(\frac{S}{L}\right)^{0.2} \cdot \left(\frac{K_g}{12 \cdot L \cdot {t_s}^3}\right)^{0.1} \tag{13}$$

Refer to appendix D for the results of the calculations of interior girder distribution factors. The appendix also explains in detail the provisions used from the AASHTO LRFD code.

The AASHTO LRFD specification uses the lever rule for the calculation of the exterior girder distribution factor, when single lane loading is used. The lever rule is a conservative method to estimate the most vulnerable case of distribution factor.

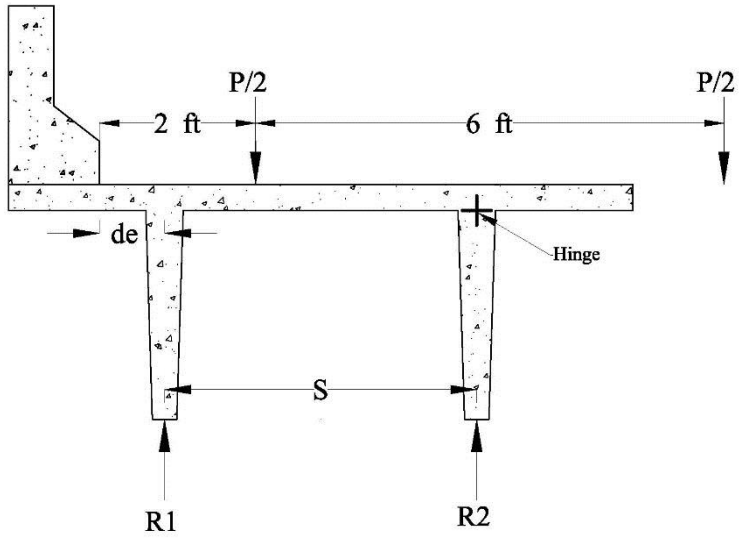

Figure 4.6 Illustration of the use of the lever rule

Figure 4.6 illustrates the model use for computing exterior girder distribution factors using the lever rule. The load is placed 2ft (0.609 m) away from the edge of the barrier. The parametric study considered an assumed barrier 14 inches wide (35.56 cm). This barrier and a minimum edge distance were also considered for the accurate calculation of distribution factors from FEM.

Assuming pin and roller supports at the stems, the lever rule sums the moments about one support to find the reaction of the other support under the assumption that the deck at the interior support is hinged (AASHTO LRFD 2010). The reaction can be written in terms of the spacing of the girders, the edge distance and the load. By summing the moments at the hinge, the exterior girder distribution factor that corresponds to the reaction of the exterior girder can be written in the form of equation (14 given the

dimensions of Figure 4.6. Note that the only parameter effectively considered by the lever rule is the girder spacing. This equation applies to all girder spacing investigated in the parametric study, since all the spacing have the interior wheel load on the far side of the hinge. Otherwise the reaction would need to be included in the static calculations.

$$GDF_{ext} = R_1 = \frac{1}{S} \cdot \frac{P}{2} \cdot (S + d_e - 2) \tag{14}$$

The specification uses equation 15 for the calculation of the exterior girder distribution factor when using two lanes loaded. The exterior girder distribution factor for this loading case is basically a multiplier of the theoretical interior girder distribution factor. Once e is calculated it is multiplied by the interior moment girder distribution factor and the exterior moment girder distribution factor is obtained.

$$e = 0.77 + \frac{d_e}{9.1} \tag{15}$$

The lever rule is used for both MGDF and SGDF for the exterior girders. Refer to Appendix E to the use of the lever rule and the calculation of theoretical exterior girder distribution factors. The interior SGDF are calculated as per Equation 16 and 17. An important observation is that the AASHTO theoretical model proposes that shear distribution factor only changes with the girder spacing.

$$SGDF_{interior} = 0.36 + \frac{S}{25} \tag{16}$$

$$SGDF_{interior} = 0.2 + \frac{S}{12} - \left(\frac{S}{35}\right)^2 \quad (17)$$

4.4 Girder Distribution Factor Comparison

The distribution factors from FEM and the predictions from AASHTO were plotted against the parameters changed in the parametric study to observe differences in response. The plots for the parametric study consider both loading cases, single and double lane loaded, for interior and exterior factors.

To illustrate the differences between the FEM and the estimated AASHTO equations, Figure 4.8 and Figure 4.7 plot the FEM and AASHTO MGDF and SGDF for all bridges investigated in the parametric study. Both plots demonstrate that the AASHTO predictions with the FEM have significant scatter Figure 4.8 and Figure 4.7 indicate that AASHTO GDF prediction are inaccurate when compared to the FEM, the coefficient of determination (R^2) is poor and the values are predicted inaccurately.

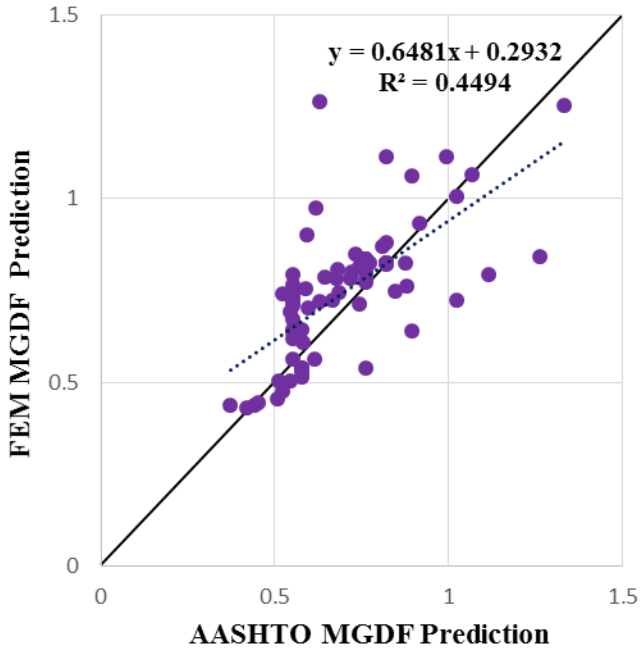

Figure 4.8 FEM vs AASHTO MGDF

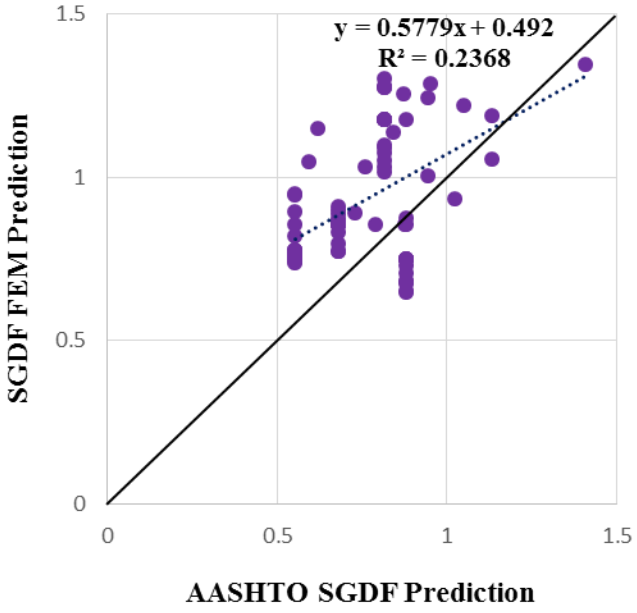

Figure 4.7 FEM vs AASHTO SGDF

4.4.1 GDF and Length

Figure 4.9 and Figure 4.10 present MGDF for interior and exterior girders for the variable span length, respectively. On Figure 4.9 the girder distribution factor decreases as the span length increases for both AASHTO and FEM. As length increases the FEM two lane loaded produces larger MGDF than AASHTO. For the one loaded case, FEM and AASHTO predictions are very similar.

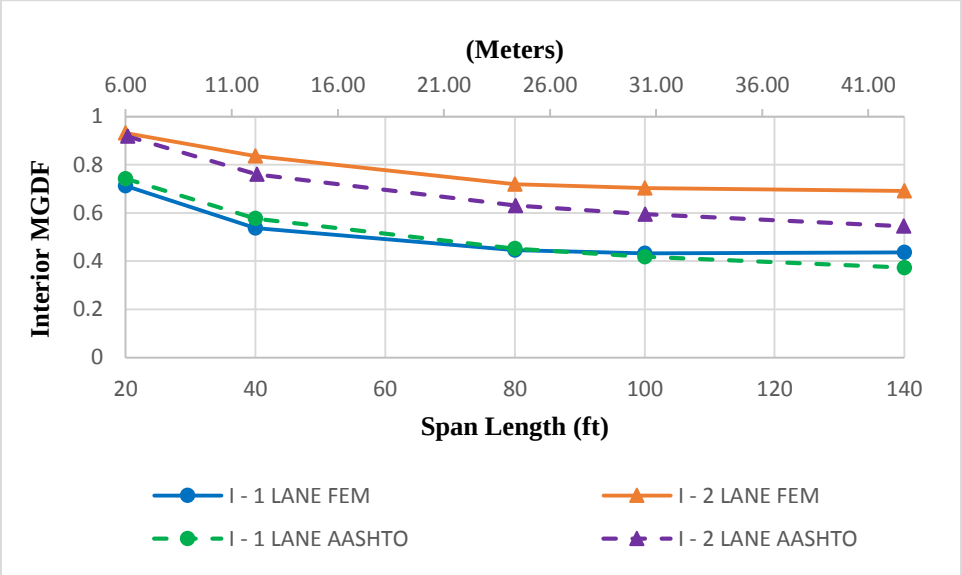

Figure 4.9 Interior MGDF for variable length

For exterior MGDF (Figure 4.10), again, all MGDF decrease as span length increases, but for the two lanes loaded case, FEM is very close to constant after the length is greater than 40 ft. (12.19 m) and for one lane loaded the AASHTO prediction is also constant for the single lane loaded due to lever rule. The exterior two lane loaded is a multiplier of the interior two lane loaded case considering only d_e. Note that in both load cases AASHTO under predicts the value of the distribution factor.

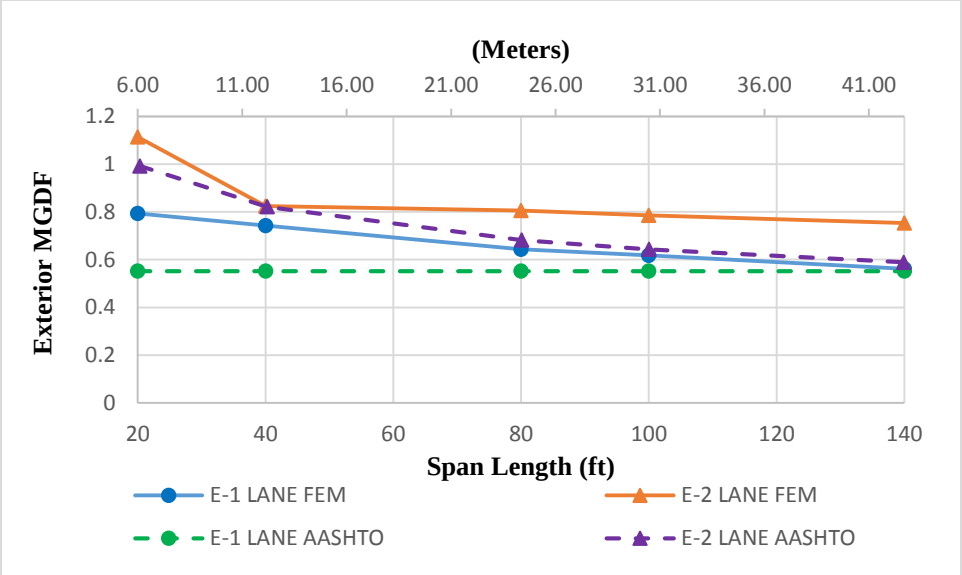

Figure 4.10 Exterior MGDF for variable length

Figure 4.11 presents the FEM and AASHTO interior SGDF as a function of length. On this case, both one and two lane loaded for FEM, plot above the AASHTO prediction. The SGDF remain relatively constant with respect to span length for all cases indicating the span length is not an important factor when computing interior SGDF.

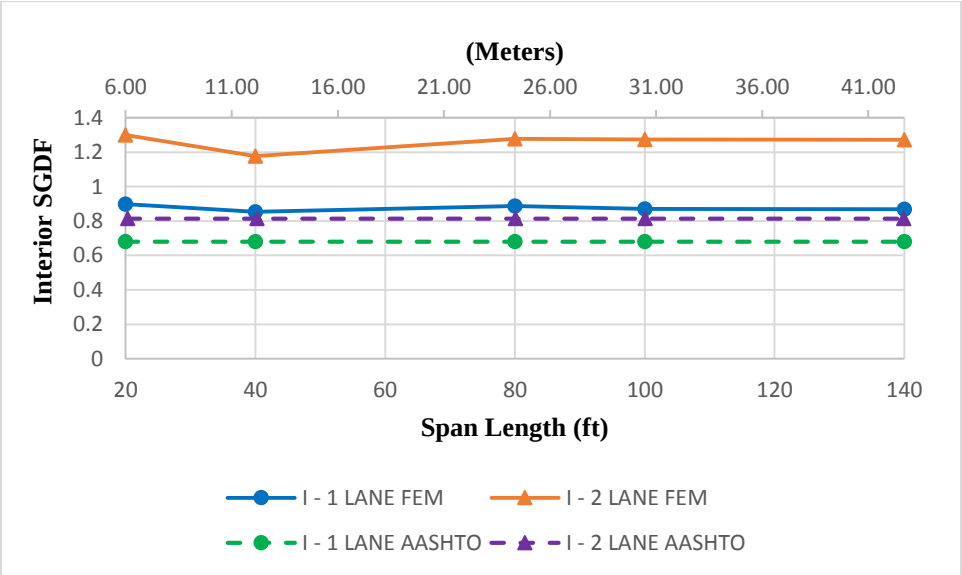

Figure 4.11 Interior SGDF for variable length

Figure 4.12 presents exterior SGDF as a function of length. The exterior AASHTO SGDF is constant, however the FEM SGDF clearly are not and vary with span length, especially the two lane case. When the span length increases, FEM approaches the AASHTO two lane lever rule for both loading cases.

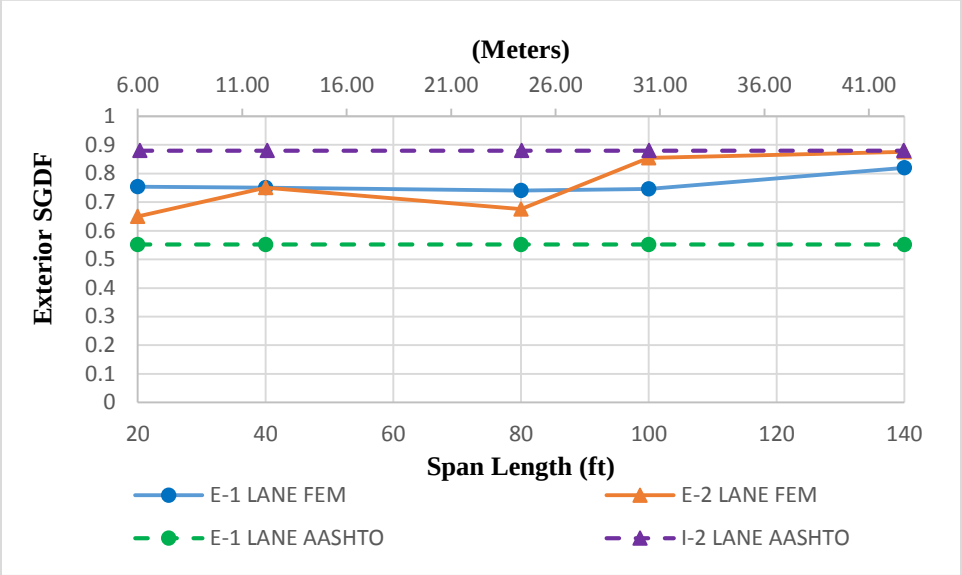

Figure 4.12 Exterior SGDF for variable length

4.4.2 GDF and Slab Thickness

On Figure 4.13 and Figure 4.14 MGDF predictions from FEM and AASHTO are plotted as a function of slab thickness. The general trend is that when slab thickness increases, the distribution factor decreases. On Figure 4.13 AASHTO and FEM are relatively similar with variation under 10%.

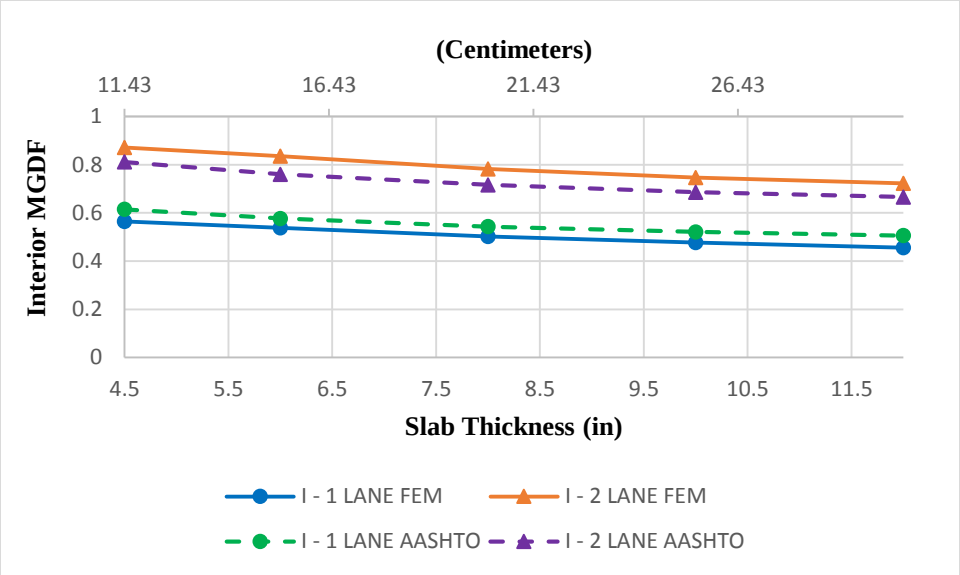

Figure 4.13 Interior MGDF for variable slab thickness

In Figure 4.14 the FEM two lane loaded prediction is constant whereas the AASHTO deceases linearly. The FEM one lane loaded decreases linearly, but the AASHTO lever rule is again constant for variable slab thickness.

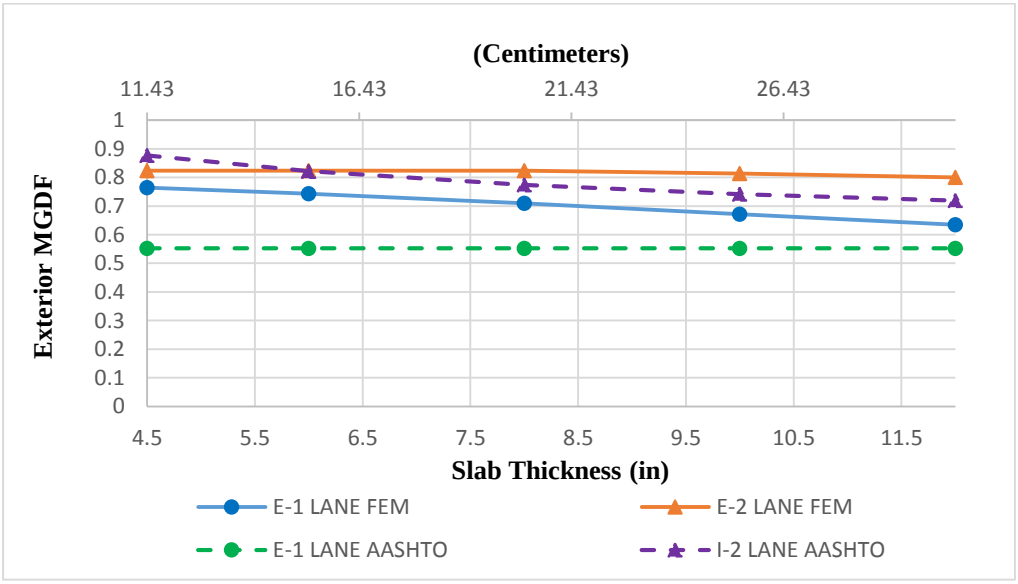

Figure 4.14 Exterior MGDF for variable slab thickness

Figure 4.15 and Figure 4.16 are plots of SGDF obtained from FEM and AASHTO for the parameter of slab thickness. Figure 4.15 demonstrates that for the FEM and AASHTO interior SGDF are relatively constant with respect to slab thickness. Both load cases of FEM plot significantly above the AASHTO predictions.

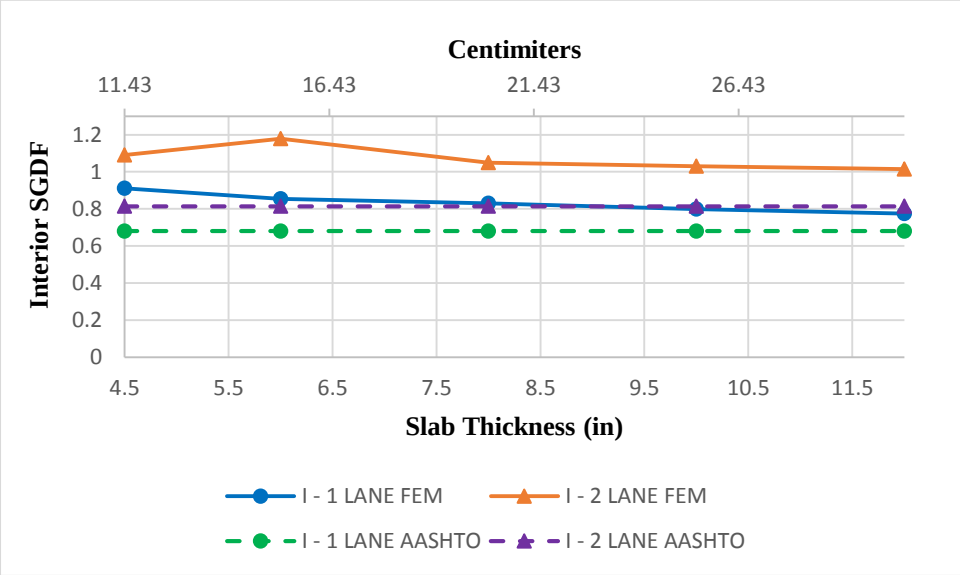

Figure 4.15 Interior SGDF for variable slab thickness

On Figure 4.16 there again is negligible change in the interior distribution factors as the slab thickness increases for FEM and AASHTO. The FEM two lane loaded plots bellow the AASHTO prediction. Note that on both figures, there is more variation in SGDF for the two lane load case.

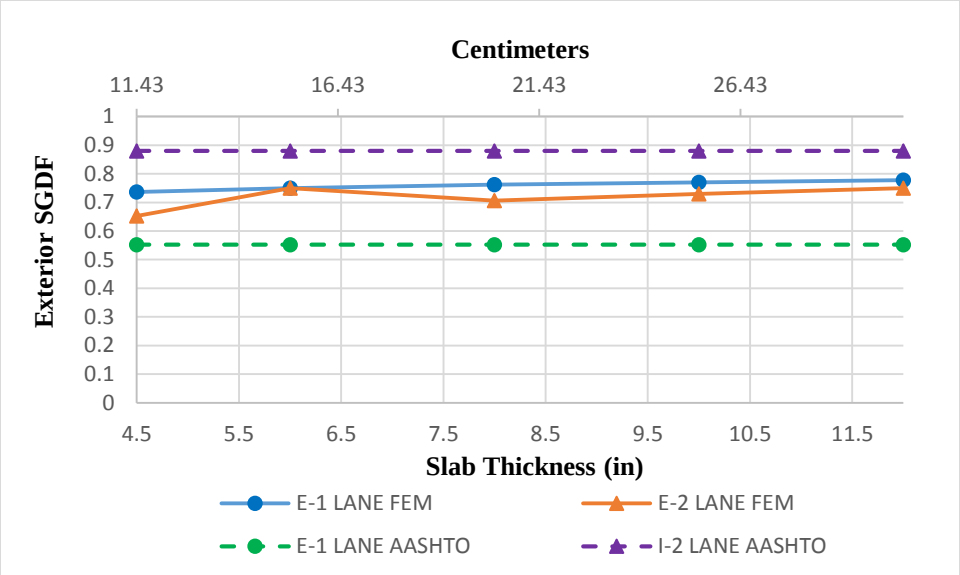

Figure 4.16 Exterior SGDF for variable slab thickness

4.4.3 GDF and Number of Girders

Figure 4.17 and Figure 4.18 show the prediction of MGDF as the parameter of number of double tees is changed respectively for interior and exterior girder distribution factors. Note that for two lane loading, two trucks is not a possible load case because the resulting model is not wide enough for two lanes. On Figure 4.17 FEM MGDF increases when the number of double tees decreases. As the number of double tees increases FEM MGDF is about constant and is well predicted by AASHTO. However, in Figure 4.18 it can be observed that MGDF for FEM is about the same for both loading cases. For exterior MGDF the percent difference of both loading cases on FEM is less that the percent difference of both loading cases for interior. This is also observable in all parameters

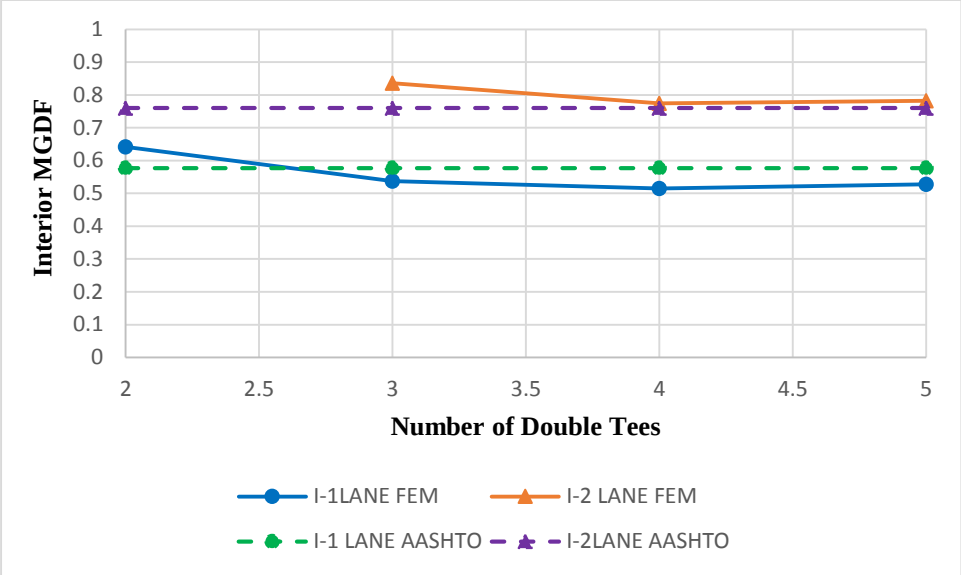

Figure 4.17 Interior MGDF for different number of girders

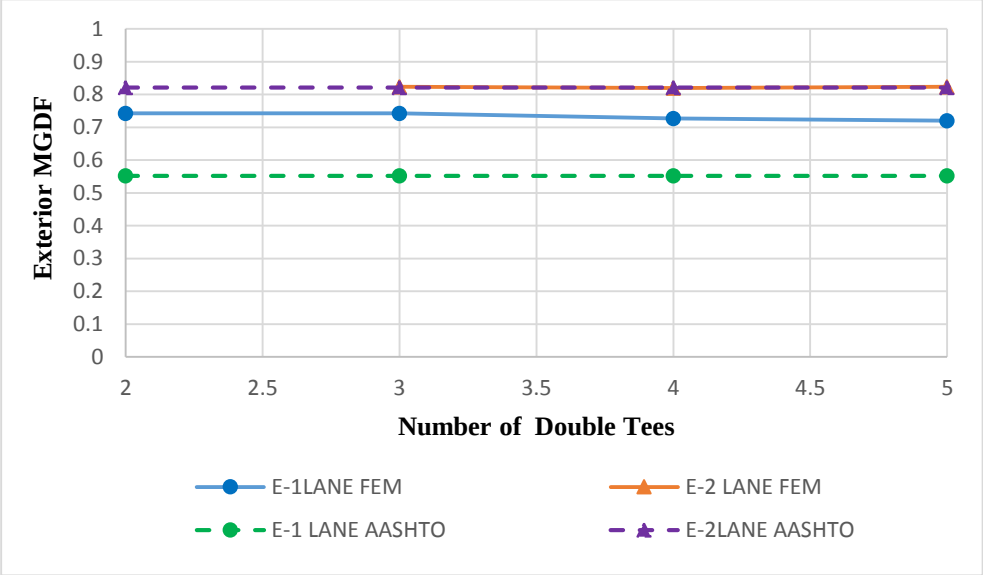

Figure 4.18 Exterior MGDF for different number of girders

Figure 4.19 and Figure 4.20 are plots of the SGDF for the parameter of number of double tees for interior and exterior factor respectively. Figure 4.17 through Figure 4.20 show that girder distribution factor does not changes significantly as the number of girders changes. There is some interaction between the number of girders and the distribution factor with FEM, but it is low. Even though the specification does not include

this parameter, the specification recommends another method for when the number of girder is less than three.

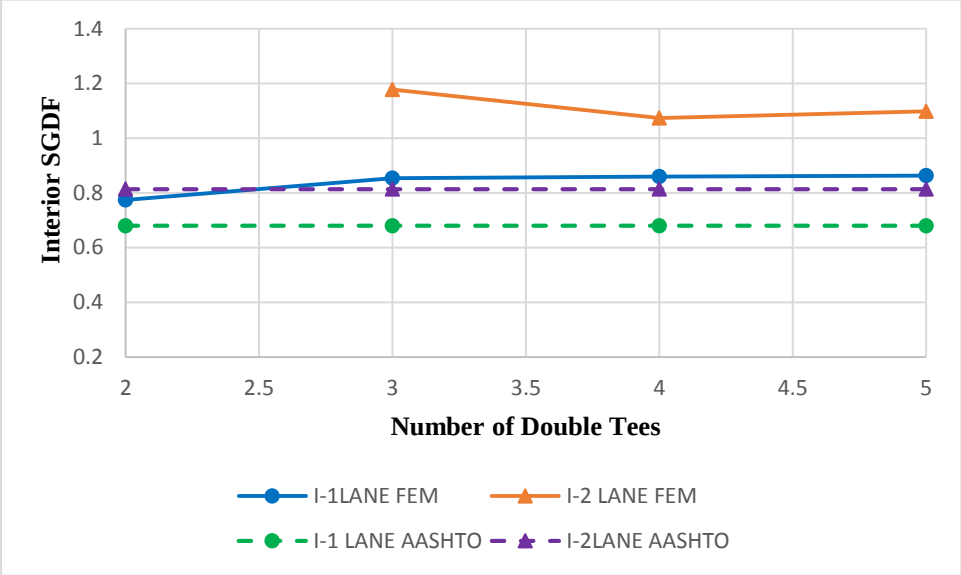

Figure 4.19 Interior SGDF for variable number of double tees

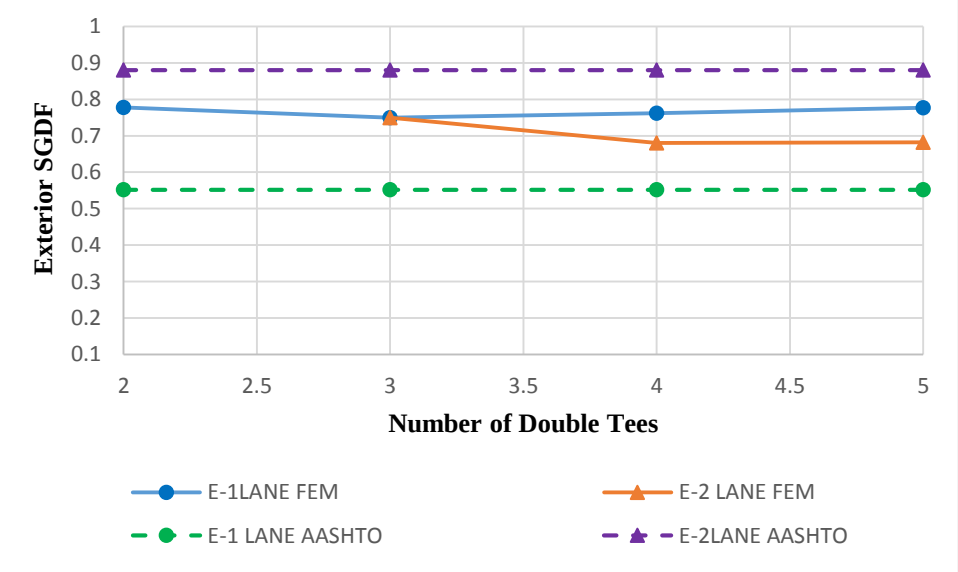

Figure 4.20 Exterior SGDF for variable number of double tees

4.4.4 GDF and Skew

Figure 4.21 and Figure 4.22 are plots of MGDF for variable skew for interior and exterior respectively. On Figure 4.21 the AASHTO and FEM values show similar variations and are relatively close, often within 10% of each other.

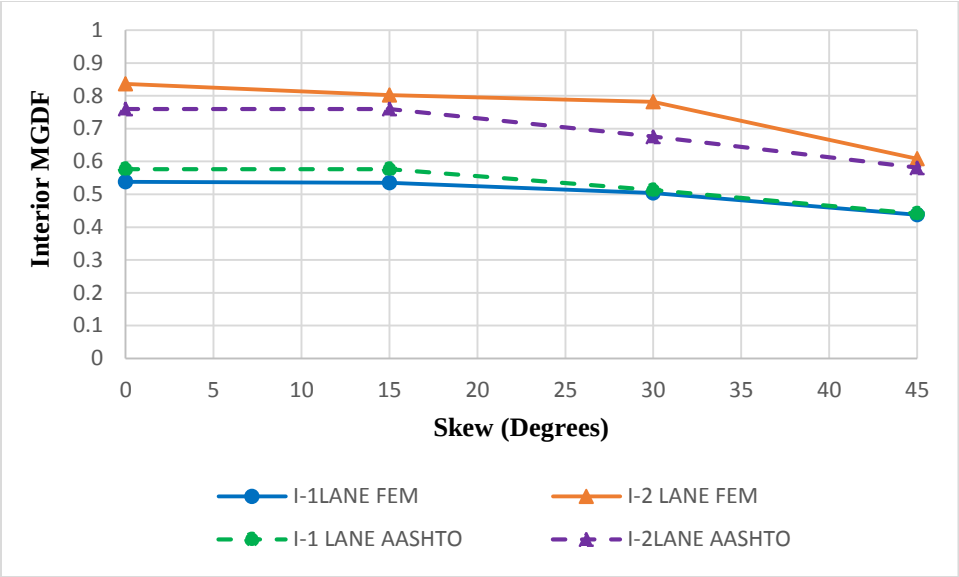

Figure 4.21 Interior MGDF for the variable skew

In Figure 4.22 the complex behavior is described by FEM that is not captured by AASHTO for the two lane SGDF, this is due to the use of the lever rule by AASHTO and the multiplier for the exterior two lane loaded case. Exterior two-lane FEM MGDF decreases as skew angle increases from 0° up to 15° and increases for both load cases as the skew angle increases from 30°.

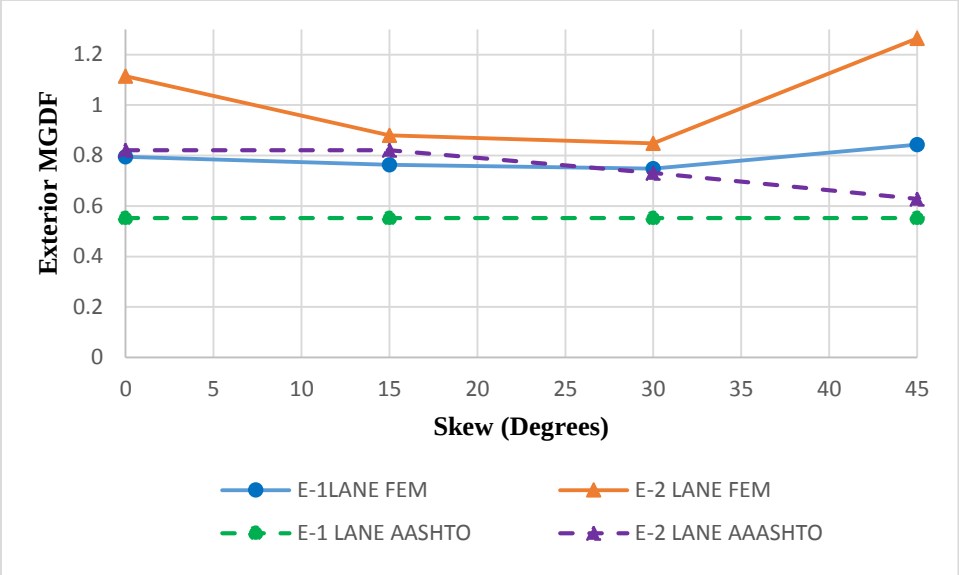

Figure 4.22 Exterior MGDF for the variable skew

Figure 4.23 and Figure 4.24 are the interior and exterior shear distribution factors for the variable skew. For interior girders the FEM SGDF clearly increases as the angle of skew increases to 15° and then slightly decreases as skew increases. For exterior stems the FEM distribution factor increases up to 15°, then slightly decreases to 30° and increases from here until 45°. The AASHTO specification proposes a linear increasing distribution factor for all cases, except for exterior single loaded which is constant, based on the lever rule. In general the lever rule produces inaccurate results and the AASHTO methods are, overall, not accurate when compared to the FEM for SGDF as skew is varied.

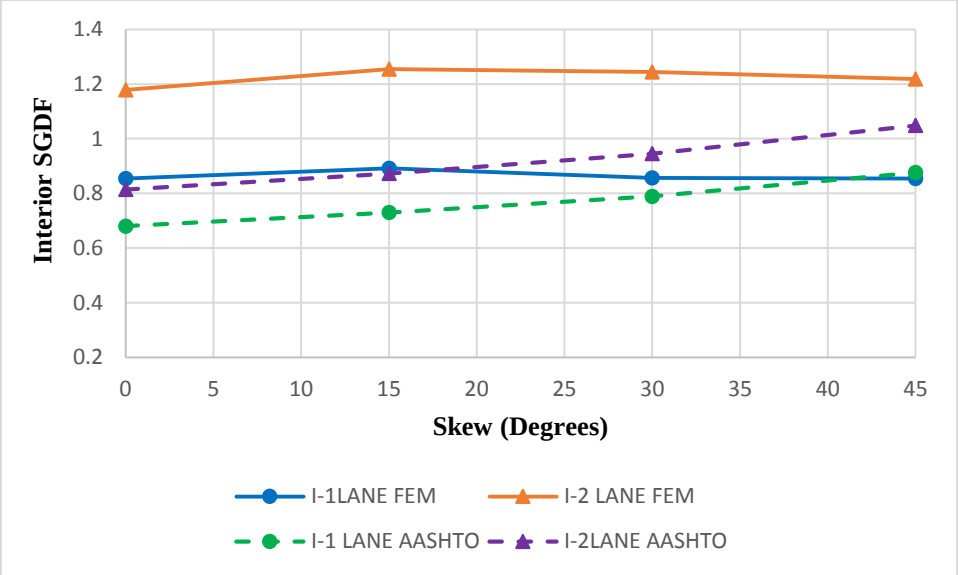

Figure 4.23 Interior SGDF for variable skew

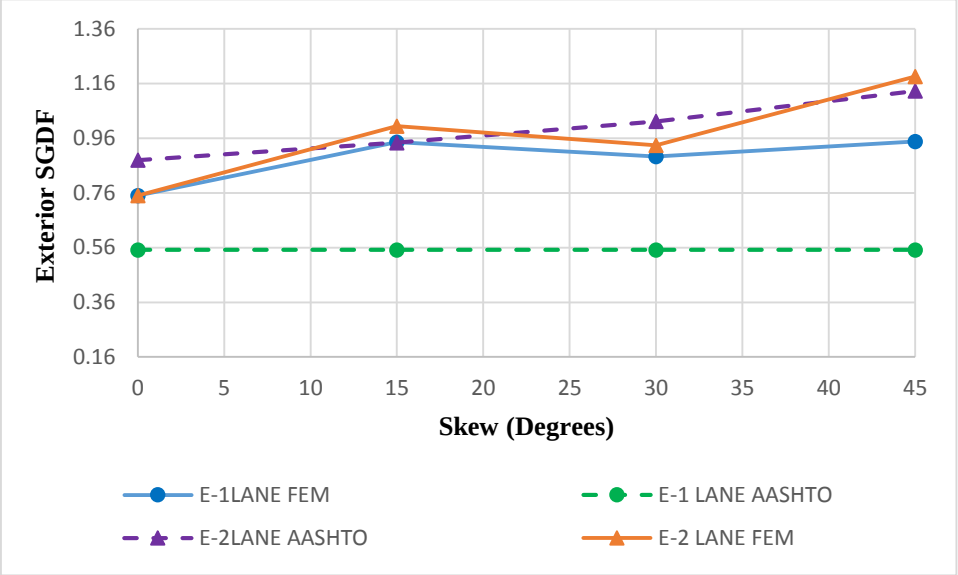

Figure 4.24 Exterior SGDF for variable skew

4.4.5 GDF and Girder Spacing

Figure 4.25 and Figure 4.26 illustrate a positive correlation for girder spacing and distribution factor both from FEM and the AASHTO prediction. In Figure 4.25 the AASHTO and FEM predictions are relatively similar. The two-lane loaded FEM is not linear, but has a similar trend to the other lines.

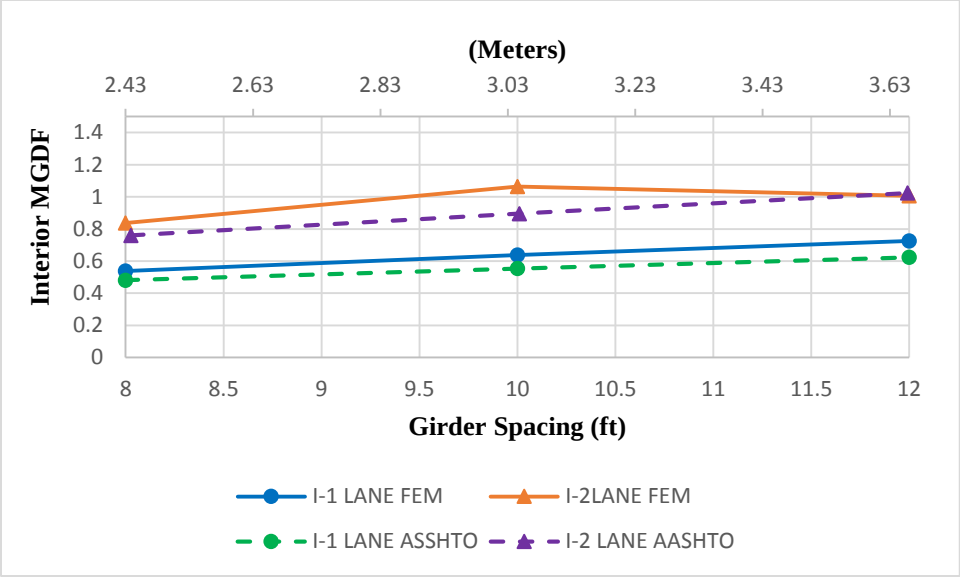

Figure 4.25 Interior MGDF for the variable girder spacing

In Figure 4.25, two lane FEM and AASHTO are nearly identical. However, the AASHTO lever rule significantly under-predicts the FEM single lane factor. Note that this is the only case where the exterior single lane loaded factor is not constant; this is due to the derivation of the lever rule which involves girder spacing when taking the sum of the moments.

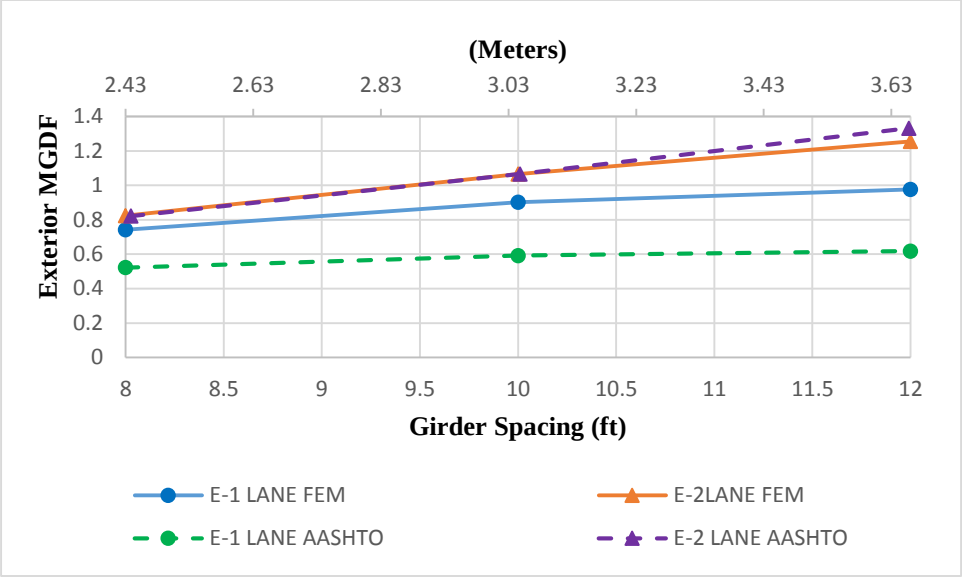

Figure 4.26 Exterior MGDF for the variable girder spacing

Figure 4.27 and Figure 4.28 plot the AASHTO and FEM SGDF for interior and exterior girders. Both plots show SGDF has a strong positive correlation with girder spacing. Also in both cases, the FEM MGDF plots higher than the AASHTO prediction. Note that in Figure 4.28 the exterior AASHTO SGDF is again controlled by the lever rule and it grossly under predicts the FEM SGDF, whereas the 2 lane AASHTO and FEM are nearly similar for larger spacing.

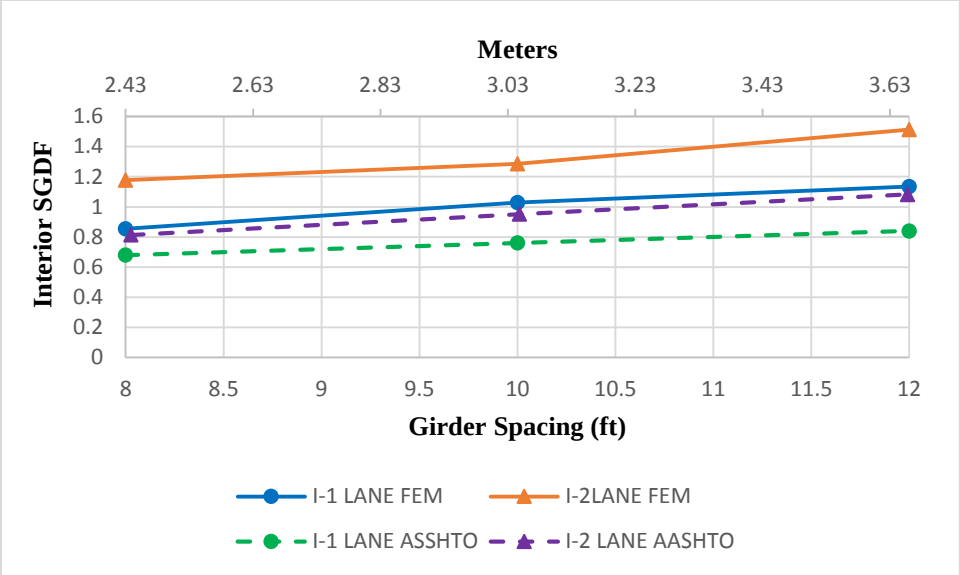

Figure 4.27 Interior SGDF for the variable girder spacing

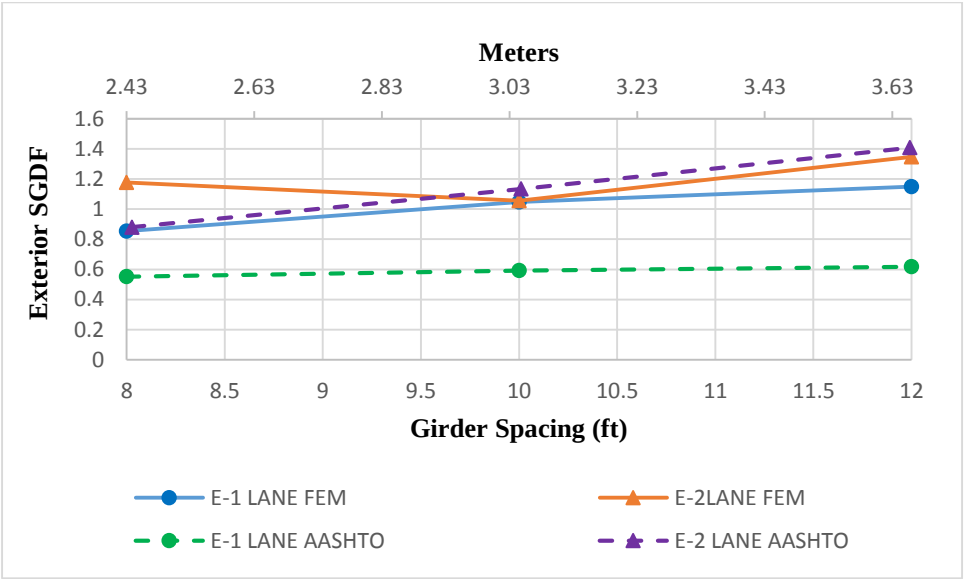

Figure 4.28 Exterior SGDF for the variable girder spacing

4.4.6 Comparison of FEM and AASHTO

Table 4.3 and Table 4.4 are the absolute percent difference (i.e., abs((AASHTO-FEM)/AASHTO*100)) in the AASHTO and FEM prediction for MGDF and SGDF

respectively. Both tables have significant percent difference for the predictions indicating that the AASHTO prediction is not accurate for the calculation of GDF.

Table 4.3 Average percent difference for AASHTO AND FEM MGDF

	Interior		Exterior	
	1 Lane	**2 Lane**	**1 Lane**	**2 Lane**
Span Length	6.2%	11.9%	16.6%	13.3%
Slab Thickness	8.9%	8.1%	21.3%	6.3%
Number of Girders	18.7%	4.6%	28.0%	0.3%
Skew	18.65%	8.19%	27.97%	6.64%
Spacing	12.60%	8.92%	33.59%	2.12%

Table 4.4 Average percent difference for AASHTO AND FEM SGDF

	Interior		Exterior	
	1 Lane	**2 Lane**	**1 Lane**	**2 Lane**
Span Length	22.3%	35.3%	27.5%	17.3%
Slab Thickness	18.2%	23.9%	27.3%	23.0%
Number of Girders	18.7%	29.6%	28.0%	20.1%
Skew	18.7%	24.8%	28.0%	6.6%
Spacing	24.2%	28.5%	41.7%	12.4%

4.5 Proposed Statistical Model

Using the data from the parametric study, a new statistical model was developed to predict the MGDF and SGDF for double tee girder bridges. The statistical model was developed using a multilinear regression model to predict the distribution factors. Multilinear regression models are based on the assumption that parameters are linearly independent and have a direct correlation with the dependent variable. Equation 18 is the basic form for the multilinear model used to predict GDFs. In Equation 18 y is the dependent variable, the distribution factor in this case. Furthermore, a_i is the coefficient that corresponds to the variable parameter x_i and c is a constant. The value ϵ corresponds

to the residual, which is used in the regression technique to calculate the fit by computing the coefficient of determination R^2.

$$y = a_1 \cdot x_1 + a_2 \cdot x_2 + \cdots + c + \epsilon \tag{18}$$

Figure 4.29 plots the FEM predictions versus the proposed models for girder distribution factor. The fitted model offers a notable improvement in the prediction of girder distribution factor. The fitted model has a coefficient of determination of 0.86. Equations 19 through 23 show the proposed multilinear regression for predicting MGDF.

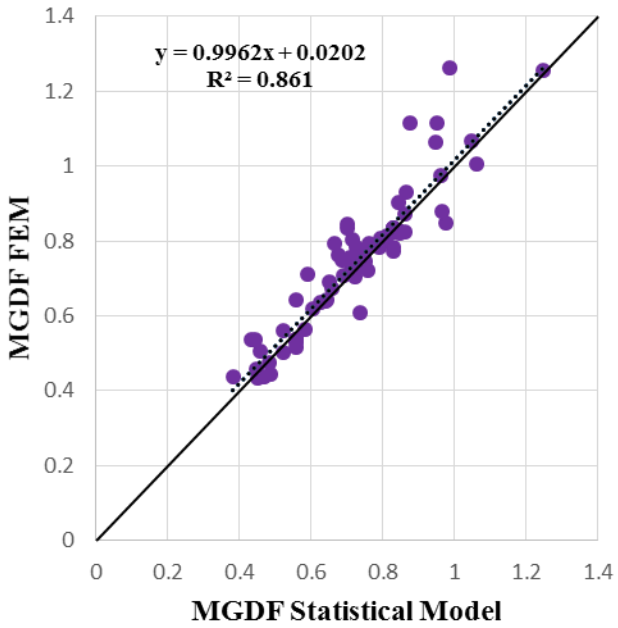

Figure 4.29 FEM vs statistical model for MGDF

Similarly, Figure 4.30 plots of the FEM prediction versus the proposed model for shear distribution factor. The fitted model provides an R^2 of 0.83.Compared to the AASHTO prediction with 0.23 R^2, the proposed model offers vast improvement. The

following equations constitute the proposed model for predicting shear distribution factor.

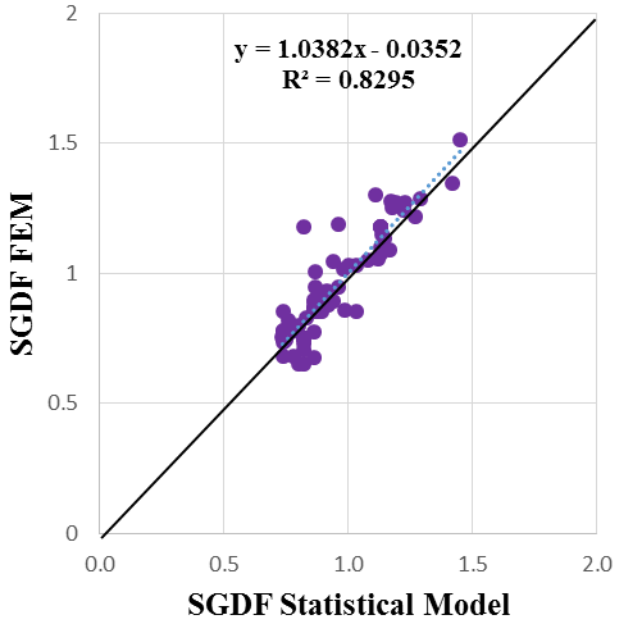

Figure 4.30 FEM vs statistical model for SGDF

The model uses the non-skew GDF to make a correction for skew and predict the skew GDF for MGDF and SGDF.

The following equations correspond to the prediction of MGDF:

For exterior two lane

$$MGDF = -\frac{7 \cdot L}{5000} - \frac{9 \cdot t_s}{1000} + \frac{S}{10} + \frac{4}{25} \tag{19}$$

For exterior single lane

$$MGDF = -\frac{L}{500} - \frac{2 \cdot t_s}{125} + \frac{3 \cdot S}{50} + \frac{21}{50} \tag{20}$$

For interior two lane

$$MGDF = -\frac{9 \cdot L}{5000} - \frac{t_s}{50} + \frac{29 \cdot S}{500} + \frac{14}{25} \quad (21)$$

For interior single lane

$$MGDF = -\frac{L}{625} - \frac{9 \cdot t_s}{500} + \frac{S}{25} + \frac{2}{5} \quad (22)$$

For skew correction

$$MGDF_{Skew} = \frac{9 \cdot MGDF}{10} - \frac{1}{20} + \frac{\theta}{1250} \quad (23)$$

Where:

- $MGDF$ = moment girder distribution factor for the respective case
- $MGDF_{Skew}$= MGDF corrected for skew
- $L =$ Span length
- t_s= Slab Thickness
- S = Stem Spacing

The following equations correspond to the prediction of SGDF:

For exterior two lane

$$SGDF = \frac{3 \cdot S}{20} + \frac{L}{1000} - \frac{NG}{25} + \frac{3}{10} \quad (24)$$

For exterior one lane

$$SGDF = \frac{S}{10} + \frac{L}{5000} - \frac{7}{100} \quad (25)$$

For interior two lane

$$SGDF == \frac{2 \cdot S}{25} + \frac{L}{1000} - \frac{t_s}{40} + \frac{3}{5} \quad (26)$$

For interior one lane

$$SGDF = \frac{7 \cdot S}{100} - \frac{2 \cdot t_s}{125} + \frac{2}{5} \quad (27)$$

For skew correction

$$SGDF_{SKEW} = \frac{7 \cdot SGDF}{10} + \frac{\theta}{250} + \frac{27}{100} \quad (28)$$

Where:

- *SGDF*= moment girder distribution factor for the respective case
- $SGDF_{Skew}$= SGDF corrected for skew
- L = Span length
- t_s= Slab Thickness
- S = Stem Spacing
- NG = Number of Double Tees

Table 4.6 through Table 4.14 show the correlation matrices used in the statistical analysis for understanding which variables were relevant to predict the GDF. Since a low correlation was obtained when all the predictions are considered, individual models were fitted to increase the correlation for the prediction. Once the models were divided into more categories, the parameters showed more correlations to the dependent variable. In some tables skew was not included because all of the values were zero skewed, which is

not valid for the correlation matrix. However the correlation matrix for skew provided the correlation between the distribution factor with no skew and the skew distribution factor.

Table 4.5 Correlation matrix for MGDF exterior two lane

	FEM	Length	Slab Thickness	No. Girders	Spacing
FEM	1				
Length	-0.3908	1			
Slab Thickness	-0.1816	-0.1415	1		
No. Girders	-0.1342	-0.1375	-0.1304	1	
Spacing	0.83324	-0.1375	-0.1304	-0.12676	1

Table 4.6 Correlation matrix for MGDF exterior single lane

	FEM	Length	Slab Thickness	No. Girders	Spacing
FEM	1				
Length	-0.61532	1			
Slab Thickness	-0.31994	-0.1320	1		
No. Girders	-0.04116	-0.0753	-0.07151	1	
Spacing	0.785338	-0.1283	-0.1218	-0.069523	1

Table 4.7 Correlation matrix for MGDF interior two lane

	FEM	Length	Slab Thickness	No. Girders	Spacing
FEM	1				
Length	-0.54542	1			
Slab Thickness	-0.35541	-0.1414	1		
No. Girders	-0.14465	-0.1375	-0.13041	1	
Spacing	0.704285	-0.1375	-0.13041	-0.126760	1

Table 4.8 Correlation matrix for MGDF interior one lane

	FEM	Length	Slab Thickness	No. Girders	Spacing
FEM	1				
Length	-0.58302	1			
Slab Thickness	-0.34662	-0.1320	1		
No. Girders	-0.18129	-0.0753	-0.07151	1	
Spacing	0.605607	-0.1283	-0.1218	-0.069523	1

Table 4.9 Correlation matrix for MGDF skew correction

	FEM	GDF	Skew
FEM	1		
MGDF-NS	0.871429	1	
Skew	-0.06427	0	1

Table 4.10 Correlation matrix for SGDF exterior two lane

	FEM	Length	Slab Thickness	No. Girders	Spacing
FEM	1				
Length	0.061625	1			
Slab Thickness	-0.12981	-0.1414	1		
No. Girders	-0.24657	-0.1375	-0.13041	1	
Spacing	0.779132	-0.1375	-0.13041	-0.126760	1

Table 4.11 Correlation matrix for SGDF exterior one lane

	FEM	Length	Slab Thickness	No. Girders	Spacing
FEM	1				
Length	-0.0748	1			
Slab Thickness	-0.09391	-0.1320	1		
No. Girders	-0.07013	-0.0753	-0.07151	1	
Spacing	0.951633	-0.1283	-0.1218	-0.069523	1

Table 4.12 Correlation matrix for SGDF interior two lane

	FEM	Length	Slab Thickness	No. Girders	Spacing
FEM	1				
Length	0.255974	1			
Slab Thickness	-0.49456	-0.1414	1		
No. Girders	-0.27284	-0.1375	-0.13041	1	
Spacing	0.706016	-0.1375	-0.13041	-0.126760	1

Table 4.13 Correlation matrix for SGDF interior one lane

	FEM	Length	Slab Thickness	No. Girders	Spacing
FEM	1				
Length	-0.03458	1			
Slab Thickness	-0.4267	-0.1320	1		
No. Girders	0.066536	-0.0753	-0.07151	1	
Spacing	0.897597	-0.1283	-0.1218	-0.069523	1

Table 4.14 Correlation matrix for SGDF Skew correction

	FEM	SGDF-NS	Skew
FEM	1		
SGDF-NS	0.754944	1	
Skew	0.307214	0	1

4.5.1 Implementation

To implement the proposed model, the GDF is calculated for the different cases of MGDF or SGDF, the maximum value is the governing GDF for moment or shear. If skew is considered, the governing factor has to be corrected for skew using the corresponding equations for MGDF and SGDF. The lever rule is not recommended to be included in this analysis as it was shown to be highly inaccurate in the above analyses, when compared to the FEM prediction.

4.5.2 MGDF and Variable Shear Connections

The parametric FEM were pinned-roller boundary condition that used a deck with rigid vertical springs modeled, which is the case of a design model. In this case, the deck is connected from girder to girder by the nodes of the shells using spring elements with variable vertical stiffness at the girders connected flanges. To observe how MGDF changed as the longitudinal stiffness of the flange connection changes a model with the dimensions of the parametric model was developed. The stiffness was varied and MGDF was computed. When there is zero stiffness for shear transfer, there is no load transfer and the wheel loads go completely into the girder they are touching. This caused the higher distribution factor for interior MGDF.

Figure 4.31 is a plot of MGDF, for interior and exterior girders, against the variable longitudinal stiffness between flanges. As the stiffness increases, both MGDF approach a constant value. Therefore, for a deteriorated bridge such as the Icy Springs Bridge that has poor shear connection, a simple rehabilitation scenario was investigated.

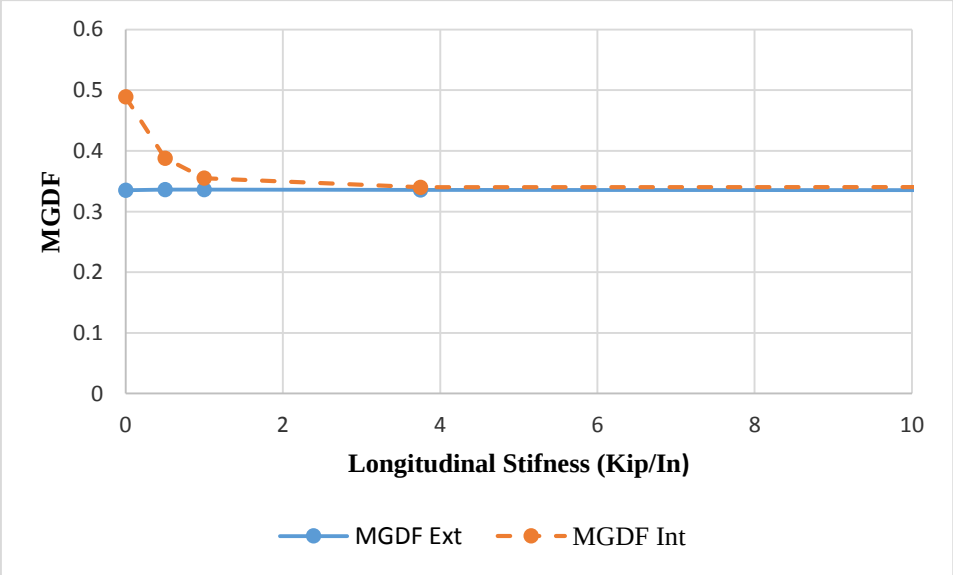

Figure 4.31 Variable MGDF for longitudinal stiffness

If one assumes a layer of asphalt or concrete is to be added to the bridge deck the resulting effect on the vertical shear transfer can be estimated from the shear modulus (see Equation 29) of the material, conservatively assuming no moment transfer. Equation 30 rearranges Equation 29 to create a spring stiffness constant that can be considered analogous to the shear transfer springs in the FEM.

$$G = \frac{\tau_{xy}}{\gamma_{xy}} = \frac{F/A}{\Delta x/l} = \frac{Fl}{A\Delta x} \tag{29}$$

$$K_{shear} = \frac{F}{\Delta x} = \frac{GA}{l} \tag{30}$$

Assuming a 1 in. asphalt (E = 500 ksi, ν = 0.35, G = 185 ksi) overlay across the deck results in a spring constant of 2160 kip/in for a 12 in. link spacing (using Equation 30). Adding this 1 in. of asphalt increases longitudinal stiffness by more than necessary to be on the flat range of MGDF as shown in Figure 4.31. From MGDF interior the FEM model slightly perceives the difference when there is no stiffness or very little stiffness, but when stiffness is increased beyond only 4 kips/in there is no additional benefit. From this information, nearly any rehabilitation, protection of the deck or embedment of flange connectors that could provide at least 4 kips/in. would allow the use of the above equations. Based on the condition of the deck, redecking or overlaying would be warranted to improve deck strength and ride.

CHAPTER 5. LIVE LOAD RATING

5.1 Bridge Rating

The Icy Springs was rated for live load flexural and load capacity according to the provisions for the AASHTO Load and Resistance Factor Rating (AASHTO LRFR). The capacity of the girders used in this analysis is the ones obtained from strain compatibility from thesis of Christopher Pettigrew (2014) about the capacity of the girders of the same Icy Springs Bridge. Table 5.1 contains the values used for the flexural capacity rating of the bridges, both experimental and theoretical.

Table 5.1 Strain compatibility flexural capacity of girders

Girder	Full Deck (kip-ft)	Half Deck (kip-ft)
1 (S4 & S3)	1,609	1,381
2 (S2 & S1)	1,623	1,383
3 (S6 &S5)	1,623	1,383

The shear capacity was obtained from Pettigrew (2014) by using the simplified analysis of the AASHTO provisions. Table 5.2 contains the values for girder distribution factors calculated from the theoretical AASHTO LRFD provisions; note that these equations are the same as used for the theoretical calculations in the parametric study. Girder 2 and 3 have the same cross sectional properties, therefore they share the same capacity from strain compatibility and girder distribution factors. Note that for half deck, the deck thickness is reduced in half, which is a conservative approach for calculating flexural capacity because the deck was significantly deteriorated. If the thickness of the slab is reduced then there is a greater need for load transfer and therefore a greater girder

distribution factor will be calculated. A significant increase in the girder distribution factor from full deck to half deck can be observed.

Table 5.2 Theoretical girder distribution factor for full deck and half deck

	Full Deck		Half Deck	
Girder	**Interior Girder**	**Exterior Girder**	**Interior Girder**	**Exterior Girder**
1	0.353	0.35	0.394	0.391
2	0.344	0.341	0..396	0.393
3	0.344	0.341	0.396	0.393

Table 5.3 presents the results of the calculations for the live load rating factor for flexure and shear. Inventory rating and operating rating are considered for theoretical and experimental cases. The bridge passes the inventory level and operating level according to the specifications for half-deck and full-deck, shear and flexure respectively. For experimental, the bridge passes the inventory level for interior, except for half deck. For exterior, the bridge rates less than one on inventory, but performs very well on operating on all cases except on exterior shear operating full deck. On this case the rating factor is 0.96, which still is very close to one. This is a reality for flexural and shear rating on all the experimental cases, therefore the bridge can be posted or improved through renovation, even though the bridge qualifies to be rated for legal load rating (operating). This bridge was not in good structural conditions, but it had potential for renovation and to remain in service for a longer period. Note that the operating rating was considered to understand where does the bridge stands in between a bridge that can carry design loads and a bridge that can carry legal loads. If the bridge does not qualify for operating the bridge qualifies for posting or renovation, before considering replacement. Appendix F has example calculations about the calculations pertaining live load rating according to

the AASHTO provisions.

Moreover, there was a rating performed from the calibrated model using a HS-20 load (the same specified in the parametric study). This rating is obtained from conditions very similar to the existing bridge and it has the advantage of using a legal design loads on the bridge. This is an example of one of the advantages of a calibrated model. In this case, we are able to estimate the flexural load distribution of a bridge that is no longer in service from a load that was never placed on the bridge.

Table 5.3 Live load rating factor for full deck and half deck

	Theoretical				**Experimental**			
	Full Deck				**Full Deck**			
Girder	**Inventory**		**Operating**		**Inventory**		**Operating**	
	Flexure	**Shear**	**Flexure**	**Shear**	**Flexure**	**Shear**	**Flexure**	**Shear**
Interior	1.59	1.28	2.06	1.65	1.11	0.889	1.44	1.152
Exterior	1.63	1.29	2.11	1.67	0.94	0.74	1.22	0.96
Girder	**Half Deck**				**Half Deck**			
	Inventory		**Operating**		**Inventory**		**Operating**	
Interior	1.26	1.28	1.63	1.65	0.93	0.95	1.18	1.23
Exterior	1.26	1.28	1.64	1.67	0.84	0.81	1.09	1.05

Table 5.4 MGDF from calibrated model and HS-20 loading

Interior	0.355
Exterior	0.329

Table 5.5 Live load rating from calibrated model and HS-20 loading

	Inventory	**Operating**
Interior	0.799	1.01
Exterior	0.84	1.089

Table 5.4 contains the flexural distribution factor values for the HS-20 loading from the calibrated model. The HS-20 is a legal load used in the design of bridges. This is the load that the bridge has to pass to perform for inventory level, which is a screening for the bridges that need to be evaluated at operating level. Since the bridge rates below 1.0 for the inventory level the bridge can be rated for legal loads and decide the need for load posting or strengthening and renovation. The bridge passes the operating stage, and could remain in operation according to the AASHTO LRFR. However, from field observation, renovation and strengthening of the bridge is suggested due to the detrimental deck conditions of the driving surface and shear connections of the girders.

CHAPTER 6. SUMMARY AND CONCLUSIONS

6.1 Summary

A 48-year-old prestressed double tee girder bridge located on Icy Springs Road in Coalville, Utah, was tested for live load testing prior to replacement by a new bridge. The bridge was load posted before testing and removal. The deck surface had significant damage and deterioration exhibiting spalling concrete and exposed rebar. The asphalt was absent in most of the locations on the surface.

The live load test considered four load cases. The truck used for testing weighed 61.7 Kips (273.98 KN). From testing, influence lines were recorded for the measurements of strain, deflection and rotation at the respective instrument locations. However, the strains gages at 2H behaved strangely and were not considered in the analysis. Data processing of the data involved zeroing the readings for initial readings and corrections the measurements for thermal drift. The plots exhibited adequate behavior for calibration and analysis.

After processing the data, the study proceeded to calibrate a finite element model (FEM) to simulate the global structural behavior measured from live load testing. The calibration used objective error functions such as: mean absolute percent error (MAPE) and absolute percent error (APE). In addition, the calibration used the R^2 value to quantify the correlation between FEM and the test measured response. Moreover, plots of the transverse distribution of live load measured and FEM predicted, were used during the calibration. The calibration consisted in a semi-automated calibration, using a programming interface to communicate to the FEM software and analyze the calibration,

and fine tuning from the calibration user. Influence lines from the measured response and the FEM prediction were plotted to demonstrate the outcome of the calibration.

A parametric study on girder distribution factor (GDF) was developed to study the influence of the variable parameters on the predictions and to compare the FEM prediction to the current specifications from AASHTO. The study considered moment and shear GDF (MGDF and SGDF) for the variable span length, slab thickness, angle of skew, number of double tees and spacing of the stems. Due to the low correlation of the AASHTO prediction and FEM GDF, a new statistical model was proposed to estimate GDF. The new prediction significantly improves the prediction of GDF and is more accurate.

Different ratings were performed to understand and better estimate the state of the bridge prior to removal. Theoretical rating and experimental ratings were performed. Also GDF from the calibrated model were considered for rating. The bridge successfully passes the operating rating and is rated below the inventory level.

6.2 Conclusions

1. A finite element model was successfully calibrated to model the global behavior of a 48-year-old double tee girder bridge that was in a state of extensive deterioration. This was possible due to the implementation of link elements along the flange connections to model the transverse load distribution.

2. After calculating MGDF for interior and exterior and different loading cases, it was observed that the exterior GDF for moment is obtained when the truck is placed

close to the edge of the exterior girder between one or two feet away from the allowable edge distance.

3. For the calculation of accurate SGDF it is necessary to use different transverse positions; the governing factor is usually obtained when the truck is placed closer to the interior girders.

4. A new statistical model was proposed for the prediction of MGDF and SGDF with a correlation superior to the AASHTO specification. The model has an R^2 of 0.86 for MGDF and 0.83 for SGDF.

5. The AASHTO specification inaccurately predicts GDF with R^2 of 0.46 for MGDF and 0.22 for SGDF for double tee girders.

6. The Icy Springs Bridge failed the inventory rating, but passed the operating rating. The low rating is due to the deteriorated transverse flange connectors. The bridge could carry legal loads if posted appropriately and also have the rating increased if renovated.

REFERENCES

ASCE, (2013). “2013 Report Card for America’s Infrastructure” Bridges 2013 Grade C+, <http://infrastructurereportcard.org> (Jan. 14, 2013).

Aktan, A. and Brownjohn, J. (2013). ”Structural Identification: Opportunities and Challenges.” *J. Struct. Eng.* 139, SPECIAL ISSUE: Real-World Applications for Structural Identification and Health Monitoring Methodologies, 1639–1647.

AASHTO (2010) AASHTO LRFR-Manual for Condition Evaluation and Load and Resistance Factor Rating (LRFR) of Highway Bridges Washington, DC.

AASHTO (2010) AASHTO LRFD Bridge Design Specifications, Washington, DC.

Bapat, Amey V.(2009) “Influence of Bridge Parameters on Finite Element Modeling of Slab on Girder Bridges” Virginia Polytechnic Institute and State University, Blacksburg, Virginia.

Bridge Diagnostics Inc. (2012a) “ST350 Operations Manual”, < http://bridgetest.com bdi-strain-transducers/ (Sept, 2015).

Bridge Diagnostics Inc. (2012b) “Tiltmeter”, < http://bridgetest.com/products/bdi-tiltmeter/ > (Sept, 2015).

Barr, P., Woodward, C., Najera, B., and Amin,M. (2006). “Long-Term Structural Health Monitoring of the San Ysidro Bridge.” J. Perform. Constr. Facil., 20(1), 14-20.

Catbas, N and Kijewski-Correa, T. (2013). “Structural Identification of Constructed Systems: Collective Effort toward an Integrated Approach That Reduces Barriers to Adoption”. ASCE Journal of Structural Engineering.

Chajes, M. J., Shenton, H. W., and O'Shea, D. (2000). "Bridge-condition Assessment and LoadRating Using Nondestructive Evaluation Methods." *Transportation Research Board: Journal of the Transportation Research Board*, Vol. 2, No. 1696, 83-91.

Chapra, S. and Canale, R. (2010*) Numerical methods for engineers 6th* Ed., McGraw-Hill Higher Education, Boston.

Collins, W. N. (2010) “Live Load Testing and Analysis of the Southbound Span Span of U.S. Route 15 Over Interstate-66” Virginia Polytechnic Institute and State University. Blacksburg, VA.

Computers and Structures Inc. (2014). *Csi Bridge 2015 - Introduction to CSi Bridge*. Berkeley, California.

Computers and Structures Inc. (2013). *CSi Analysis Reference Manual for SAP2000, ETABS, SAFE, and Csi Bridge*. California.

Gere, J.M., and Goodno, B.J. (2009) Mechanics of Materials, 7th Ed., Cengage Learning, Ohio.

Goble, G., Schulz, J., and Commander, B. (1992). "Load predictions and structural response." Final Rep. *FHWA DTFH61-88-C-00053* Univ. of Colorado, Boulder, Colorado.

Hardyniec, Andrew B.(2009) "Dynamic Testing and Modeling of a Superelevated Skewed Highway Bridge" Virginia Polytechnic Institute and state University. Blacksburg, Virginia.

Hodson, D., Barr, P., and Halling, M. (2012). "Live-Load Analysis of Posttensioned Box-Girder Bridges." *J. Bridge Eng.*, 17(4), 644-651.

Ibrahimbegovic, A., Wilson, E. (1991). A Unified Formulation for Triangular and Quadrilateral Flat Shell Finite Elements with Six Nodal Degrees of Freedom . Communications in Applied Numerical Methods, 7(1), 1-9.

Karoumi, R. Andersson, A. Sundquist, H. (2006) "Static and Dynamic Load Testing of the New Svinesund Arch Bridge." The International Conference on Bridge Engineering. Hong Kong.

Kim, S. and Nowak, A. (1997). "Load Distribution and Impact Factors for I-Girder Bridges." *J. Bridge Eng.*, 2(3), 97–104

Maguire, M., Moen, C., Roberts-Wollmann, C., and Cousins, T. (2015). "Field Verification of Simplified Analysis Procedures for Segmental Concrete Bridges." *J. Struct. Eng.* 141, SPECIAL ISSUE: Field Testing of Bridges and Buildings, D401400.

Moon, F. and Catbas, N. (2013) Structural Identification of Constructed Systems. Structural Identification of Constructed Systems: pp. 1-17.

Nilson,A.H., Darwing,D., Dolan, C.W. (2010) Design of Concrete Structures, 14th Ed, McGraw Hill, New York.

Pettigrew, C. S., "Flexural, Shear, and Punching Shear Capacity of Three 48-Year-Old Prestressed Lightweight Concrete Double-Tee Bridge Girders" (2014). *All Graduate Theses and Dissertations.* Paper 3852.

Ren, W., Lin, Y., and Peng, X. (2007). "Field Load Tests and Numerical Analysis of Qingzhou Cable-Stayed Bridge." *J. Bridge Eng.*, 12(2), 261–270.

Sanayei, M., Phelps, J., Sipple, J., Bell, E., and Brenner, B. (2012). "Instrumentation, Nondestructive Testing, and Finite-Element Model Updating for Bridge Evaluation Using Strain Measurements." *J. Bridge Eng.*, 17(1), 130–138.

Vaghefi, K., Oats, R., Harris, D., Ahlborn, T., Brooks, C., Endsley, K., Roussi, C., Shuchman, R., Burns, J., and Dobson, R. (2012). "Evaluation of Commercially Available Remote Sensors for Highway Bridge Condition Assessment." *J. Bridge Eng.* 17, SPECIAL ISSUE: Nondestructive Evaluation and Testing for Bridge Inspection and Evaluation, 886–895.

Zokaie, T. (2000). ”AASHTO-LRFD Live Load Distribution Specifications.” *J. Bridge Eng.*, 5(2), 131–138.

Wang, X., Swanson, J., Helmicki, A., and Hunt, V. (2007). ”Development of Static-Response-Based Objective Functions for Finite-Element Modeling of Bridges.” *J. Bridge Eng.*, 12(5), 544–551.

APPENDIX A Live Load Experimental Data

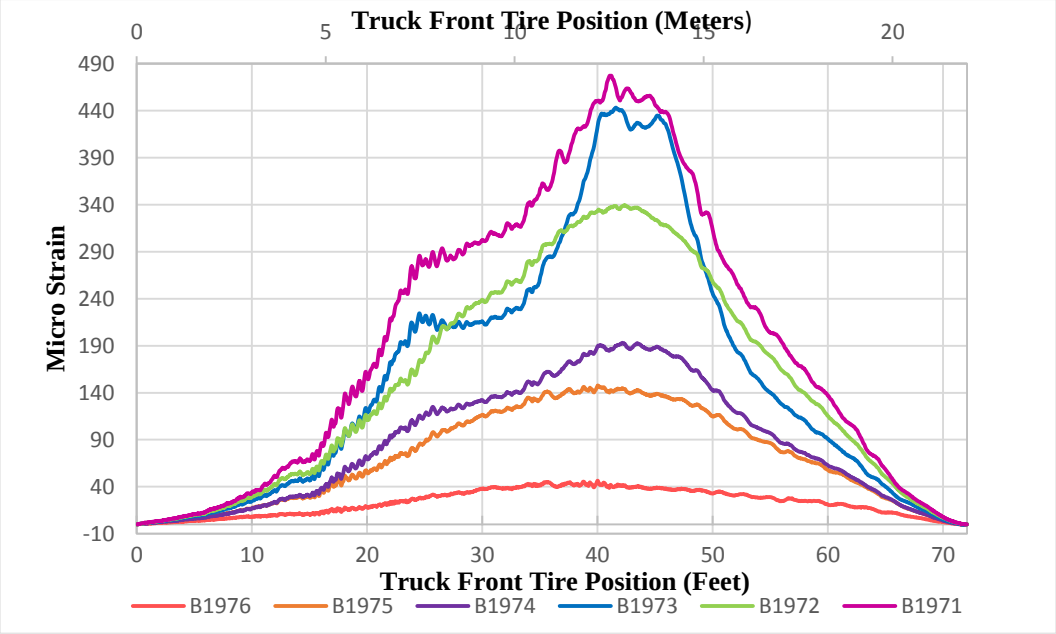

Figure A.1 Midspan gages for LC-A

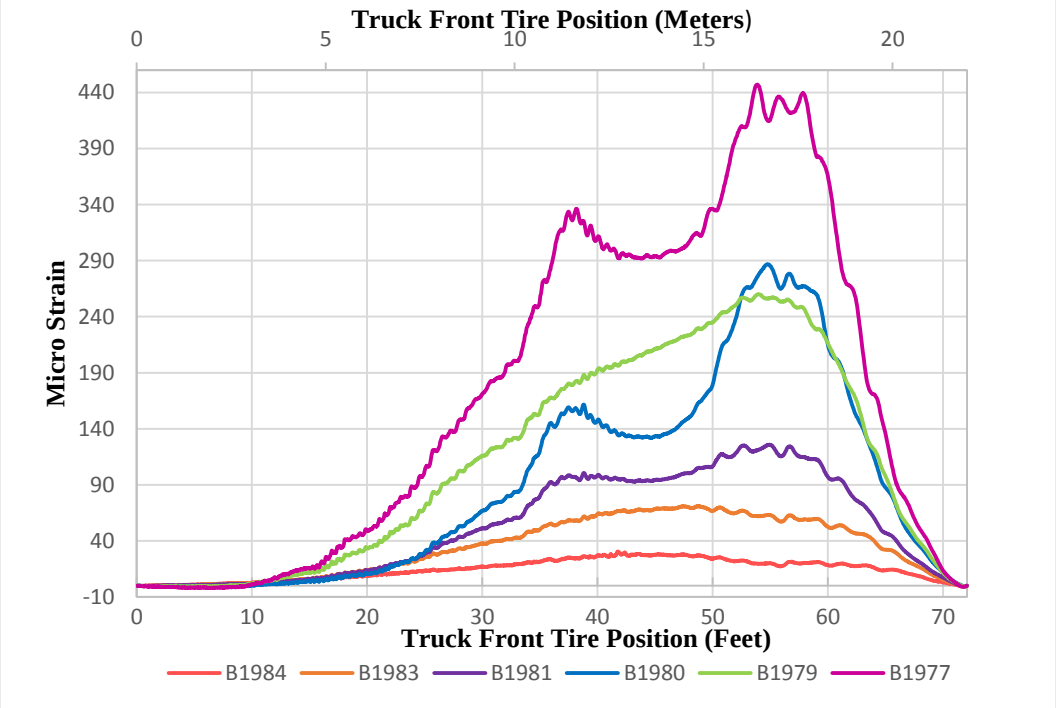

Figure A.2 Quarter span gages for LC-A

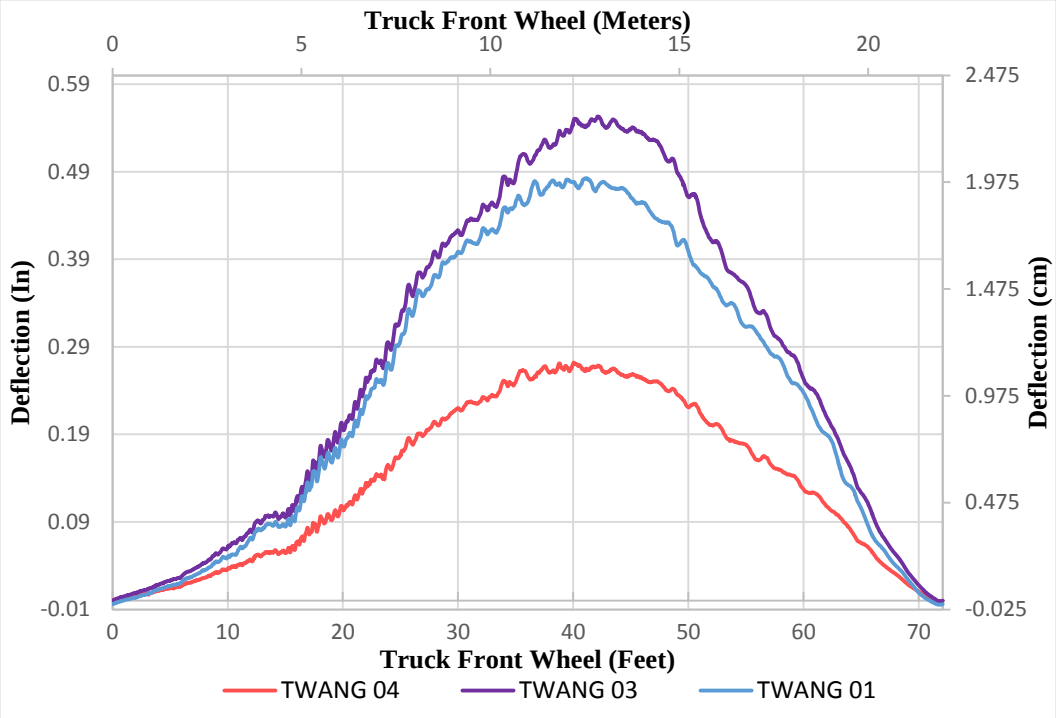

Figure A.3 Deflections at midspan for LC-A

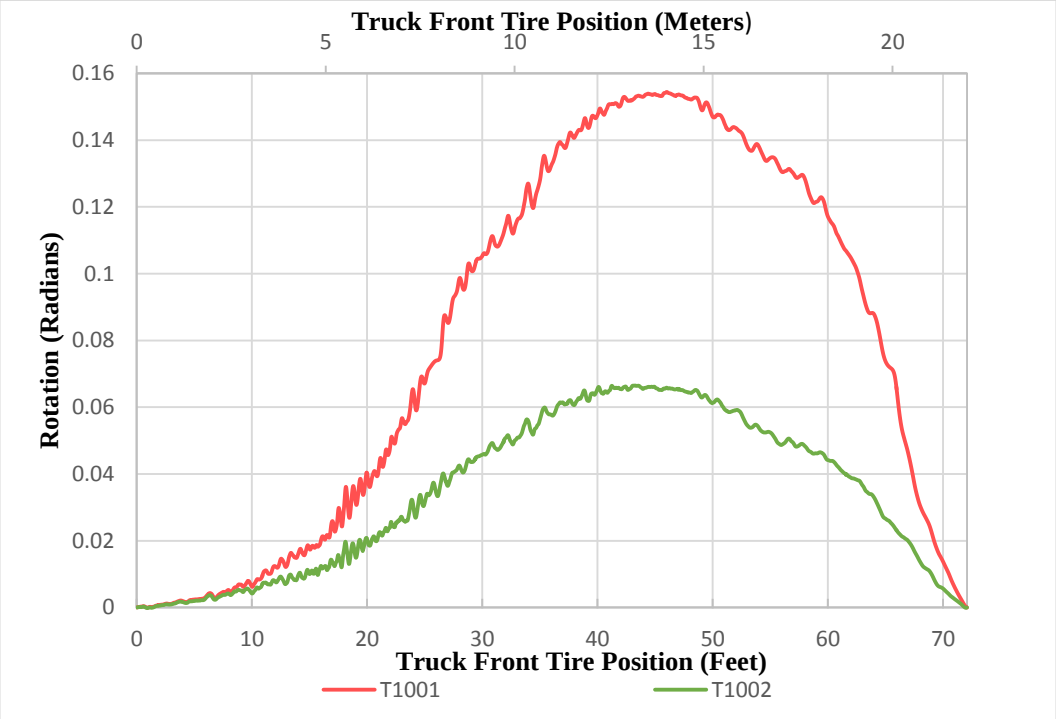

Figure A.4 Rotations for LC-A

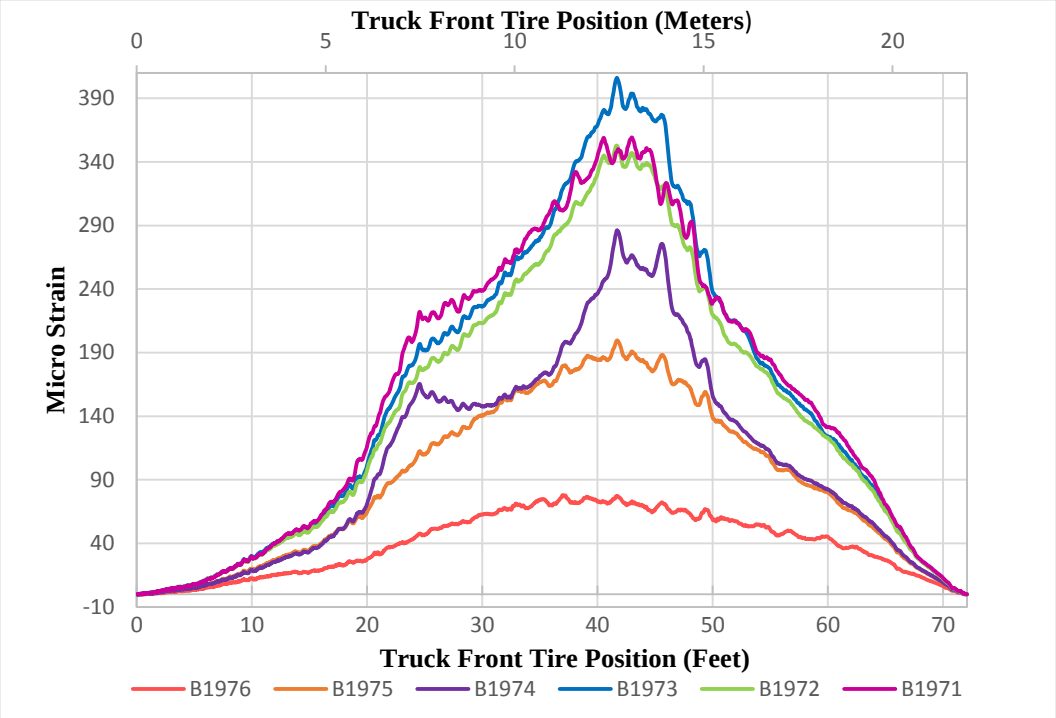

Figure A.5 Midspan gages for LC-B

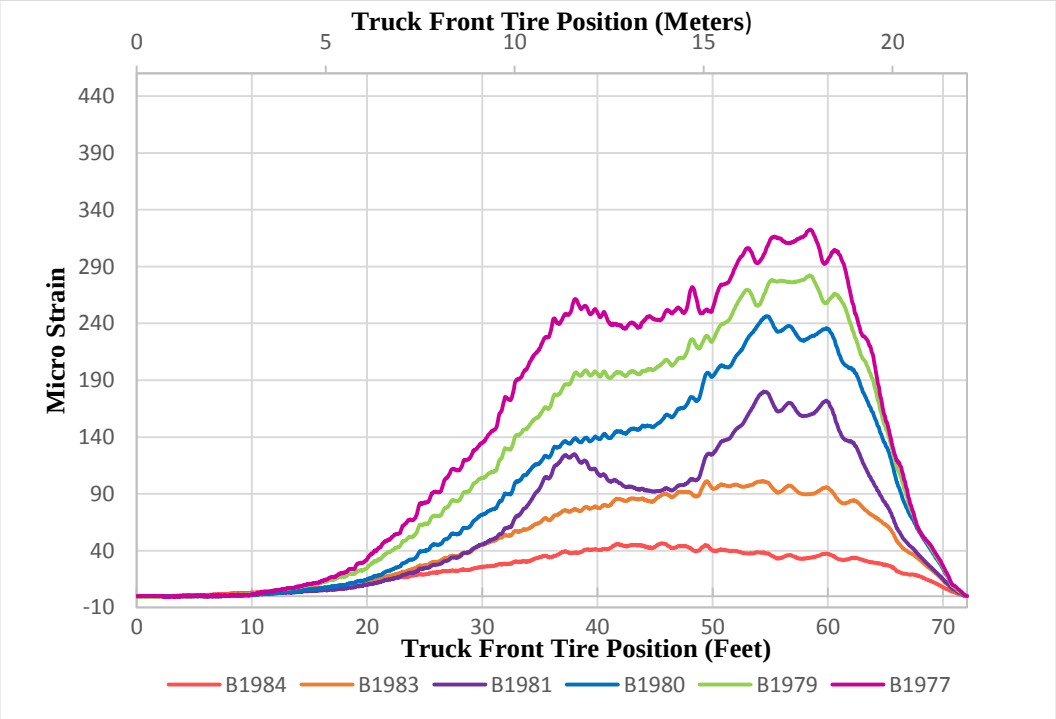

Figure A.6 Quarter span gages for LC-B

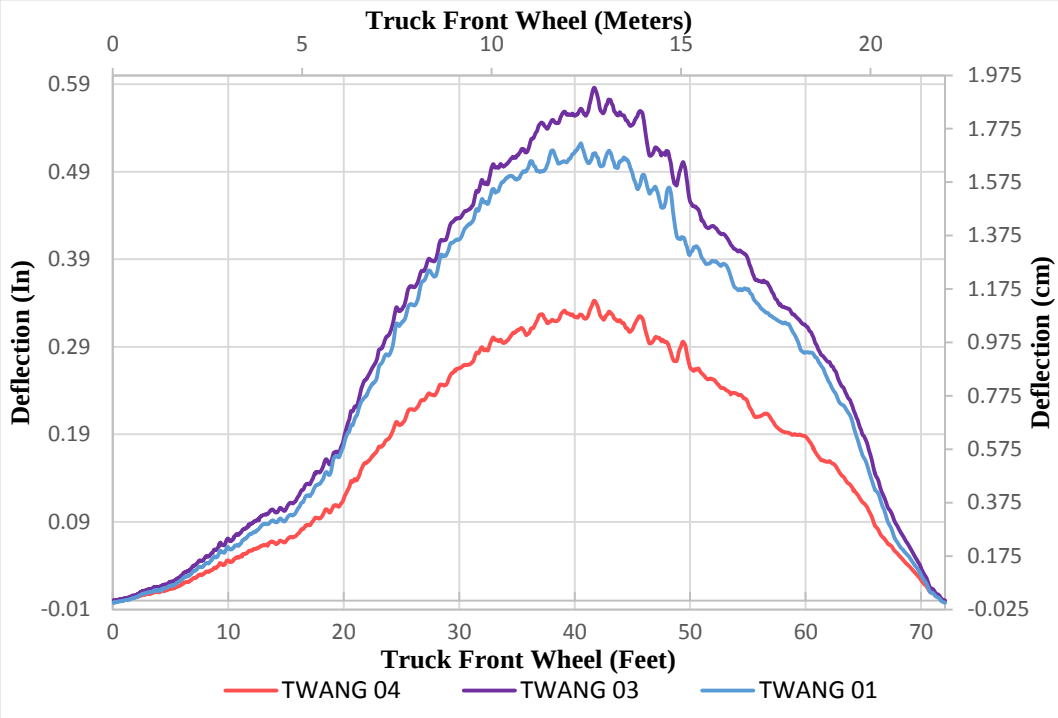

Figure A.7 Deflections at midspan for LC-B

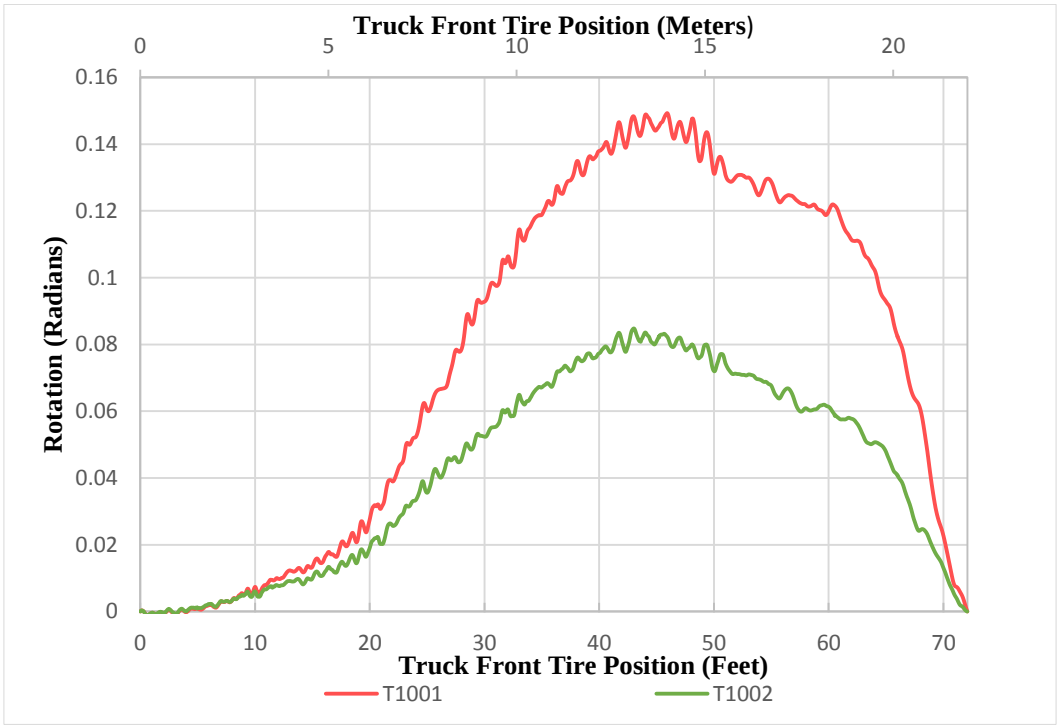

Figure A.8 Rotations for LC-B

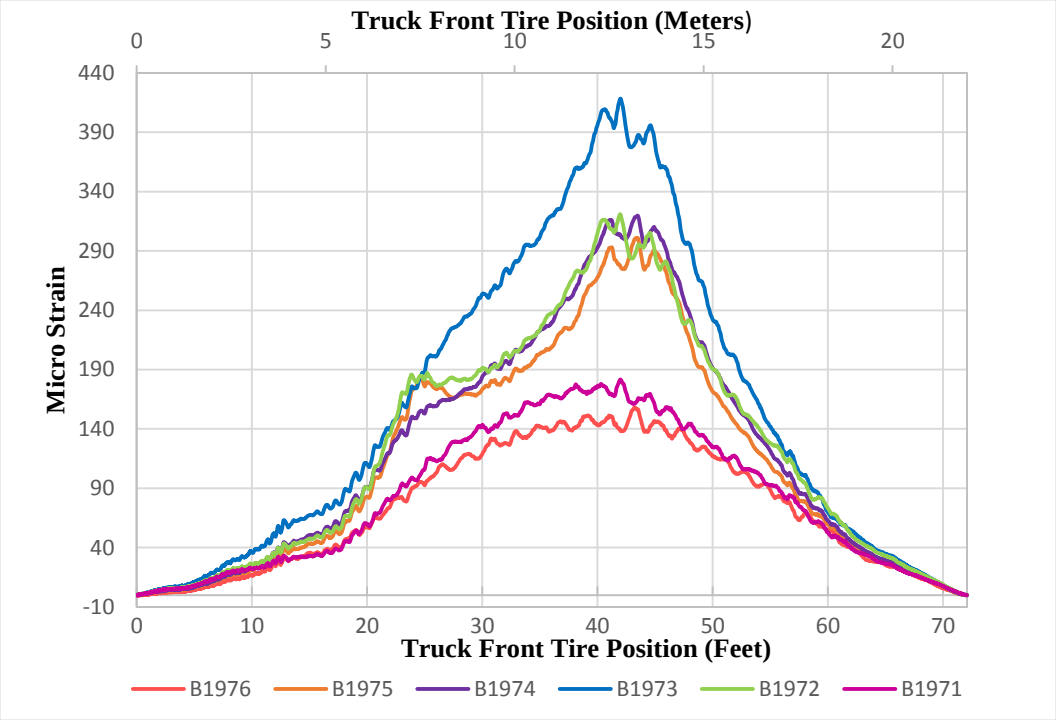

Figure A.9 Midspan gages for LC-C

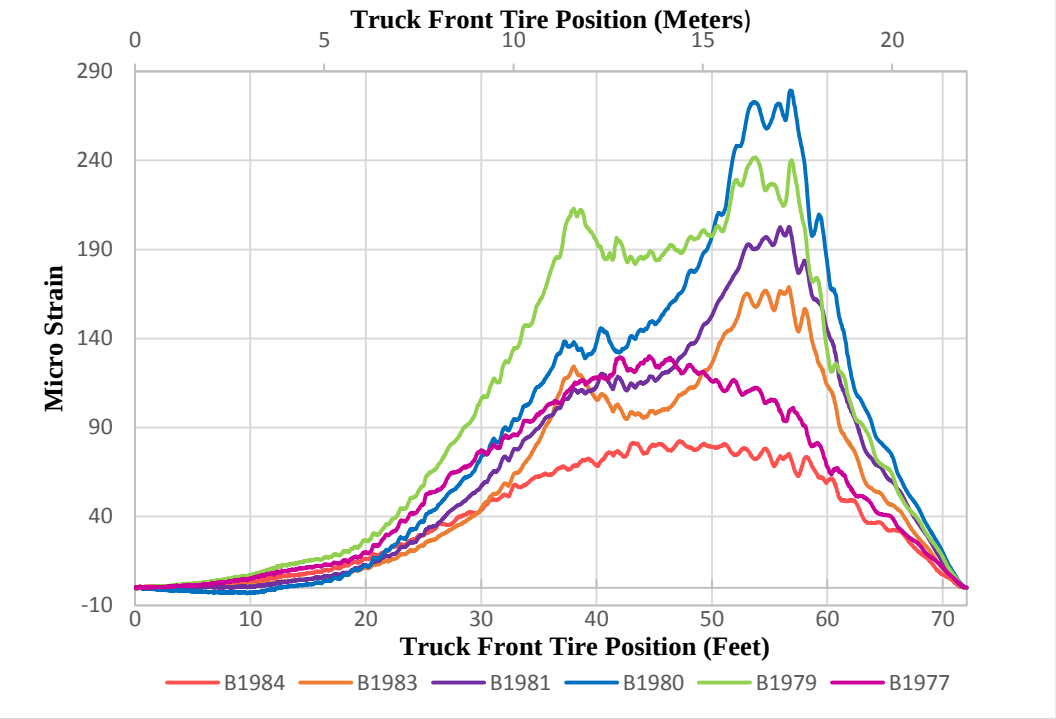

Figure A.10 Quarter span gages for LC-C

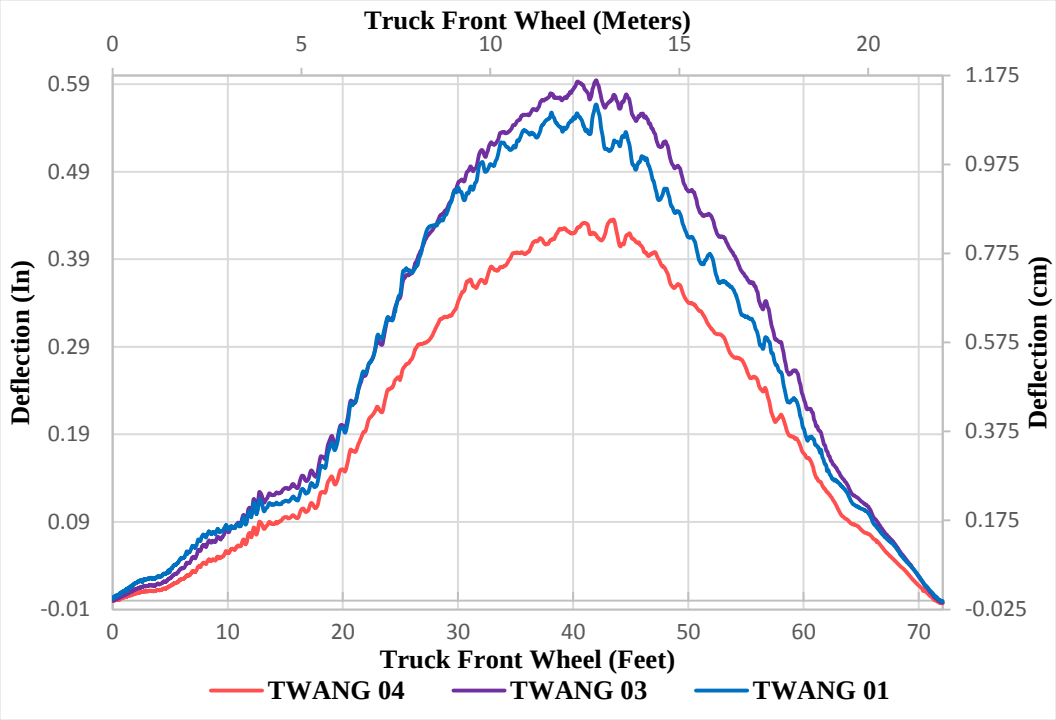

Figure A.11 Deflections at midspan for LC-C

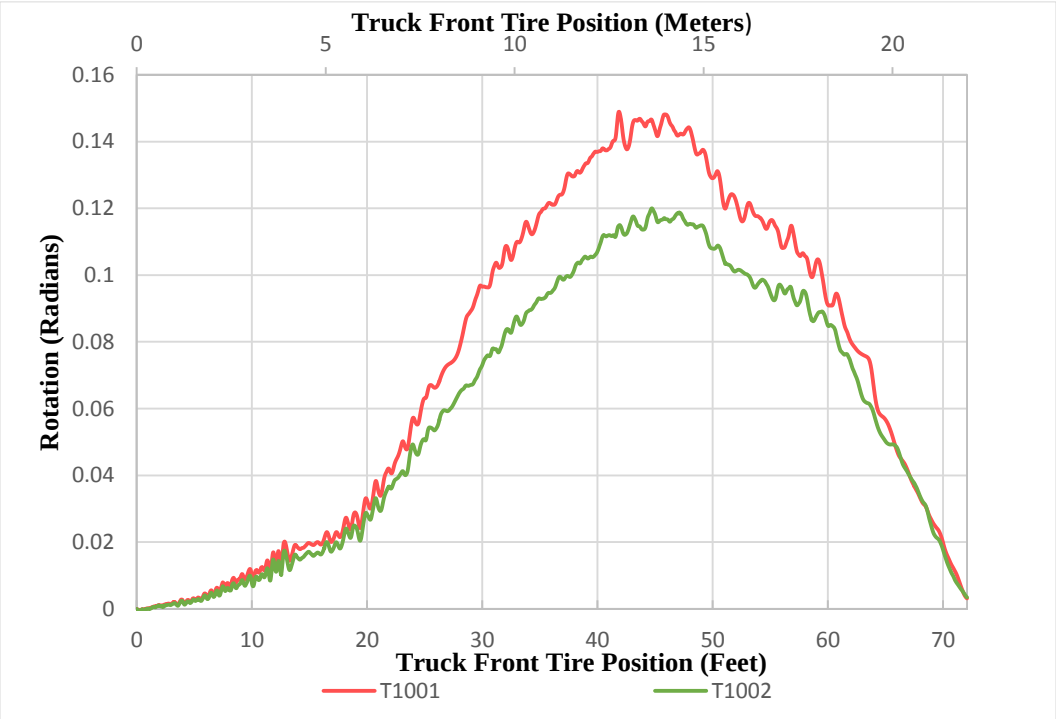

Figure A.12 Rotations for LC-C

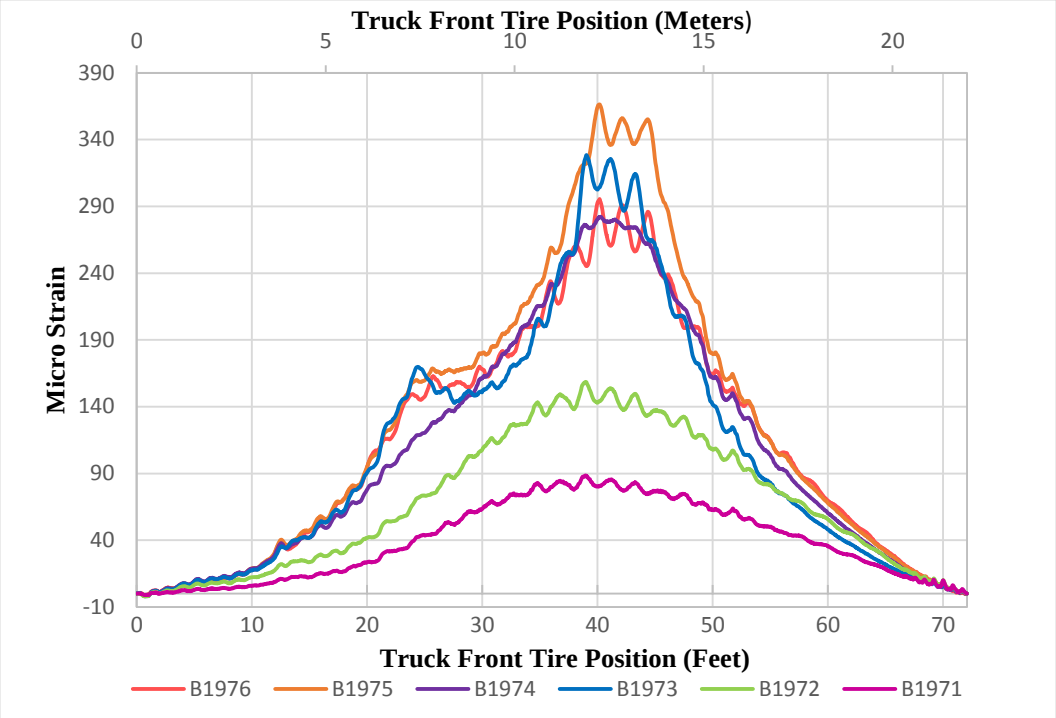

Figure A.13 Midspan gages for LC-D

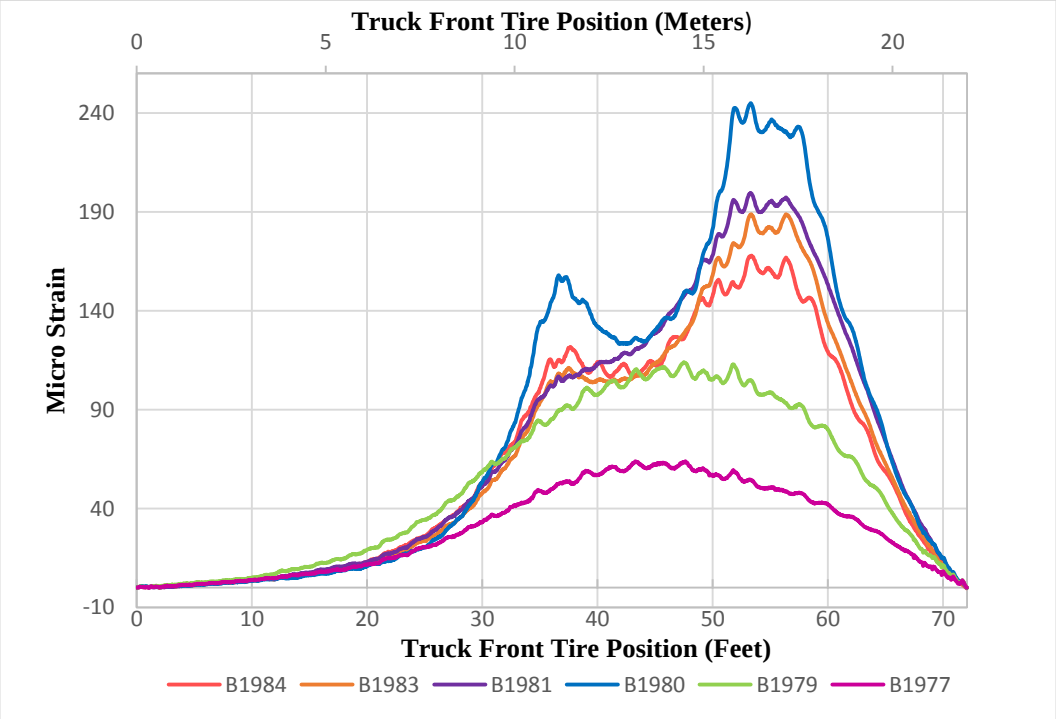

Figure A.14 Quarter span gages for LC-D

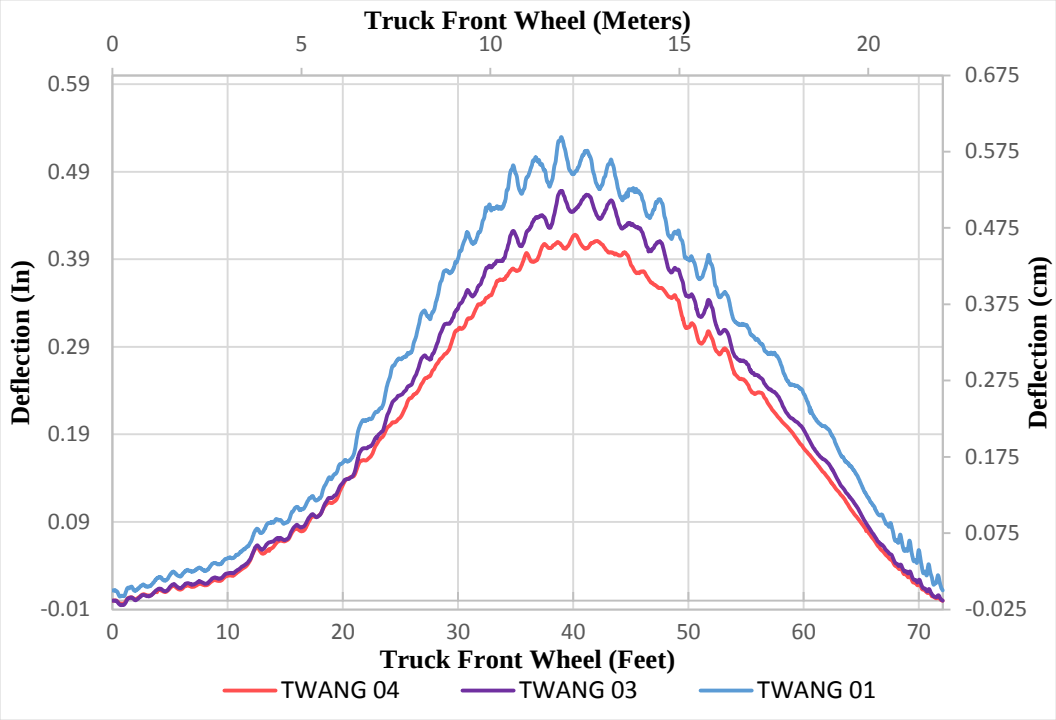

Figure A.15 Deflections at midspan for LC-D

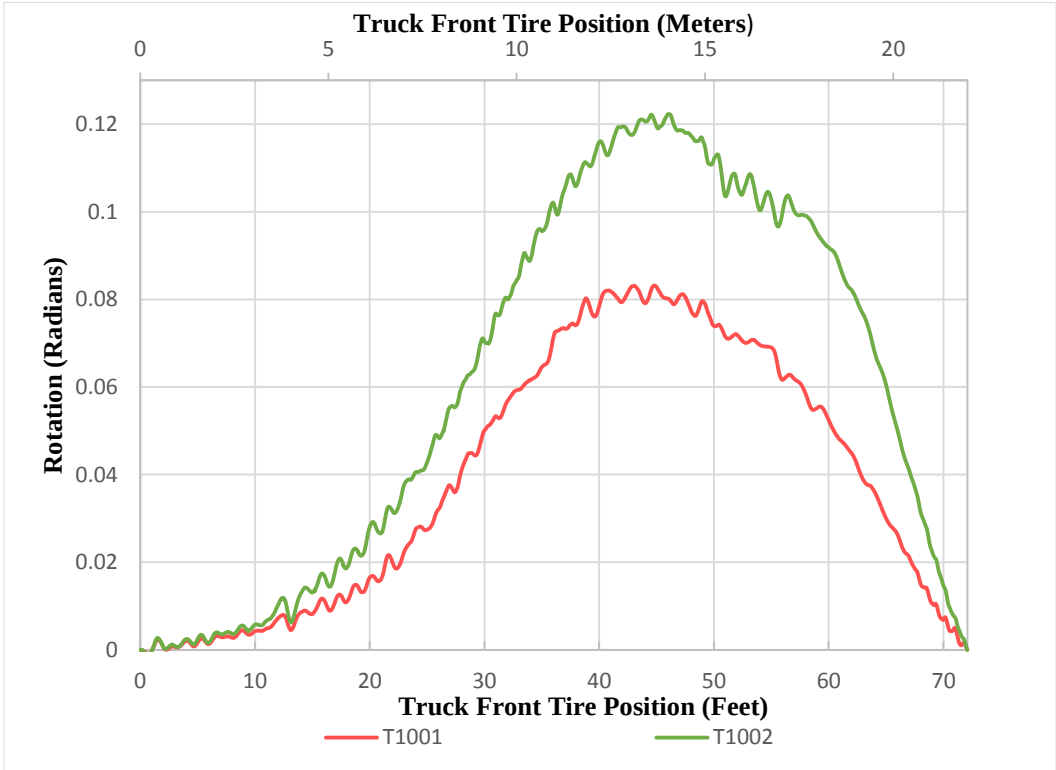

Figure A.16 Rotations for LC-D

APPENDIX B Lateral Load Distribution

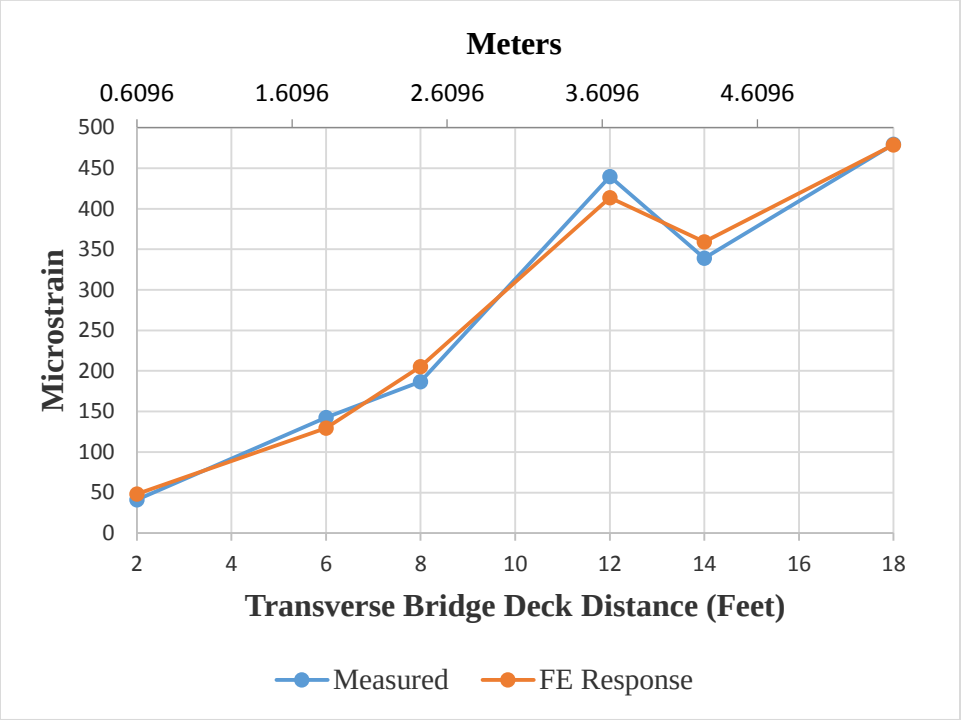

Figure B.1 LC-A transverse distribution

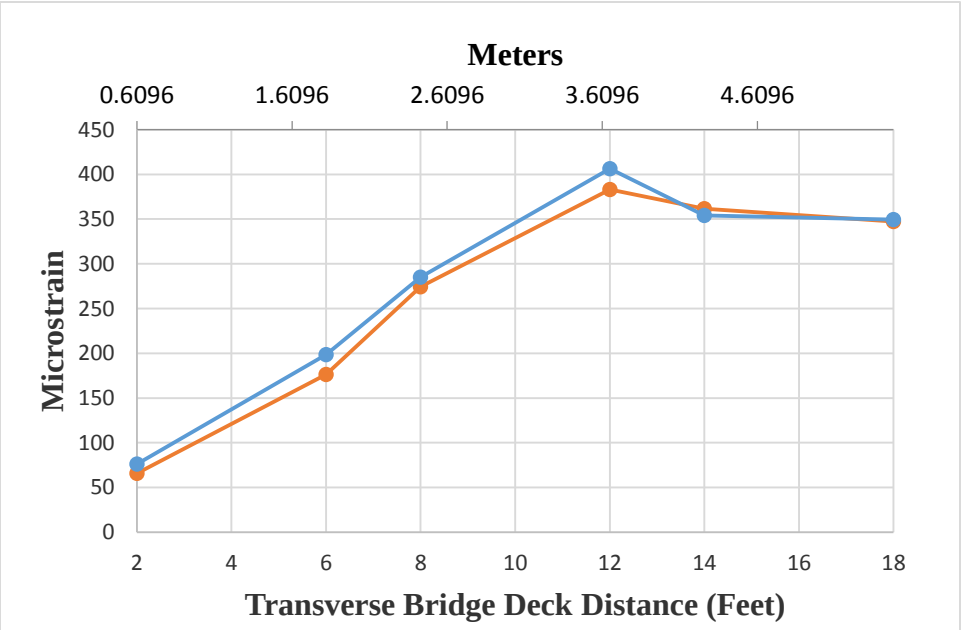

Figure B.2 LC-B transverse distribution

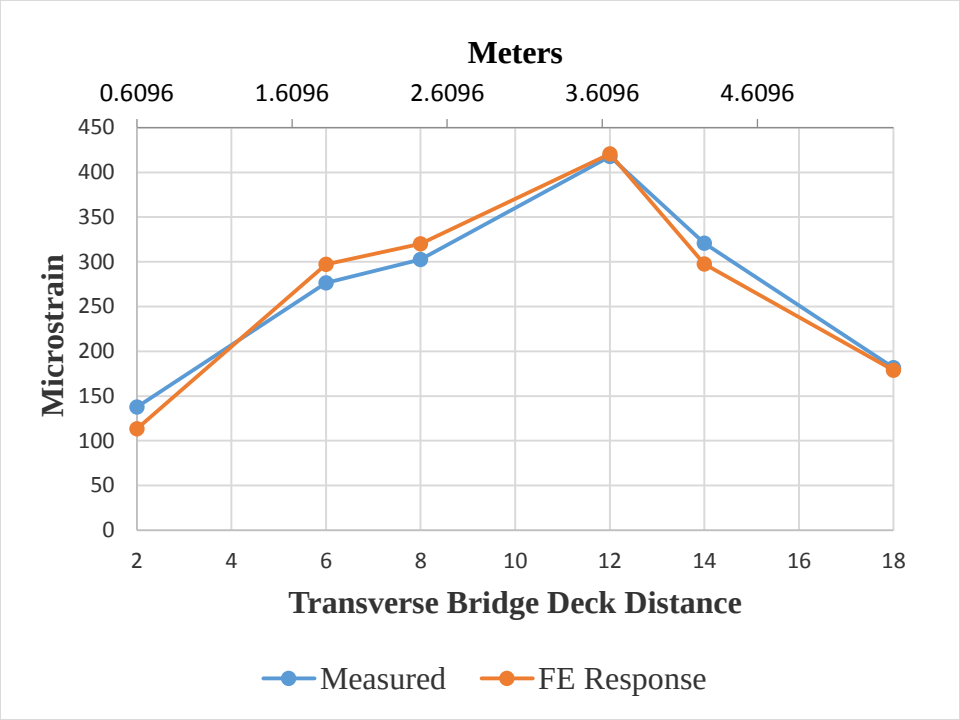

Figure B.3 LC-C transverse distribution

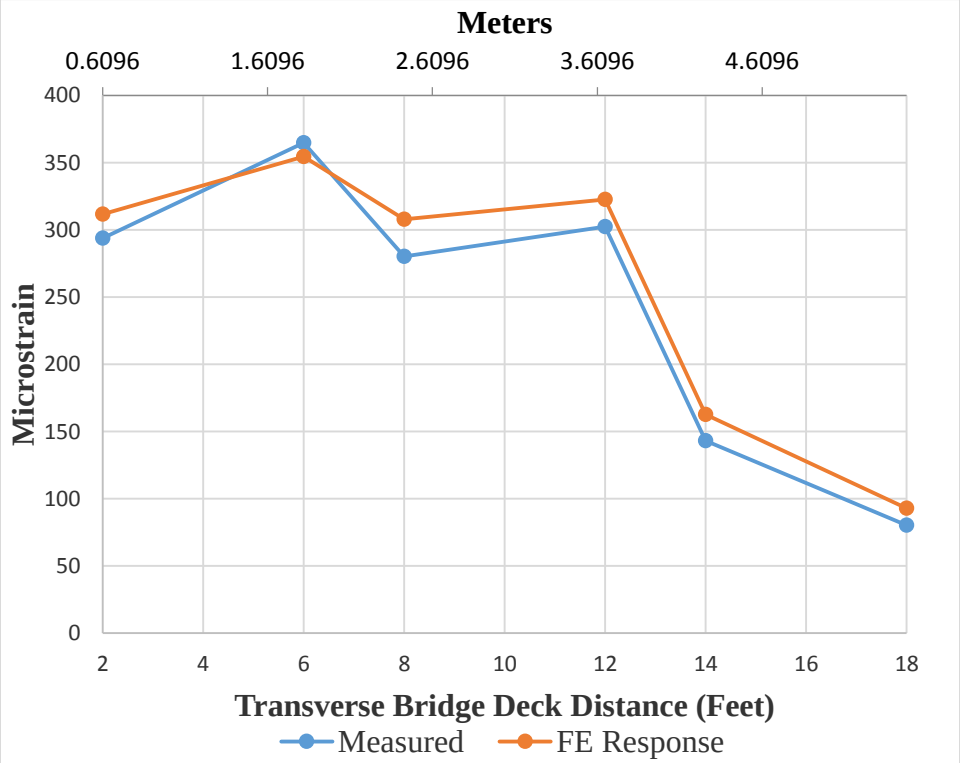

Figure B.4 LC-D transverse distribution

APPENDIX C Experimental & Calibration Comparison

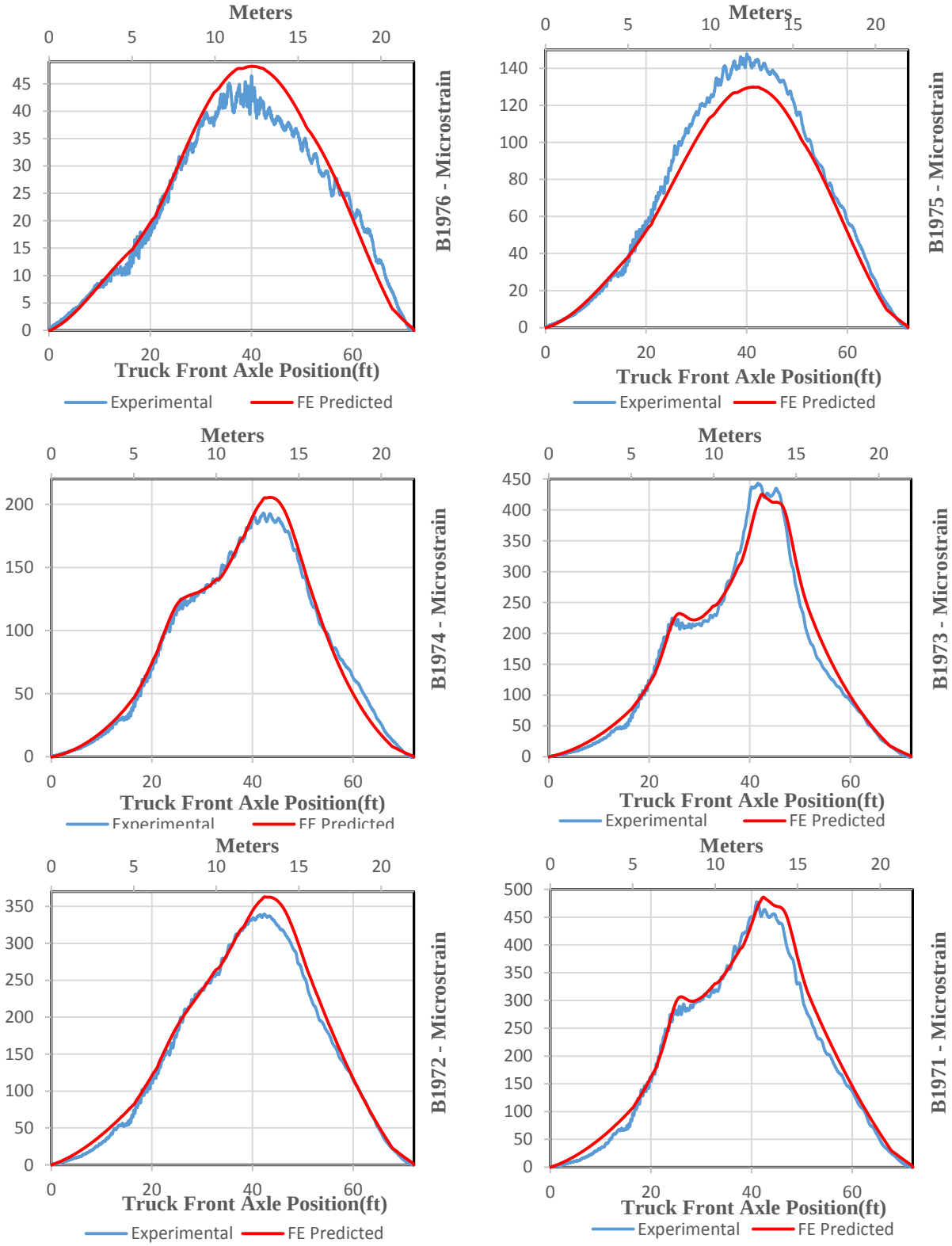

Figure C.1 B1971 through B1971 comparison for LC-A

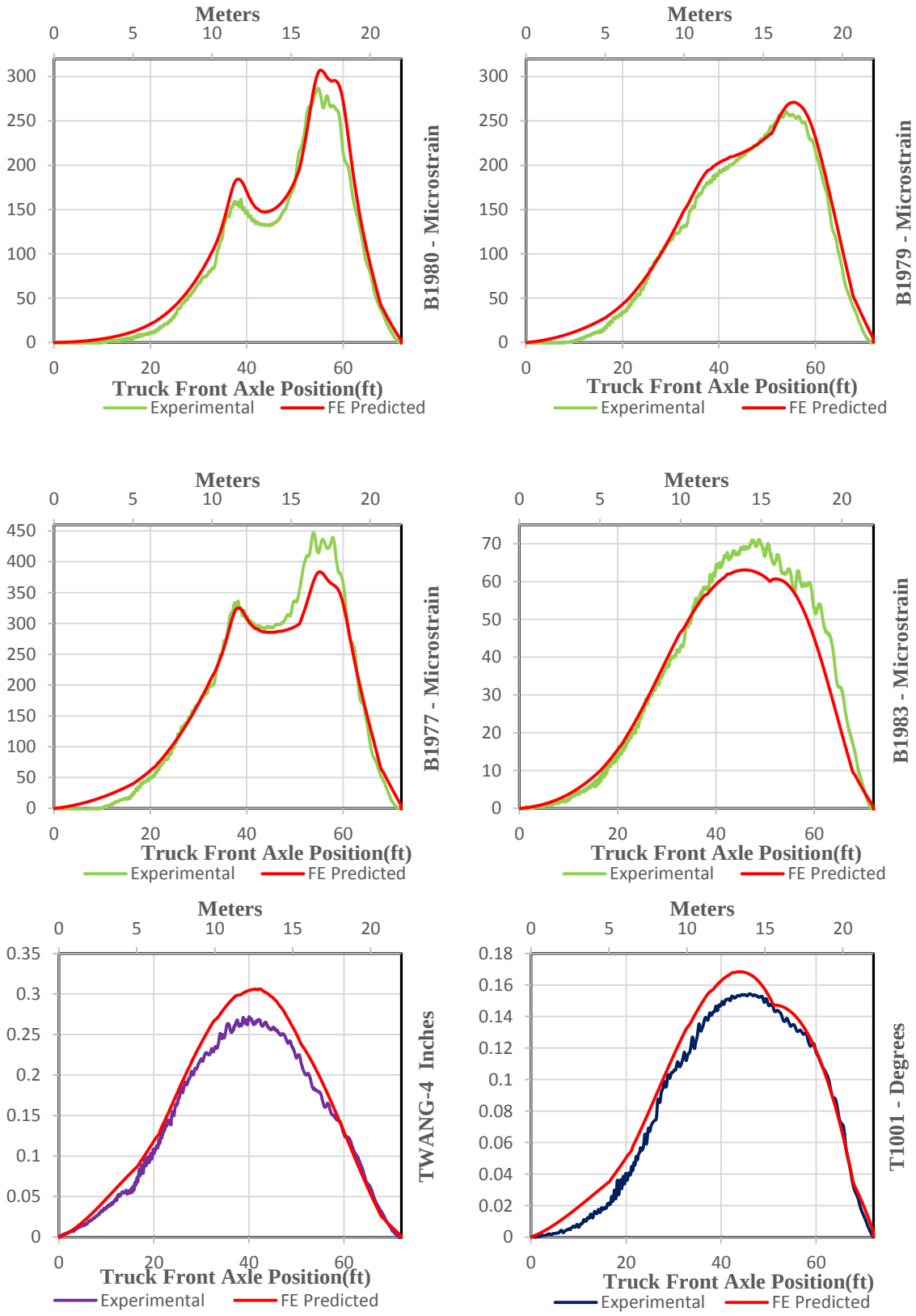

Figure C.2 B1977, 79, 80 & 83, TWANG-4 & T001 for LC-A

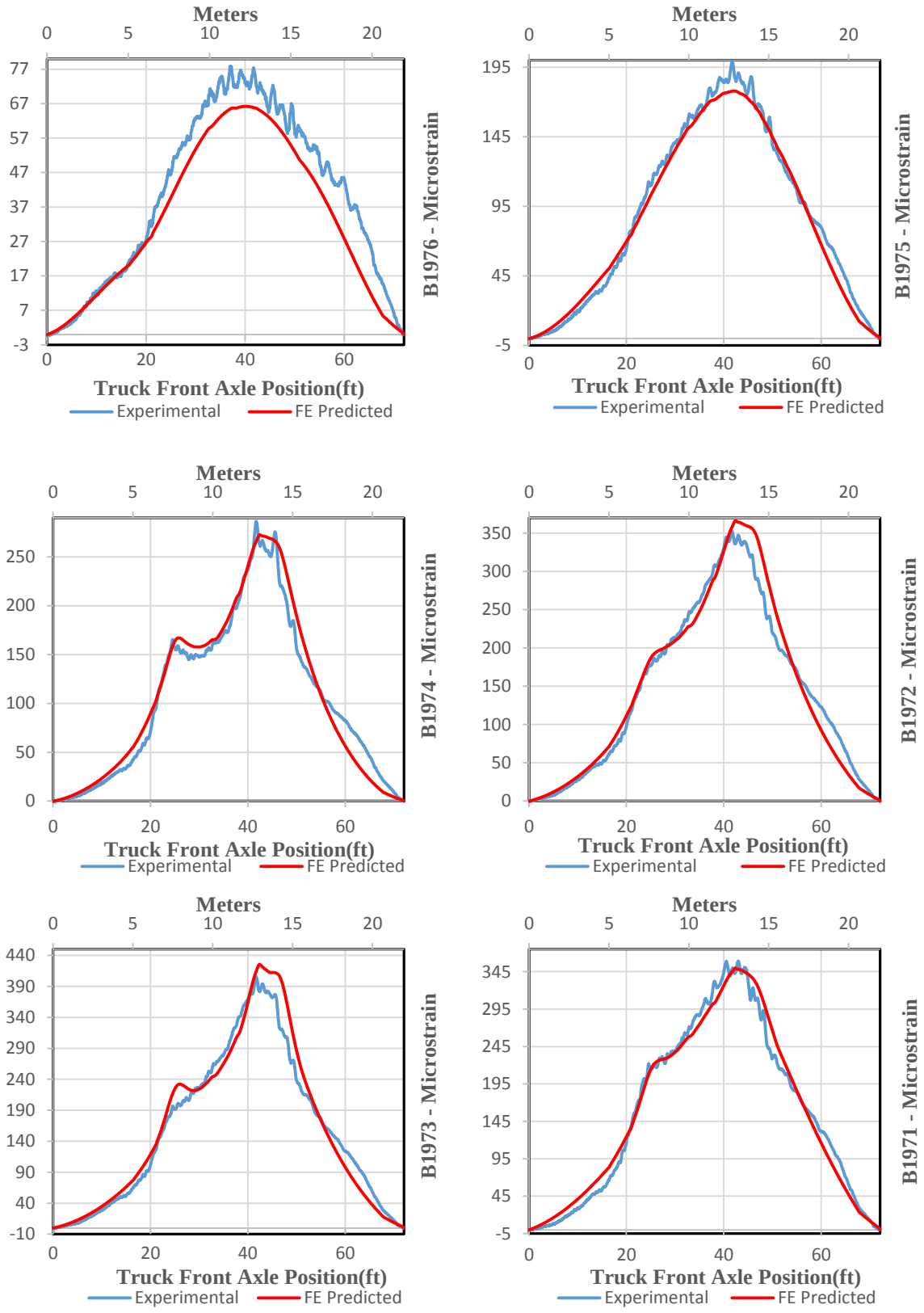

Figure C.3 B1971 through B1971 comparison for LC-B

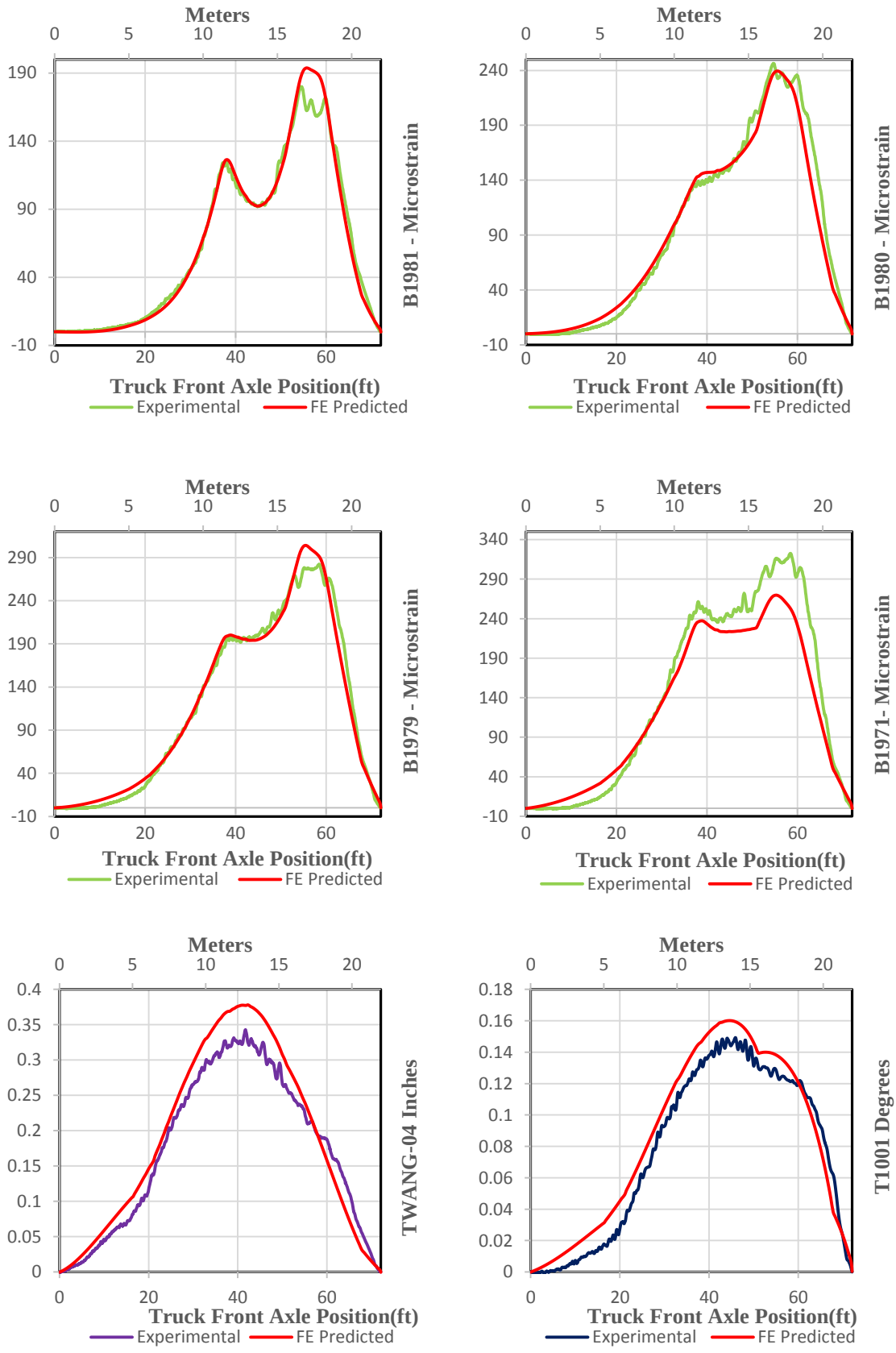

Figure C.4 B1971, 79, 80 & 81, TWANG-4 & T001 for LC-B

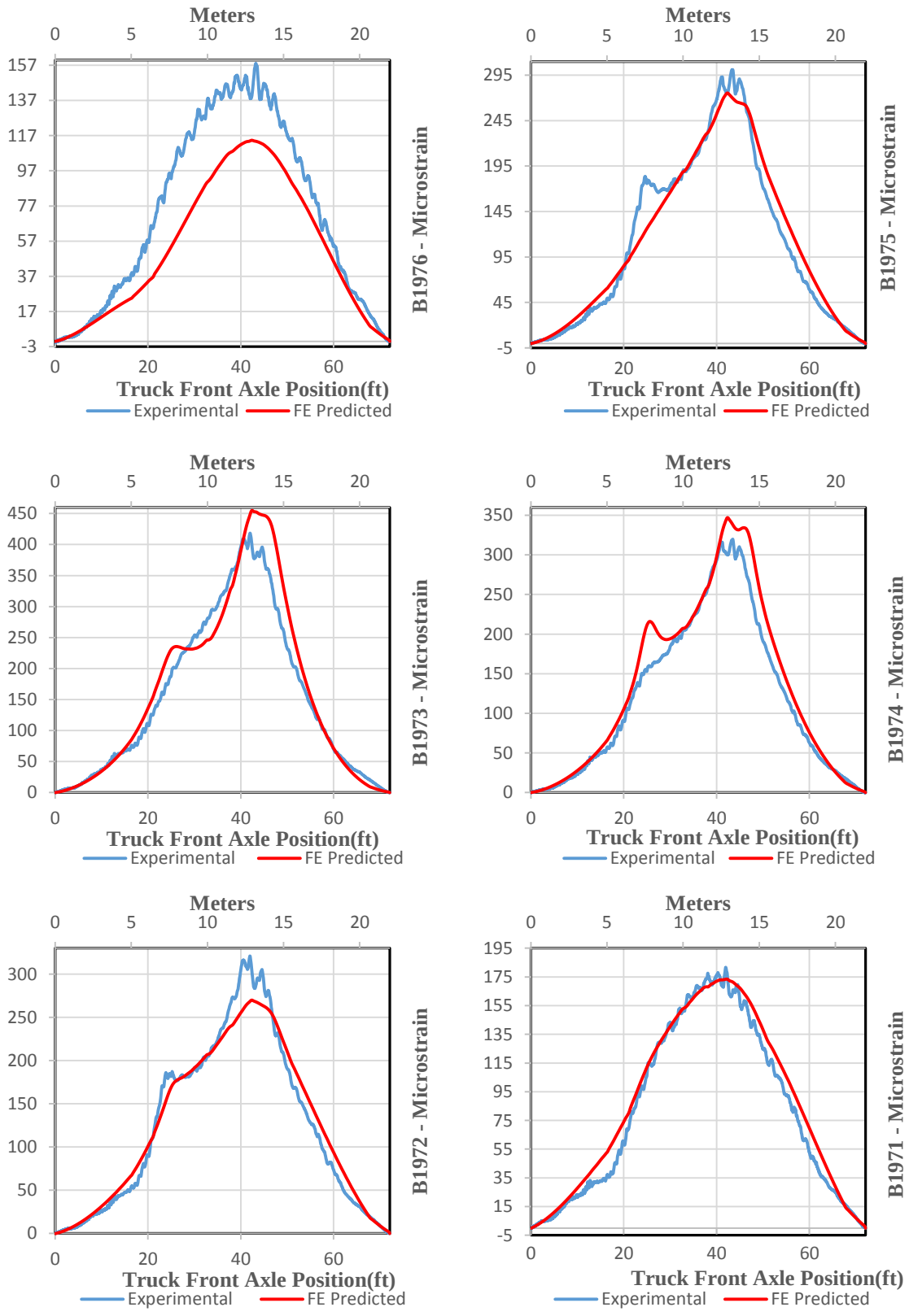

Figure C.5 B1971 through B1971 comparison for LC-C

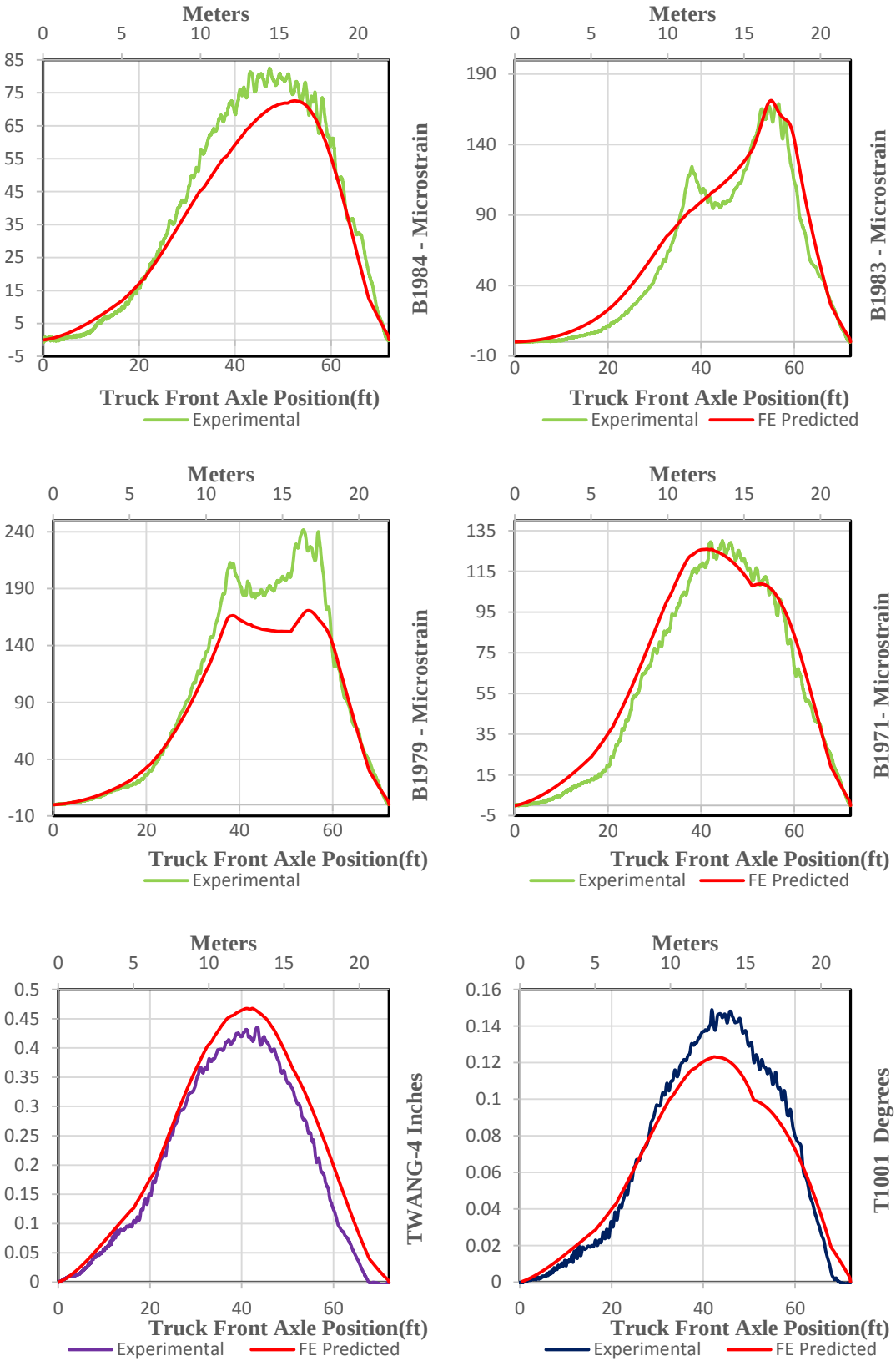

Figure C.6 B1971, 79, 83 & 84, TWANG-4 & T001 for LC-C

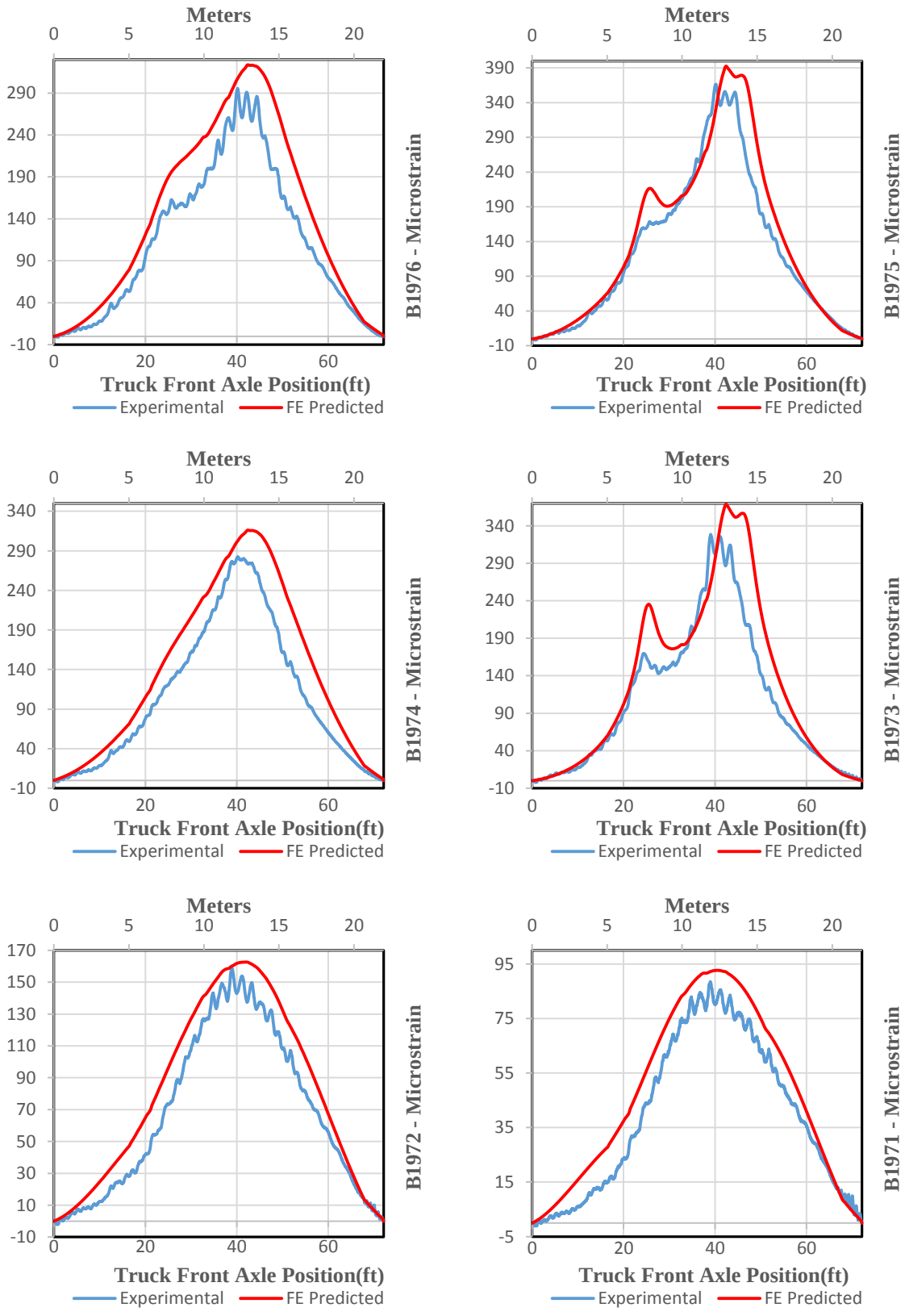

Figure C.7 B1971 through B1971 comparison for LC-D

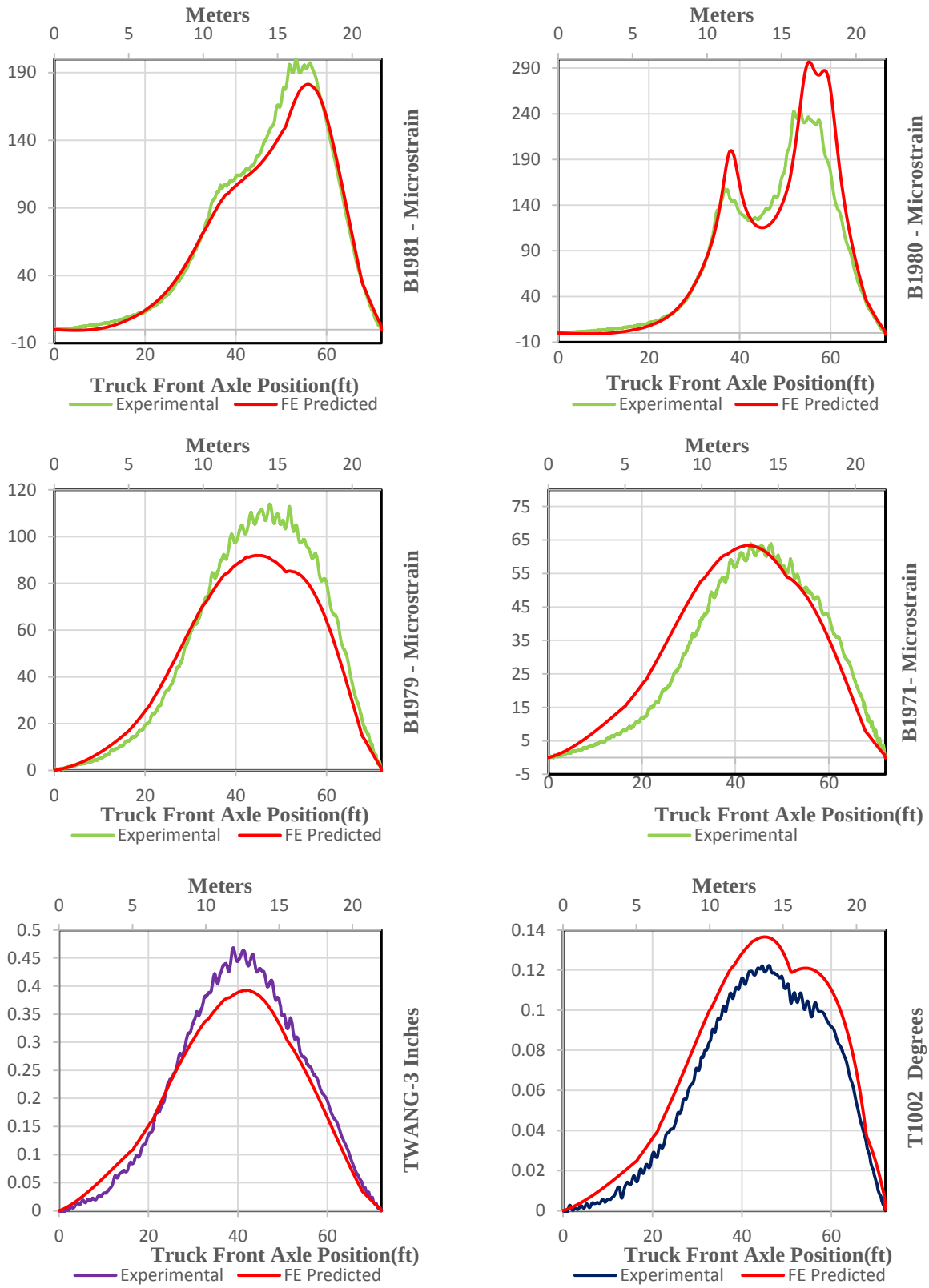

Figure C.8 B1971, 79, 80 & 81, TWANG-3 & T001 for LC-D

APPENDIX D AASHTO Interior Girder Distribution Factor

From AASHTO LRFD table 4.6.2.2.2.b-1 "Distribution of Live Loads per Lane for Moment in Interior Beams" using double T-Sections as the type of superstructure.

- One design lane loaded:

$$GDF_{interior} = 0.06 + \left(\frac{S}{14}\right)^{0.4} \cdot \left(\frac{S}{L}\right)^{0.3} \cdot \left(\frac{K_g}{12 \cdot L \cdot {t_s}^3}\right)^{0.1}$$

- Two or more design lanes loaded

$$GDF_{interior} = 0.075 + \left(\frac{S}{9.5}\right)^{0.6} \cdot \left(\frac{S}{L}\right)^{0.2} \cdot \left(\frac{K_g}{12 \cdot L \cdot {t_s}^3}\right)^{0.1}$$

Applicable when:

$$3.5 \leq S \leq 16$$
$$4.5 \leq t_s \leq 1290879$$
$$20 \leq L \leq 240$$
$$N_b \geq 4$$
$$10{,}000 \leq K_g \leq 7{,}000{,}000$$
$$K_g = n \cdot \left(I + A \cdot {e_g}^2\right) \qquad AASHTO\ (4.6.2.2.1 - 1)$$
$$n = \frac{E_b}{E_D}$$

Nomenclature

S = Spacing of beams or webs (ft.)

L = Span of beam (ft.)

t_s = depth of concrete slab (ft.)

N_b = Number of beams, stringers or girders

K_g= Longitudinal Stiffness parameter (in^4.)

n= modular ratio

e_g= Distance between the center of gravity of the stem and the deck (in.)

Assuming the same modulus for deck and girder the modular ratio is a unit value.

Table D.1 Cross sectional properties for calculations

Girder Spacing	Slab Thickness	A (in^2)	$\bar{y}$ (in)	I_x (in^4)	e_g (in)	K_g(in^4)
8	6	880	28.8242	90,879.48	9.176	164,971.35
10	6	1024	29.6927	96,031.31	8.307	166,698.81
12	6	1168	30.3470	100,019.34	7.653	168427.24
8	4.5	736	27.1757	78,629.28	9.324	142,619.01
8	8	1072	30.6468	107,263.57	9.353	201,044.65
8	10	1264	32.2194	124,781.81	9.781	245,696.22
8	12	1456	33.6410	144,217.7	10.359	300,459.43

According to section 3.6.1.1.2 of the code the GDF for one lane is to be divided by a multiple presence factor of 1.2

In addition, for skewed bridges, section 4.6.2.2e specifies the use of Table 4.6.2.2.2e-1 for the reduction of factors.

$$1 - c_1 \cdot (\tan(\theta))^{1.5}$$

$$c_1 = \left(\frac{K_g}{12 \cdot L \cdot {t_s}^3}\right)^{0.25} \cdot \left(\frac{S}{L}\right)^{0.5}$$

Table D.2 Reduction skew factor

θ(°)	c_1	Reduction Factor
15	N/A	N/A
30	0.252	0.889
45	0.236	0.764

Table D.3 Different model variations and the calculated distribution factor

Parameter	#Double T	L (ft)	S (ft)	t_s(in)	θ(°)	GDF 1 Lane	GDF 2 Lane +
Base Model	3	40	8	6	0	0.577	0.76
# of Girders	2	40	8	6	0	0.577	0.76
# of Girders	4	40	8	6	0	0.577	0.76
# of Girders	5	40	8	6	0	0.577	0.76
Length	3	20	8	6	0	0.742	0.918
Length	3	80	8	6	0	0.452	0.631
Length	3	100	8	6	0	0.418	0.595
Length	3	140	8	6	0	0.373	0.545
Skew	3	40	8	6	15	0.577	0.76
Skew	3	40	8	6	30	0.513	0.676
Skew	3	40	8	6	45	0.441	0.581
Slab Thickness	3	40	8	4.5	0	0.615	0.811
Slab Thickness	3	40	8	8	0	0.543	0.716
Slab Thickness	3	40	8	10	0	0.521	0.686
Slab Thickness	3	40	8	12	0	0.506	0.6656
Spacing	3	40	10	6	0	0.665	0.895
Spacing	3	40	12	6	0	0.748	1.024

APPENDIX E AASHTO Exterior Girder Distribution Factors

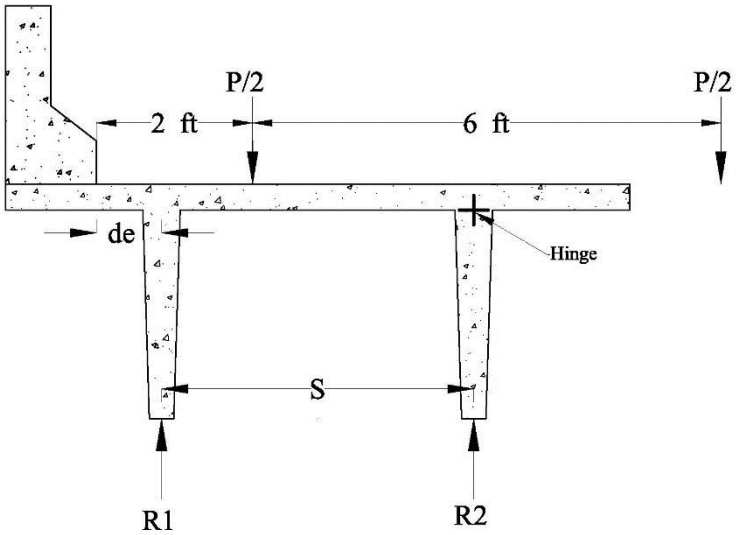

Figure E.1 Illustration of the lever rule model

Nomenclature

- R1 & R2 = Girder Reactions.
- P = Live Load corresponding to the truck load.
- d_e = horizontal distance from the centerline of the exterior girder to the curb or traffic barrier (ft.).

Assumptions

- The load is placed two feet from the curb or traffic barrier.
- The load is separated eight feet.
- The interior girder is considered to be hinged.
- A 14" traffic barrier was assumed.
- The overhang flange is halve of the spacing between the stems.

Calculation

For the cases of the study the second load is at the right of the hinge on all cases. Therefore its contribution does not affect the left side of the hinge. The exterior girder distribution factor is the same as the reaction R1 as a function of P. By summing the moments at the hinge the exterior girder distribution factor can be obtain.

$$\sum M_{Hinge} = R_1 \cdot S = \frac{P}{2} \cdot (S + d_e - 2)$$

$$GDF_{ext} = R_1 = \frac{1}{S} \cdot \frac{P}{2} \cdot (S + d_e - 2)$$

For one design lane loaded

- S=8 ft.

$$d_e = \frac{S}{2} - \left(\frac{14"}{12"}\right)' = 2.833\ ft$$

$$GDF_{ext} = R_1 = 0.552 \cdot P$$

- S=10 ft.

$$d_e = 3.833\ ft$$

$$GDF_{ext} = R_1 = 0.592 \cdot P$$

- S=12 ft.

$$d_e = 4.833\ ft$$

$$GDF_{ext} = R_1 = 0.618 \cdot P$$

For two or more design lane loaded

Applicable when $-1 \leq d_e \leq 5.5$ Table 4.6.2.2.2d-1 AASHTO 2010 LRFD

- S=8 ft.

$$GDF_{exterior} = e \cdot GDF_{interior}$$

$$e = 0.77 + \frac{d_e}{9.1} = 1.081$$

- S=10 ft.

$$e = 1.191$$

- S=12 ft.

$$e = 1.301$$

Table E.1 Results for the exterior girder distribution factor from lever rule

Spacing	$\boldsymbol{GDF_{exterior}}$ **1 Lane**	**e**	$\boldsymbol{GDF_{interior}}$ **2 Lane +**	$\boldsymbol{GDF_{exterior}}$ **2 Lane +**
8	0.552	1.081	0.76	0.822
10	0.592	1.191	0.895	1.066
12	0.618	1.301	1.024	1.332

APPENDIX F Experimental Load Rating Calculations Example

$$RC = \frac{C - \gamma_{DC} \cdot DC - \gamma_{DW} \cdot DW + \gamma_p \cdot P}{\gamma_l \cdot (LL + IM)}$$ Equation 6.1 AASHTO LRFR

$$C = \varphi_c \cdot \varphi_s \cdot \varphi \cdot R_n$$

$$\varphi_c \cdot \varphi_s \geq 0.85 \quad \text{Lower Limit}$$

AASTO LRFD Nomenclature

RF= Rating factor

C= Capacity

R_n = Nominal member resistance (as-inspected)

DC=Dead load effect due to structural components and attachments

DW= Dead load effect due to wearing surface and utilities

P= Permanent loads other than dead load

LL= Live load effect

IM= Dynamic load allowance

γ_{DC} = LRFD load factor for structural components and attachments

γ_{DW} = LRFD load factor for wearing surfaces and utilities

γ_p = LRFD load factor for permanent loads other than dead loads =1.0

γ_L = Evaluation live – load factor

φ_c = Condition factor

φ_s=System factor

φ = LRFD resistance factor

Load Analysis

$$W_{barrier} = 4.022 \ \frac{lbf}{ft}$$

$$W_{pavement} = 7.03 \ \frac{lbf}{ft}$$

$$W_{Girder} = 324.5\ \frac{lbf}{ft}$$

$$LL_{truck} = 645.75\ kip\ ft \quad For\ HL-93\ Truck\ and\ 51\ ft\ span$$

$$LL_{Lane} = 640\frac{lbf}{ft} \cdot \frac{L^2}{8} = 208.08\ kip - ft$$

Moments

$$DC = \frac{W_{barrier} \cdot L^2}{8} + \frac{W_{girder} \cdot L^2}{8}$$

$$DW = \frac{W_{pavement} \cdot L^2}{8} = 26.6665\ kip - ft$$

Shear

$$DC = \frac{W_{barrier} \cdot L}{2} + \frac{W_{girder} \cdot L}{2}$$

$$DW = \frac{W_{pavement} \cdot L}{2}$$

Girder No 2

$\varphi_c = 0.85$ For Poor Condition Table 6-2 p6-15

$\varphi_c = 1$ For flexure and shear

$\varphi_c \cdot \varphi_s = 0.723 \geq 0.85$

$IM = 33\%$

$g_{exp} = 0.2943$ Experimental girder distribution factor

Strength I Limit States Inventory Level for Prestressed Concrete on Flexure

$\gamma_{DC} = 1.25 \quad \gamma_{DW} = 1.50 \quad \gamma_l = 1.75 \quad Table\ 6-1 \quad AASHTO\ LRFR$

Flexural Analysis

R_n = 1623/2 kip-ft
R_n Corresponds to the full deck-strain compatibility (Pettigrew 2014). The value is divided by because the experimental girder factor is calculated for one T section.

$$LL = [LL_{truck} \cdot (1 + IM) + LL_{lane}] \cdot g_{exp} = 313.97\ kip - ft$$

$$C = 0.85 \cdot R_n = 689.775\ \ kip - ft$$

$$RC = \frac{C - \gamma_{DC} \cdot DC - \gamma_{DW} \cdot DW + \gamma_p \cdot P}{\gamma_l \cdot (LL + IM)} = 0.94$$

Shear Analysis

$$LL = [LL_{truck} \cdot (1 + IM) + LL_{lane}] \cdot g_{exp} = 313.97\ kip - ft$$

$$C = 0.85 \cdot R_n = 689.775\ \ kip - ft$$

$$RC = \frac{C - \gamma_{DC} \cdot DC - \gamma_{DW} \cdot DW + \gamma_p \cdot P}{\gamma_l \cdot (LL + IM)} = 0.94$$